

**Volume 6, Issue 2, 2024**

**Print ISSN: 2663-1024  
Online ISSN: 2663-1016**

# **EURASIA JOURNAL OF SCIENCE AND TECHNOLOGY**



**Copyright© Upubscience Publisher**



# **Eurasia Journal of Science and Technology**

**Volume 6, Issue 2, 2024**



**Published by Upubscience Publisher**

**Copyright© The Authors**

Upubscience Publisher adheres to the principles of Creative Commons, meaning that we do not claim copyright of the work we publish. We only ask people using one of our publications to respect the integrity of the work and to refer to the original location, title and author(s).

Copyright on any article is retained by the author(s) under the Creative Commons Attribution license, which permits unrestricted use, distribution, and reproduction in any medium, provided the original work is properly cited.

Authors grant us a license to publish the article and identify us as the original publisher.

Authors also grant any third party the right to use, distribute and reproduce the article in any medium, provided the original work is properly cited.

**Eurasia Journal of Science and Technology**

**Print ISSN: 2663-1024 Online ISSN: 2663-1016**

**Email: [info@upubscience.com](mailto:info@upubscience.com)**

**Website: <http://www.upubscience.com/>**

# Table of Content

<b>STUDY ON PHOSPHOGYPSUM-BASED LOW-CARBON ROAD BASE MATERIALS</b> Girts Sinka	1-4
<b>PROGRESS IN THE INVESTIGATION OF MARINE DEEPWATER DRILLING FLUID SYSTEMS</b> S.Z. Lim	5-9
<b>ADVANCED OPTICAL DIAGNOSTIC TECHNOLOGY APPLICATION PROGRESS IN COMBUSTION TESTING OF ENERGETIC MATERIALS</b> Steven Bhattacharya	10-24
<b>DESIGN OF A DISPOSABLE WOODEN TABLEWARE PACKAGING INSPECTION DEVICE</b> JianWu Hou, TianYue Jiang*, JiBo Li, HaoJun Zhao	25-30
<b>RESEARCH ON THE LAUNCH AND RECOVERY METHODS OF UAV</b> JinHui Ge, RenJun Zhan*	31-36
<b>AIRLINE INTERNATIONAL CREDIT CARD PAYMENT RISK CONTROL SYSTEM</b> XiangNan Li, DouDou Li*, LingNan Meng, HaoRan Sun, WeiMing Yi, WeiDong Meng	37-41
<b>INVESTIGATION ON THE REMOVAL OF SE(IV) FROM AQUATIC SYSTEMS USING ORGANIC AND INORGANIC SORBENTS</b> CaiYu Liu, ZhongShan Zhao*, Yue Sun	42-46
<b>RESEARCH ON TALENT CULTIVATION IN CYBERSECURITY UNDER THE BACKGROUND OF NEW ENGINEERING DISCIPLINES</b> Xiong Wei, BangChao Wang*, Hang Luo, YingKai Yuan	47-50
<b>TRUXENONE AND ISOTRUXENONE-BASED POROUS ORGANIC POLYMERS AS METAL-FREE, HETEROGENEOUS PHOTOCATALYSTS FOR VISIBLE-LIGHT-PROMOTED REDUCTION OF LUNG CANCER A549 CELLS</b> YongLi Tan*, YeMu Zhu, HaiFeng Duan	51-65
<b>DEEP APPLICATION OF BIM + 3D SCANNING IN STEEL STRUCTURE AND CURTAIN WALL ENGINEERING</b> XueLiang Qiao1*, XiYan Wang2, GuangYu Qiao3, SuYao Wei3, Hang Xing3, XingBin Tang3	66-72



# STUDY ON PHOSPHOGYPSUM-BASED LOW-CARBON ROAD BASE MATERIALS

Girts Sinka

*Department of Building Materials and Products, Riga Technical University, Riga, Latvia.*

**Abstract:** Phosphogypsum is a by-product emitted from the wet phosphoric acid production process. The massive accumulation of phosphogypsum occupies land resources and pollutes groundwater. Predecessors have made contributions to the utilization of phosphogypsum resources, especially the preparation of pavement base materials using phosphogypsum. It is more conducive to realizing its large-scale utilization. The paper introduces the physical and chemical properties of phosphogypsum, this review summarizes the phosphogypsum modified pavement base materials, Phosphogypsum-cement pavement base material and its hydration mechanism were analyzed. The problems existing in the research on phosphogypsum-based pavement base materials are summarized. Suggestions on resource utilization of phosphogypsum in pavement base materials were also put forward.

**Keywords:** Phosphogypsum; Pavement base materials; Resource; Hydration mechanism

## 1 PHYSICAL AND CHEMICAL PROPERTIES OF PHOSPHOGYPSUM

Phosphogypsum is a solid by-product emitted during the production of wet phosphoric acid [1]. Among them, for every 1t of phosphoric acid produced (as  $P_2O_5$  (calculated) Emissions 4.5 ~ 5.5t off-white or off-black phosphogypsum. The main component of phosphogypsum is  $CaSO_4 \cdot 2H_2O$ , due to soluble phosphorus and many harmful impurities, phosphogypsum cannot be directly utilized[2]. Currently, the global stockpile of phosphogypsum reaches 6 billion tons[3]. my country is the largest by-product country of phosphogypsum, mainly distributed in the five provinces of Hubei, Yunnan, Guizhou, Sichuan, and Anhui. The stock of phosphogypsum has reached 400 million tons, and 50 million tons of phosphogypsum are added every year, but the comprehensive utilization rate is not high. to 40% [4]. The high accumulation of phosphogypsum occupies a large amount of cultivated land, and also pollutes groundwater, soil and atmospheric environment, seriously restricting the high-quality and rapid development of the phosphorus industry [5].

In order to promote the resource utilization of phosphogypsum, researchers have made contributions to the study of the utilization of phosphogypsum in the extraction of valuable components, cement retarder, production of fertilizers, soil conditioners and calcination to prepare sulfuric acid [6-10]. However, phosphogypsum has not been utilized on a large scale and its comprehensive utilization rate is still low. Pavement base material is an important part of the road construction structure and maintains the quality, performance and safety of the road [11]. Preparing pavement base material from phosphogypsum is one of the effective ways to utilize resources. The paper summarizes the physical and chemical properties of phosphogypsum, and systematically summarizes the utilization status and mechanism of phosphogypsum in pavement base materials. Finally, the existing problems in the research on phosphogypsum-based pavement base materials were discussed, and suggestions were put forward for the resource utilization of phosphogypsum low-carbon building materials in the future.

Phosphogypsum is gray-white or gray-black powdery solid particles. The bulk density of phosphogypsum is 2.27~2.4 g/cm<sup>3</sup>, the volume density is 0.9~1.7g/cm<sup>3</sup>. The main mineral phase of phosphogypsum is dihydrate gypsum  $CaSO_4 \cdot 2H_2O$  (mass fraction 75% ~ 95%), moisture content 20% ~ 25%, pH value 1.5 ~ 5.5 [13]. Phosphogypsum is the product of the reaction between phosphate rock and sulfuric acid during the production of wet phosphoric acid. The main chemical components of phosphogypsum are CaO (30%~40%),  $SO_3$  (37% ~50%),  $P_2O_5$  (1% ~3%) and a small amount of  $SiO_2$ , MgO,  $Al_2O_3$ ,  $Fe_2O_3$ , F[14].

## 2 RESEARCH STATUS OF PHOSPHOGYPSUM-BASED PAVEMENT BASE MATERIALS

Phosphogypsum is a solid waste produced in the wet phosphoric acid leaching process. Its efficient utilization of resources can reduce environmental pressure and is also an important way for my country to achieve sustainable development. In order to comprehensively understand the research progress of phosphogypsum in road base materials, the relevant research status was systematically summarized.

### 2.1 Phosphogypsum Modified Pavement base Material

The performance of pavement base materials can be improved by using the modification function of phosphogypsum. For example, Shen Weiguo et al. [15] studied the performance of phosphogypsum-modified lime pavement base materials. The results show that phosphogypsum modification can greatly improve the performance of pavement base materials. early strength and water stability, while maintaining stable development of later strength. The erosion resistance of the pavement base material after modification by phosphogypsum is greatly improved, so the performance

of the pavement base material modified by phosphogypsum is good. Wu Kaiquan et al. [16] explored the use of waste phosphogypsum to modify lime gravel pavement base material. The results show that compared with the conventional lime pavement base material using phosphogypsum modified lime pavement base material, its strength development, water stability, and erosion resistance have been greatly improved. In addition, material costs and environmental pollution are reduced, which has social and economic benefits. Shen Weiguo et al. [17] studied the mix proportion design method of phosphogypsum modified lime pavement base material. The results show that through experimental research on the mix ratio of phosphogypsum-based pavement base materials, and based on the strength formation principle of phosphogypsum-modified pavement base materials, a mix proportion design method based on volume analysis method was developed. The above calculation method can basically determine the mix ratio of phosphogypsum modified pavement base material, its maximum dry density and optimal moisture content, which can make up for the shortcomings of complex experimental work in conventional design.

## 2.2 Phosphogypsum-Cement Pavement base Material

The synergistic utilization of phosphogypsum and cement can prepare green and low-carbon pavement base materials. Liu Chao et al. [18] studied phosphogypsum-cement stabilized gravel pavement base material. The results show that suitable phosphogypsum fine aggregate is beneficial to filling pores, causing the pavement base material to form a high-density skeleton structure. Phosphogypsum can also promote the synthesis of expanded ettringite (AFt). When the phosphogypsum content is 8%, compared with conventional cement-stabilized gravel road base materials, the strength of the cement-phosphogypsum pavement base material after curing for 7 days increased by 26.7%, and the dry shrinkage strain decreased by 40.3% at 28 days. Du Tingting et al. [19] studied phosphogypsum-cement pavement base material. The results show that the phosphogypsum-cement pavement base material prepared from modified or improved phosphogypsum has good water stability and the unconfined compressive strength is significantly improved. The improved phosphogypsum-cement pavement base material can meet the requirements of different levels of traffic. Strength requirements. Zhou Mingkai et al. [20] studied the properties of phosphogypsum-cement pavement base material. The results show that the phosphogypsum content of 8%, the cement content of 1%, and reducing the aggregate gradation are beneficial to improving the strength of the phosphogypsum-cement pavement base material. Compared with conventional cement-stabilized gravel materials, phosphogypsum-cement-based pavement base materials have excellent properties. Wu Shangfeng et al. [21] studied the application of phosphogypsum-cement pavement base material on highways. The results show that when the ratio of phosphogypsum:cement:gravel in the phosphogypsum-cement pavement base material is 40:7:60, its unconfined compressive strength meets the industry standard requirements. Phosphogypsum-cement pavement base material (40% phosphogypsum) saves about 20% in material cost compared with conventional pavement base materials, and slows down the accumulation of phosphogypsum.

## 2.3 Hydration Reaction Mechanism of Phosphogypsum-Based Pavement base Material

Xu Fang et al. [22] studied the microstructure and mechanical properties of perthion gypsum slag cement pavement base material. The results show that the main mineral phases of phosphorus gypsum slag cement are quartz ( $\alpha$ -SiO<sub>2</sub>), dihydrate gypsum (CaSO<sub>4</sub>·2H<sub>2</sub>O) and the hydration product ettringite. These mineral components and microstructure affect the unconfined compressive strength and water stability of the pavement base material, and the anti-scouring ability is consistent with its unconfined compressive strength; when the content of persulfate gypsum slag cement is 5%, the unconfined compressive strength of the pavement base material after 7 days of maintenance can meet the standard requirements. Li Xia [23] studied the properties of cement-stabilized phosphogypsum base material and found that the gel product produced by the hydration reaction can fill the inter-particle pores of the pavement base material, resulting in the formation of a high-density structure between the particles, thereby improving the overall quality of the pavement base material. Strength and stability. In addition, Yu Changyun [24] studied the feasibility of phosphogypsum-modified cement-lime stabilized red mud road base material and analyzed the strength formation mechanism of phosphogypsum-modified pavement base material. The hydration products CSH, CASH, NASH gel and ettringite have cementing and filling effects; at the same time, the filling mechanism of ettringite in the pores of the pavement base material was revealed, and it was found that ettringite mainly fills the pore size range of 0.1~1  $\mu$ m. of pores.

## 3 CONCLUSION AND RECOMMENDATIONS

The paper sorts out the physical and chemical properties of phosphogypsum. Phosphogypsum is a powdery solid particle whose main chemical components are CaO, SO<sub>3</sub> and P<sub>2</sub>O<sub>5</sub> etc. The main mineral in phosphogypsum is gypsum CaSO<sub>4</sub>·2H<sub>2</sub>O, which reacts with hydration in the pavement base material to form ettringite, which can improve the early strength of the road base material. In addition, it is introduced that the modified function of phosphogypsum and the synergistic utilization of phosphogypsum cement can improve the overall strength of the road base material. performance, and summarized the hydration reaction mechanism of phosphogypsum-based pavement base material. At present, the research and development of phosphogypsum-based pavement base materials are mostly in the experimental stage, and the impact of P<sub>2</sub>O<sub>5</sub>, fluoride ions and other harmful elements in phosphogypsum on the environmental performance of pavement base materials has not been studied in depth. Therefore, suggestions for the

future low-carbon research and development of phosphogypsum-based pavement base materials are put forward, which are summarized as follows:

- a. Preparing the pavement base material with a high content of phosphogypsum will affect its setting time. Thinking from another perspective, the setting time of the pavement base material can be controlled based on the retarding characteristics of phosphogypsum.
- b. Phosphogypsum contains a large amount of gypsum, and the hydration process will generate excess ettringite (hydrated calcium sulfoaluminate), causing volume expansion and cracking of the hardened body of the pavement base. The pavement base material itself has dry shrinkage phenomenon. Therefore, the expansion characteristics of phosphogypsum can be used to compensate for the shrinkage of the pavement base material.
- c. When phosphogypsum is mixed alone to prepare pavement base materials, it is difficult to achieve high-volume application of solid waste. If phosphogypsum is used to cooperate with various solid wastes to prepare low-carbon pavement base materials with a high content of solid waste, the effect of "treating waste with waste" can be achieved.
- d. Phosphogypsum is an industrial solid waste that contains a large amount of  $P_2O_5$ , fluoride ions and other harmful elements. It is necessary to ensure that the environmental performance of the phosphogypsum-based pavement base material is qualified, and to conduct research on the curing mechanism of harmful elements in phosphogypsum.
- e. Phosphogypsum contains phosphorus and fluorine elements. Based on chemical coordination theory and charge balance effect, through the silicon-oxygen tetrahedron and the four-coordination isomorphic effect of silicon, phosphorus elements and fluorine ions can be fully utilized to generate new chemical products. Realize the synergistic solidification and stable utilization of phosphorus and fluorine.

## COMPETING INTERESTS

The authors have no relevant financial or non-financial interests to disclose.

## REFERENCES

- [1] Deng Hua, Hou Shuomin, Li Zhongjun. Current status and prospects of comprehensive utilization of phosphogypsum. *Inorganic Salt Industry*, 2023. DOI: 10.19964/j.issn.1006-4990.2023-0278.
- [2] Huang Di, Zong Shirong, Ma Navigation. Research and application progress of phosphogypsum resource utilization technology. *Phosphate Fertilizer and Compound Fertilizer*, 2023, 38(5): 17-22.
- [3] Yan Chao, Peng Qiugui, Zhu Miao. Review of comprehensive utilization and impurity removal methods of phosphogypsum. *Phosphate Fertilizer and Compound Fertilizer*, 2023, 38(2): 27-33.
- [4] Zhou Miaoqin, Tao Snow, Liao fast. Research progress on phosphogypsum production and emission and resource utilization. *Yunnan Chemical Industry*, 2022, 49(12): 4-8.
- [5] Wu Hao, Han Chaonan, Tang Yu. Research progress on resource utilization of phosphogypsum in my country. *Modern Chemicals*, 2023, 43(3): 18-21.
- [6] Pan Keliang, Li Na, Hu Jingping. Research progress on the extraction and recovery of rare earth elements in phosphogypsum. *Journal of Huazhong University of Science and Technology (Natural Science Edition)*, 2023, 51(10): 77-83.
- [7] Yi Hui. A review of research on modified phosphogypsum as cement retarder. *Sichuan Building Materials*, 2016, 42(3): 23-24.
- [8] Zhou Jiliang. Research on the technology of using phosphogypsum to produce medium element fertilizer. *Liaoning Chemical Industry*, 2023, 52(5): 746-749.
- [9] Yang Hua, Qi Jiamin, Li Bin. Research progress on phosphogypsum soil improvement. *Phosphate Fertilizer and Compound Fertilizer*, 2023, 38(5): 40-44.
- [10] Ma Xiaoling, Tan Hongbin, Hou male. Research status and development trends of phosphogypsum production of sulfuric acid co-production of cement. *New Building Materials*, 2021, 48(3): 71-76.
- [11] Shen Weiguo, Zheng Xiaoping, Li Hongzhen. A review of the classification of pavement base materials and their service status. *Journal of Wuhan University of Technology*, 2021, 43(9): 1-5.
- [12] Li Pengpeng, Ren Qiangqiang, Lu Qinggang. A review of low-carbon cement raw material/fuel substitution technologies for dual carbon. *Clean Coal Technology*, 2022, 28(8): 35-42.
- [13] Kai Jun, Xie Weimin, Dong Xiongbo. Research progress on comprehensive utilization of phosphogypsum materials. *Materials Herald*, 2023, 37(16): 167-178.
- [14] Li Ming, Liang Huan, follow Jiefei. Progress and prospects of phosphogypsum resource utilization in my country. *Phosphate Fertilizer and Compound Fertilizer*, 2020, 35(7): 30-36.
- [15] Shen Weiguo, Jiang Ship, Zhang Korea. Research on the performance of phosphogypsum modified lime pavement base material. *Highway*, 2008(1): 141-145.
- [16] Wu Kaiquan, Lu Yong, Zhang military. Discussion on modified fly ash gravel base with waste phosphogypsum. *Road Construction Machinery and Construction Mechanization*, 2007(11): 56-58.
- [17] Shen Weiguo, Zhou Mingkai, Cha Enter. Research on the mix proportion design method of phosphogypsum modified fly ash pavement base material. *Comprehensive Utilization of Fly Ash*, 2004(3): 13-15.
- [18] Liu Chao, Zhao Deqiang, Ma Qian. Research and application of cement-phosphogypsum stabilized gravel pavement base material. *Bulletin of Silicates*, 2023, 42(6): 2121-2130.

- 
- [19] Du Tingting, Li Zhiqing, Zhou Yingxin. Research on cement phosphogypsum stabilizing materials used in pavement base. *Highway*, 2018, 63(2): 189-195.
- [20] Zhou Mingkai, Zhang Xiaoqiao, Chen Xiao. Study on the properties of cement phosphogypsum stabilized gravel pavement base material. *Highway*, 2016, 61(4): 186-190.
- [21] Wu Shangfeng, Cao Penghui. Application and economic benefit analysis of cement phosphogypsum stabilized gravel materials in highways. *Low Carbon World*, 2021, 11(11): 114-116.
- [22] Xu Fang, Li Heng, Sun Tao. Microstructure and mechanical properties of perthionate gypsum slag cement pavement base material. *Journal of Building Materials*, 2022, 25(3): 228-234.
- [23] Li Xia. Research on the properties and application of cement-stabilized phosphogypsum base material. Chengdu: Chongqing Jiaotong University, 2023.
- [24] Yu Changyun. Feasibility study on phosphogypsum modified cement-lime stabilized red mud road base material. Nanjing: Southeast University, 2022.

# PROGRESS IN THE INVESTIGATION OF MARINE DEEPWATER DRILLING FLUID SYSTEMS

S.Z. Lim

*Faculty of Science, Universiti Putra Malaysia, 43400 UPM Serdang, Selangor, Malaysia.*

**Abstract:** With the development of the petroleum industry, offshore oil and gas resources have become a key area of petroleum development. As one of the key technologies in current deepwater oil and gas exploration and development, deepwater drilling technology is related to the success or failure of drilling operations. The technical problems of marine deepwater drilling are analyzed: well wall stability, drilling fluid rheology adjustment at low temperature, natural gas hydrate generation and formation decomposition, wellbore cleaning, etc., and the research progress of marine deepwater drilling fluid systems is reviewed, including water-based drilling fluids. system, oil-based drilling fluid system, synthetic-based drilling fluid system.

**Keywords:** Deepwater drilling; Deepwater drilling fluid; Well wall stability; Constant rheology

## 1 TECHNICAL DIFFICULTIES FACED BY OFFSHORE DEEPWATER DRILLING

In recent years, the exploitation of land and offshore oil and gas resources in various countries around the world has been close to saturation. The development of oil and gas resources has gradually turned to the ocean, especially the exploitation of deep-sea oil and gas resources, which has gradually become the top priority in the current field of petroleum development [1]. my country's marine oil and gas resources are abundant. Petroleum geological resources account for approximately 19.01% of the country's oil and gas resource reserves, and natural gas geological resources account for approximately 23.14%, most of which are contained in deep water. The development of deepwater oil and gas resources requires high drilling technology, and the current deepwater drilling fluid system still has many problems that need to be improved. In view of this, the author provides a reference for the study of deepwater drilling fluid systems on the basis of analyzing the technical problems of ocean deepwater drilling.

Ocean deepwater drilling is different from shallow water drilling. There are more technical issues that need to be considered during the drilling process, including poor stability of loose wellbore walls in seafloor mud shale, rheology adjustment of drilling fluids at low temperatures, and natural gas hydrate generation that blocks pipes and wellbores. The cleaning rock carrying strength is not enough [2-6]. These problems often affect the normal development of on-site operations, and also put forward higher requirements for drilling technology. Therefore, an overview of the progress in developing efficient and rapid drilling technology is intended to improve the performance of offshore deepwater drilling fluid systems and high-performance The marine deepwater drilling fluid system is one of the important issues that need to be solved urgently in current marine deepwater drilling.

### 1.1 Well Wall Stability Issues

In the oceanic deepwater drilling area [7], due to the complexity of the formation, the difference in rock deposition speed and water content, some rock layers are replaced by seawater, making the rocks in this formation extremely active. However, oceanic deepwater drilling areas are often far away from the coast, and seawater The sediment carried is not enough to compact the ground layer, so the cementation properties of the rock layer are poor, and it is easy to disperse and expand. A large number of solid particles combine with the drilling fluid, thus seriously affecting the performance of the drilling fluid.

During actual drilling operations, in China, appropriate amounts of inorganic salts, polymeric alcohols with cloud points, and polyamine inhibitors are generally added to inhibit the hydration and dispersion of shale; while abroad, synthetic-based drilling fluids are used to enhance the stability of seafloor rocks. In deepwater drilling areas, there is often a thick siliceous soft mud layer in the shallow part of the seabed. The water content is generally above 50%. Its shear strength is low and its bearing capacity is poor. The formation fracture pressure is similar to the pore pressure, which will lead to the density window of the drilling fluid. Therefore, it is necessary to rationally use and develop efficient lost circulation materials to solve the problem of lost circulation in deep sea drilling.

### 1.2 Drilling Fluid Rheology Adjustment Issues at Low Temperatures

The temperature of the seafloor gradually decreases with the increase of depth. The temperature of the mud-liquid line on the deep seabed is generally about 4°C. The low temperature causes the rheology of the drilling fluid [8-9] to go out of control, which brings hidden dangers to on-site drilling operations. Experiments have shown that in the range of 4 ~ 65 °C, the rheology of water-based drilling fluid is difficult to accurately control, especially under low temperature (below 4 °C) conditions. In a low-temperature environment, the viscosity and shear force of water-based drilling fluids will increase significantly, and the thickening effect of oil-based mud will be even more obvious, resulting in excessive

equivalent circulation density and increasing the risk of lost circulation; at the same time, at low temperatures Under high-pressure environments, the probability of natural gas hydrate formation increases, leading to pipeline blockage and safety accidents.

In response to the above problems, the problem of rheology adjustment of drilling fluid at low temperature is generally solved by using a constant rheology drilling fluid system. At the same time, the equivalent circulation density should be detected to avoid the occurrence of underground safety accidents.

### 1.3 Issues of Natural Gas Hydrate Generation and Formation Decomposition

As deep-sea drilling depth advances, the seafloor temperature drops below 0°C and the static pressure reaches over 30MPa, providing good conditions for the generation of natural gas hydrates [10]. On the one hand, when the dissolved natural gas hydrate near the wellhead re-condensates in pipelines such as risers and kill pipes due to the cooling effect, it will block the pipelines, hinder normal downhole pressure monitoring, and even cause serious downhole accidents. In order to control the formation of natural gas hydrates, natural gas hydrate thermodynamic inhibitors (such as NaCl, KCl, etc.) are generally used at work sites to inhibit the formation of natural gas hydrates. On the other hand, during drilling operations, when the drill encounters a gas hydrate formation, the temperature and pressure changes caused by the agitation of the drilling tool and the invasion of drilling fluid cause a large amount of natural gas hydrate to decompose, and a large amount of gas and water to be analyzed, increasing the The pore pressure between the formations is reduced, which reduces the strength of the formation, easily causes the instability of the well wall, and increases the risk of well collapse. Therefore, it is extremely important to develop and optimize a high-performance marine deepwater anti-collapse drilling fluid system.

### 1.4 Wellbore Cleaning Issues

During deep sea drilling, due to the large diameter of the riser pipe, the annulus area is large, making it difficult for the mud to maintain a high flow rate when returning, and cannot achieve the purpose of cleaning the wellbore, especially when the well deviation is large. obvious. In order to increase the drilling fluid displacement and improve the cuttings carrying capacity of the mud, the drilling fluid is generally required to have a high viscosity while maintaining a low shear rate. This requires optimizing the rheological parameters of the drilling fluid. For water-based Drilling fluids can be added with polymer flow pattern regulators to effectively improve the mud's rock-carrying capacity. Compared with water-based drilling fluids, oil-based/synthetic-based drilling fluids have better rock-carrying and wellbore cleaning capabilities. However, deep-sea drilling fluids generally require larger quantities and higher costs. Once leakage occurs downhole, the drilling fluid will be damaged. Handling and accident handling are even more disadvantageous.

## 2 CURRENT STATUS OF RESEARCH ON MARINE DEEPWATER DRILLING FLUID SYSTEMS

### 2.1 Deepwater Water-Based Drilling Fluid System

Compared with oil-based/synthetic-based drilling fluid systems, water-based drilling fluid systems are environmentally friendly and low-cost, and are widely used in deepwater drilling. Currently commonly used deepwater water-based drilling fluid systems include: high-salt/PHPA polymer drilling fluid system, CaCl<sub>2</sub>/polymer drilling fluid system, silicate drilling fluid system, and high-performance water-based drilling fluid system. High-performance water-based drilling fluid systems are generally composed of polyamine strong inhibitors, coating agents, plugging agents, fluid loss agents, environmentally friendly lubricants and other treatment agents. Their performance is similar to that of synthetic-based drilling fluid systems. Through multiple The combination of the two treatment agents has the characteristics of strong inhibition, superior lubrication performance, increased drilling speed, and stable well wall.

ULTRADRILL drilling fluid system [11-12] is a high-performance deepwater water-based drilling fluid system launched by the foreign company M-ISWACO. It was first put into use in China's Bohai Oilfield in 2004. The system is mainly composed of the strong inhibitor Ultrahib, the coating agent Ultracap, the lubricant Ultrafree, the speed-increasing agent Ultrafree, etc. It has strong inhibitory effect, superior lubrication performance, can effectively solve the problem of mud ball coating, is easy to maintain, and is environmentally friendly. Friendly and other characteristics, it has good on-site application effects for high-activity mud shale and complex drilling environment strata.

The Hydro-Guard drilling fluid system [13] is a high-performance water-based drilling fluid launched by the foreign company Halliburton Baroid that has properties close to those of oil-based drilling fluids. The system is mainly composed of polyamine inhibitor BORE-HIB, coating agent EZ-MUD DP, blocking agent BARO-TROLPLUS, etc. It does not contain soil phase, can effectively inhibit the hydration and dispersion of shale, and can withstand high temperatures of 150°C., and the mud is easy to discharge, making it suitable for environmentally sensitive areas. The Hydro-Guard drilling fluid system has been successfully used in deepwater wells in Brazil and Angola.

The HEM drilling fluid system [14-15] is a high-performance deepwater water-based drilling fluid system developed by CNOOC Oilfield Chemical Division. The inhibitor is PF-UHIB, the coating agent is PF-UCAP, and the lubricant is PF-HLUB, supplemented by flow pattern regulator, fluid loss agent, NaCl and other materials, is suitable for complex formations and formations with high environmental performance requirements. The formula of this system is: seawater+Na<sub>2</sub> CO<sub>3</sub>+PF-FLO+XCH+PF-UHIB+ PF-HLUB+KCl+PF-UCAP+NaCl+barite. In 2011, the HEM drilling fluid system was successfully applied to 15 wells in the South China Sea, with the deepest operating depth of 1,300 m,

the deepest well depth of 4,239 m, and the lowest mudline temperature of 3°C. It effectively solved the problem of difficult to control the rheology of water-based drilling fluids at low temperatures. Problems such as narrow density window and downhole leakage.

Zhao Xin et al. [16] aimed at problems such as the difficulty in adjusting the rheology of deepwater drilling fluids at low temperatures and the formation of natural gas hydrates. They synthesized a strong polyamine inhibitor SDJA through the polymerization of polyetherdiamine and ethylene oxide, and constructed it by optimizing treatment agents. A set of high-performance polyamine deepwater water-based drilling fluid system was developed. The formula of this system is: 3% seawater bentonite slurry+0.15%XC+3%SDJA+ 0.1%KPAM+4%SD-101+1%JLS-1+1%SD-505+1.5%FT-1+20% NaCl. Indoor experiments have shown that this system has good rheology at 2°C and 25°C, can withstand high temperatures of 150°C, and can basically meet the requirements of drilling operations at a depth of 1500m. It has good suppression performance, superior environmental protection performance, and good anti-pollution ability.

Gao Han et al. [17] analyzed the effects of temperature and pressure within a specific range on the rheology of drilling fluid, and combined with the rheological model, initially proposed the rheological mechanism of constant rheology water-based drilling fluid and the "structural compensation-performance" based on molecular morphology. "Controlled release" structure-activity relationship, and introduced the T/P factor into Casson's initial equation, established a dynamic rheology equation suitable for constant rheology water-based drilling fluids, and revealed the constant rheology nature of water-based drilling fluids.

Geng Tie et al. [18] used acrylamide, alkyl quaternary ammonium salts and 2-acrylamido-2-methylpropanesulfonic acid as monomers and used aqueous solution polymerization to synthesize low molecular weight polymer coatings for deepwater drilling. agent, and on this basis, a set of water-based drilling fluid system with high temperature resistance and strong inhibition was constructed by optimizing other treatment agents. The formula of the system is: 5% seawater bentonite slurry + 0.2% Na<sub>2</sub> CO<sub>3</sub> + 0.2% NaOH + 1.0% flow pattern regulator FLOTROL + 1.0% high temperature fluid loss agent HTFL + 0.5% new coating inhibitor Cap+ 3.0% blocking agent FT-1+1.0% polyamine inhibitor+2.0% high temperature stabilizer STBHT+3.0% lubricant+5.0%NaCl+10.0% potassium formate+barite. This system has good suppression performance, good rheological properties at low temperatures, and can withstand high temperatures of 160°C. It has been successfully used in four wells in a deepwater oil field in the South China Sea. The construction was smooth, the wellbore was more stable, the drilling cycle was short, and no downhole complications occurred.

## 2.2 Deepwater Oil-Based Drilling Fluid System

Compared with water-based drilling fluids, oil-based drilling fluids [19] have better temperature resistance and rheological controllability, and can still maintain good drilling fluid performance under a narrow density window. Different from land drilling, offshore deepwater drilling areas are generally environmentally sensitive areas, requiring oil-based drilling fluids with low toxicity and environmental protection. Therefore, offshore deepwater oil-based drilling fluids generally use base oils with low aromatic content (such as white oil, gas to oil) to minimize the impact of the drilling fluid system on marine life.

Since oil-based drilling fluids tend to become viscous and even gel at lower temperatures, how to maintain good rheological properties of deepwater drilling fluids in the special low-temperature environment of the deep seabed is an important step in ensuring the success of deepwater drilling operations.. Patel et al. first proposed the concept of "constant rheology" as an indicator to test the performance of deepwater drilling fluids. "Constant rheology" means that the AV and PV values of deepwater drilling fluid are relatively stable in the range from low temperature to high temperature. In 2015, Knox et al. [20] of the British BP company gave detailed technical indicators for the ocean deep water constant rheology system: PV (4.4 °C) <2.5PV (49 °C), Gel (10 min) <1.7Gel (10s ), Gel (30min) <1.3Gel (10 min), YP (4.4 °C) < 1.2YP (49 °C). Compared with traditional oil-based drilling fluid systems, deepwater oil-based drilling fluid systems [21] mainly control the rheological properties of the drilling fluid system by adjusting the amount of organic soil and using flow pattern regulators. Since oil-based drilling fluid systems cause great damage to the marine environment and are costly, and there is a large gap between domestic deep-water oil-based drilling fluid systems compared to foreign countries, deep-water oil-based drilling fluid systems are rarely used in China. With the gradual development of easily recoverable oil reserves on land and the increase in offshore deepwater drilling depth, the development of offshore deepwater oil-based drilling fluid systems has become an inevitable trend in the exploration of oil and gas resources.

Xing Xijin et al. [22] constructed a deepwater constant-rheology oil-based drilling fluid system through indoor optimization of several base oils and treatment agents. This system mainly achieves the constant rheology characteristics of oil-based drilling fluid through the use of an amide thermosensitive polymer and organic soil. The formula is: refined white oil + 4.0% emulsifier + 2.0% wetting agent + 3.0 % calcium chloride aqueous solution + 0.5% calcium oxide + 2.0% cutting agent + 2.0% tackifier + 3.0% fluid loss agent + 1.5% organic soil + barite. Indoor rheological tests show that the rheological values of this system do not change much in the range of 4~65°C.

Hu Sanqing et al. [23] used white oil as the base oil and added an appropriate amount of treatment agent to construct a low-toxic oil-based drilling fluid system suitable for deep water. The formula of this system is: base oil (white oil: CaCl<sub>2</sub> aqueous solution = 70:30) + 3.0% main emulsifier + 0.5% auxiliary emulsifier + 1.5% wetting agent + 1.5% organic soil + 3.0% fluid loss agent + 1.0 % alkalinity regulator + aggravating agent. This system can still maintain

good rheological properties at 5°C, and has strong salt resistance, high temperature resistance, and strong reservoir protection capabilities.

### 2.3 Deepwater Synthetic-Based Drilling Fluid System

The synthetic-based drilling fluid system is an inverse emulsification drilling fluid system composed of artificially synthesized organic matter as the continuous phase, brine as the dispersed phase, and adding treatment agents such as emulsifiers and fluid loss agents. The synthetic-based deepwater constant rheology drilling fluid system is obtained by adding a polymer flow pattern regulator to the original synthetic-based drilling fluid and then combining it with organic soil. Its viscosity and shear force fluctuate less within a certain temperature range. The synthetic-based drilling fluid system is similar to the oil-based drilling fluid system in terms of inhibition performance. It has strong high-temperature resistance, is environmentally friendly, and is easy to discharge. It is especially suitable for use in marine deepwater and ultra-deep water wells. It is a relatively mature deepwater drilling fluid in recent years.

Rheliant drilling fluid system [24-25] is a constant-rheology synthetic-based drilling fluid system in a wide temperature range launched by Schlumberger MISWACO. The system is mainly composed of the main emulsifier SUREMUL, the auxiliary emulsifier SUREWET, the flow pattern regulator Rheflat, etc. It has excellent rock-carrying ability, strong wellbore cleaning ability, and can effectively solve the problem of downhole leakage.

Accolade drilling fluid system [26] is an environmentally friendly synthetic-based drilling fluid system launched by Halliburton Baroid Company. The base fluid is a mixture of esters and internal olefins, which can be completely degraded in the ocean. It has good rheological properties and is equivalent to The circulation density is low, the wellbore cleaning ability is strong, and it can effectively perform deepwater drilling operations. When operating in deep water areas in Mexico, the application effect was good and there were basically no underground accidents.

Yue Qiansheng et al. [27] found that emulsifier type, oil-water ratio, organic soil addition, etc. are the main factors affecting the low-temperature rheology of gas-to-oil synthetic-based drilling fluid systems.

Luo Jiansheng and others constructed a deepwater FLAT-PRO synthetic-based drilling fluid system using low-viscosity gas-to-liquids as the base fluid. The formula is: gas-to-liquids + 0.8% primary emulsifier PF-FSEMUL + 1.0% auxiliary emulsifier PF-FSCOAT+1.0% wetting agent PF-FSWET+25%CaCl<sub>2</sub> solution+2.5% organic soil PF-FSGEL+0.5% flow pattern regulator PF-FSVIS+3.0%CaO+2.5% fluid loss agent PF-FSHFR+barite. Indoor tests show that this system has basically unchanged dynamic shear force, static shear force and  $\Phi_6$  value in the range of 4~65°C, has good rheological properties, and the emulsion has good stability and is not prone to settling. It has good application results in an oil field in the western South China Sea. It has strong rock-carrying ability and small ECD value, which meets the needs of downhole operations in low-density windows.

Zhao Jingfang et al. [28] developed an environmentally friendly synthetic base fluid BIO-OIL. The basic physical and chemical properties, viscosity-temperature characteristics, carbon number distribution, biological toxicity, and emulsion microrheology of this base fluid and conventional base fluids were studied indoors. etc., and constructed a set of deep water synthetic base drilling fluid with this base fluid. Indoor tests show that this system basically meets the needs of on-site drilling and has good biodegradability. When applied in three wells in the western South China Sea, the wellbore was stable, the rheological properties were good, the rock carrying capacity was strong, and no downhole complications occurred.

Hu Wenjun et al. [29] used Saraline185V gas-to-liquid as the base oil, and constructed a set of FLAT-PRO deep water constant rheology synthetic base drilling fluid suitable for deep water drilling by optimizing emulsifiers, organic soils, fluid loss agents and other treatment agents. system, its formula is: Saraline185V + (0.8% ~ 1.0%) FSEMUL + (1.0% ~ 1.2%) FSCOAT + 1.2% FSWET + 2% organic soil FSGEL + 25% CaCl<sub>2</sub> + 2.5% PF-MOALK + 2% PF-HFR+0.1%FSVIS+barite, oil to water ratio is (70:30) ~ (85:15). Indoor tests show that this system has good rheological properties in the range of 4~65°C, meets constant rheological characteristics, has strong rock-carrying ability, is easy to discharge, and has strong reservoir protection capabilities. The application effect is good in the LS-A ultra-deep water well in the South China Sea. The ECD value is small, the well hole is regular, tripping is smooth, and the drilling cycle is short.

## 3 CONCLUSION

Marine deepwater drilling faces technical requirements such as drilling fluid rheology adjustment, well wall stability, wellbore cleaning, and natural gas hydrate generation at low temperatures, which puts forward higher requirements for the performance of deepwater drilling fluid systems. Deepwater water-based drilling fluids should focus on the development and research of core treatment agents, focusing on the development of modification additives based on natural polymer materials and agricultural and sideline products. It should ensure that the drilling fluid system has both good performance and superior Environmentally friendly performance. Deepwater oil-based/synthetic-based drilling fluids should pay attention to the screening of base fluids, try to select low-toxic, non-toxic, and environmentally friendly base fluids, and pay attention to the development of major additives such as emulsifiers and flow regulators to enhance the resistance of treatment agents. Research on temperature and salt resistance and performance of deepwater and ultra-deepwater well drilling fluids.

## COMPETING INTERESTS

The authors have no relevant financial or non-financial interests to disclose.

## REFERENCES

- [1] Wang Song, Song Mingquan, Liu Erping. Progress in foreign deepwater drilling fluid technology. *Petroleum Drilling Technology*, 2009, 37(3): 8-12.
- [2] Hu Youlin, Zhang Yan, Wu Bin. Research progress on drilling fluids for ocean deepwater drilling. *Drilling and Completion Fluids*, 2004, 21(6): 50-52.
- [3] Zhang Zhen. Research on key technologies of marine deepwater drilling and completion fluids. *Petrochemical Technology*, 2016, 23 (5): 155.
- [4] Chen Bo. Research on key technologies of offshore deepwater drilling and completion fluids. *China Petroleum and Chemical Industry Standards and Quality*, 2019, 39(2): 198-199.
- [5] Bao Haiwen. Research on marine deepwater drilling fluid technology. *China Petroleum and Chemical Industry Standards and Quality*, 2013, 33(18): 128.
- [6] He Song, Xing Xijin. Brief analysis of marine deepwater drilling fluid system. *Inner Mongolia Petrochemical Industry*, 2017, 43(6): 63-64.
- [7] Zhang Yongjun. Research on Optimization of Marine Deepwater Collapse-proof Drilling Fluids. Qingdao: China University of Petroleum (East China), 2016.
- [8] Li Zhaochuan. Construction and performance evaluation of ocean deepwater constant rheology water-based drilling fluid system. Qingdao: China University of Petroleum (East China), 2016.
- [9] Huo Baoyu, Yan Zhiyi, Zhang Xiaowei. Low-temperature rheology experiments and formula optimization of marine deepwater water-based drilling fluids. *Journal of Northeast Petroleum University*, 2013, 37(6): 94-100.
- [10] Luo Jiansheng, Li Zili, Luo Man. The development status of deepwater drilling fluids at home and abroad. *Drilling and Completion Fluids*, 2018, 35(3): 1-7.
- [11] Huang Haoqing. Safe and environmentally friendly new water-based drilling fluid ULTRADRILL. *Drilling and Completion Fluids*, 2004, 21(6): 4-7.
- [12] Kong Qingming, Chang Feng, Sun Chengchun. Application of ULTRADRILLTM water-based drilling fluid in Zhanghai 502FH well. *Drilling and Completion Fluids*, 2006, 23(6): 71-74.
- [13] WATSON P, KOLSTAD E, BORSTMAYER R. An innovative approach to development drilling in deepwater gulf of Mexico. SPE-79809-MS, 2003.
- [14] Luo Jiansheng, Li Zili, Liu Gang. Application practice of HEM polyamine deepwater drilling fluid in the South China Sea. *Petroleum Drilling and Production Technology*, 2015, 37(1): 119-120.
- [15] Luo Jiansheng, Li Zili, Li Huaike. Research and application of HEM deepwater polyamine drilling fluid system. *Drilling and Completion Fluids*, 2014, 31(1): 20-23, 96.
- [16] Zhao Xin, Qiu Zhengsong, Shi Bingzhong. Experimental study on deep water polyamine high-performance drilling fluid. *Petroleum Drilling Technology*, 2013, 41(3): 35-39.
- [17] Gao Han, Xu Lin, Xu Mingbiao. Research on the rheological properties of deepwater water-based constant rheology drilling fluid. *Drilling and Completion Fluids*, 2018, 35(3): 60-67.
- [18] Geng Tie, Qiu Zhengsong, Tang Zhichuan. Development and application of water-based drilling fluid with high temperature resistance and strong suppression for deepwater drilling. *Petroleum Drilling Technology*, 2019, 47(3): 82-88.
- [19] Guo Xiaoxuan. Research on marine deepwater oil-based drilling fluid. Daqing: Northeast Petroleum University, 2015.
- [20] KNOX D, BULGACHEV R, CAMERON L. Defining fragile the challenge of engineering drilling fluids for narrow ECD windows. SPE-173059-MS, 2015.
- [21] Qiu Zhengsong, Liu Kouqi, Cao Jie. Experimental study on low-temperature rheological properties of oil-based drilling fluid. *Drilling and Completion Fluids*, 2014, 31(3): 32-34.
- [22] Xing Xijin, Qiu Zhengsong, Liu Shujie. Indoor study on advection oil-based drilling fluid system for deep water drilling. *Journal of Chongqing University of Science and Technology (Natural Science Edition)*, 2016, 18(4): 8-11.
- [23] Hu Sanqing, Yu Jiaomei, Hu Zhipeng. Indoor research on low-toxic deepwater oil-based drilling fluid. *Chemical and Biological Engineering*, 2008, 25(11): 48-50.
- [24] Van OORT E, LEE J, FRIEDHEIM J. New flatrheology synthetic-based mud for improved deep water drilling. SPE- 90987-MS, 2004.
- [25] YOUNGS, FRIEDHEIMJE, LEEJ. A new generation of flatrheology invert drilling fluids. SPE-154682-MS, 2012.
- [26] BURROWSK, EVANSJ, HALLJ. New low viscosity ester is suitable for drilling fluids in deep water applications. SPE-66553-MS, 2001.
- [27] Yue Qiansheng, Liu Shujie, He Baosheng. Research on the performance of new mineral oil-based drilling fluids based on deepwater drilling. *Journal of Petroleum and Natural Gas*, 2011, 33(8): 114-118.
- [28] Zhao Jingfang, Liu Xuejing, Geng Tie. Development and field test of BIO-OIL environmentally friendly base fluid. *Petroleum Drilling Technology*, 2019, 47(3): 75-81.
- [29] Hu Wenjun, Xiang Xiong, Yang Honglie. FLAT-PRO deepwater constant rheology synthetic-based drilling fluid and its application. *Drilling and Completion Fluids*, 2017, 34(2): 15-20.

# ADVANCED OPTICAL DIAGNOSTIC TECHNOLOGY APPLICATION PROGRESS IN COMBUSTION TESTING OF ENERGETIC MATERIALS

Steven Bhattacharya

*Department of Electrical and Computer Engineering, University of Missouri, Columbia, MO, USA.*

**Abstract:** Based on different optical principles, laser-induced fluorescence (LIF), coherent anti-Stokes Raman scattering (CARS), particle imaging velocimetry (PIV), and tunable are reviewed from three aspects: light scattering, optical emission and absorption, and imaging. Testing principles of optical diagnostic technologies such as semiconductor laser absorption spectroscopy (TDLAS), laser-induced breakdown spectroscopy (LIBS), radiation method, remote sensing Fourier transform infrared spectroscopy (RS-FTIR) and schlieren method, and their use in combustion tests of energetic materials The application progress of optical diagnostic technology in combustion testing is analyzed. The superiority of optical diagnostic technology compared with other traditional contact diagnostic methods and the applicability, measurement objects, advantages and disadvantages of various optical diagnostic methods are analyzed; the microscopic combustion products, flame temperature, The development prospects of testing technologies such as combustion flow field velocity and flame structure in combustion diagnosis of energetic materials; it is pointed out that future work should combine multi-diagnostic methods and develop multi-dimensional measurements to obtain richer and multi-dimensional microscopic data information.

**Keywords:** Physical chemistry; Combustion of energetic materials; Optical diagnostic technology; Laser-induced fluorescence; Laser absorption spectroscopy; Schlieren method

## 1 INTRODUCTION

The control and regulation of the combustion properties of energetic materials are of great significance for efficient energy release and meeting the application needs of different weapons and equipment. Different from the combustion of other fuels, the combustion of energetic materials is generally more complex. During combustion, it can produce high temperature and high pressure, and undergo a series of complex physical and chemical changes from solid phase to liquid phase or gas phase. The combustion environment is usually accompanied by high pressure, vibration and other external factors. Solid propellant produces soot particles during the combustion process, and the burning surface of metal-containing propellant is accompanied by agglomeration of metal particles and other phenomena. Different from conventional gas or liquid fuels, energetic materials themselves contain oxidants and combustibles, and can independently carry out redox reactions under certain external stimuli. They can burn under anaerobic conditions and release a large amount of gas and heat. Regarding the combustion behavior of energetic materials, although researchers have established many relevant combustion models, there is still a lack of clearer understanding of the combustion of energetic materials with different formulas and the flame structure and reaction mechanism of combustion in the combustion chamber of high-pressure rocket engines. The development of theoretical simulations lacks the new full range of information provided by experiments. In order to obtain the essential laws of the combustion process, understand the detailed dynamics of the combustion reaction and the changing characteristics of the combustion flow field, reveal the combustion mechanism of energetic materials from a microscopic perspective and adjust the combustion efficiency, obtaining combustion information needs to be microscopic, systematic, and real-time online.

With the continuous development of combustion diagnostic technology, traditional contact experimental diagnostic methods, such as thermocouple temperature probes, gas sampling probes, etc., will inevitably cause disturbances to the combustion flow field. The complex combustion test environment of energetic materials also limits The accuracy and application range of the probe have been reduced, and it has gradually become difficult to meet the needs for more effective fast online real-time measurement. Non-contact optical diagnosis methods, because they only require the detection of flame emission or absorption characteristic spectral information, reduce or avoid aerodynamic, thermal or chemical disturbances, can withstand high temperatures and harsh environments, and have higher spatial and temporal resolution.

This article distinguishes based on the principles of optical diagnosis. From the three aspects of light scattering, optical emission and absorption, and imaging, the laser-induced fluorescence (LIF) and coherent anti-Stokes Raman scattering methods in recent years are distinguished. (CARS), laser absorption spectroscopy (LAS), laser-induced breakdown spectroscopy (LIBS), radiation method, remote sensing Fourier transform infrared spectroscopy (FTIR), particle imaging velocimetry (PIV) and schlieren method in energy-containing The applications in materials and engine combustion diagnosis are reviewed, and the advantages and disadvantages of specific methods in realizing real-time detection of information such as combustion flame temperature, flame structure, product component concentration, and combustion flow field velocity under different environmental conditions are analyzed.

Prospects for future diagnostic technologies and needs in the field of energetic material combustion are proposed.

**Table 1** Common advanced optical diagnostic methods for energetic material combustion

principle	Classification	name	application
light scattering	First-order scattering Third-order nonlinear scattering	inelastic LIF, PLIF CARS	Detect group components such as NO, OH, CH, CN and metal atoms such as Fe and Al. Flow field temperature measurement detects CO and N <sub>2</sub> , H <sub>2</sub> Isomolecule and flow field temperature measurement
Optical emission and absorption	emission	radiation method RS-FTIR LIBS	Combustion flow field temperature measurement and flame structure Remotely measure flame temperature Qualitative and quantitative analysis of non-metals such as C and O and metallic elements such as Al and Ir
	absorb	LAS	CO, CO <sub>2</sub> and other molecular concentrations and temperature measurement
light imaging		PIV schlieren	Combustion flow field velocity measurement (overall) Density gradient, combustion flow field changes

## 2 LIGHT SCATTERING MEASUREMENT

The energy is  $h\nu_0$ . When a multi-phase combustion flow field composed of molecules and particles is irradiated by a laser, light absorption is not considered, and the scattered light is classified according to the emission frequency, which can be divided into first-order elastic scattering processes such as Rayleigh scattering and Mie scattering, first-order inelastic scattering processes such as laser-induced fluorescence (LIF), and third-order nonlinear scattering processes such as coherent anti-Stokes Raman scattering (CARS). Light scattering method is essentially a spectroscopic method, which uses the analysis of spectral signals as the basis for diagnosis. The following is a review of LIF and CARS technologies that are widely used in the field of energetic materials and have great development prospects.

### 2.1 Laser-Induced Fluorescence (LIF)

Laser-Induced Fluorescence (LIF) is the use of a frequency-adjustable laser to generate laser light to irradiate atoms or groups, causing them to transition from a metastable state to an excited state. Since the excited state is not stable, it will spontaneously radiate energy to a lower energy level and return to the ground state., the energy generated during the process is released in the form of fluorescence, and the fluorescence signal is then detected and analyzed by the testing technology (see Figure 1). In principle, it is a first-order inelastic scattering process, and the fluorescence survival time is  $10^{-10} \sim 10^{-5}$  s. LIF technology can measure one-dimensional component concentration, temperature and other parameters of the combustion environment in real time, and has good spatial resolution, and can measure OH and NO, etc.  $10^{-6}$  amount of active ingredient. The LIFs of different components and quantum states are different and specific. There is a functional relationship between the concentration of the component and its fluorescence signal intensity. Using a laser with a specific frequency of a certain component for excitation, and collecting the signal of the corresponding frequency can complete the concentration of the target component. Therefore, PLIF technology is used in online diagnosis of combustion product concentration and flame structure [1-4]. It has a wide range of applications: analyzing the changes in combustion wave structure by measuring the concentration and spatial distribution of free radicals, thereby helping to understand the combustion mechanism of energetic materials. This technology has become an important experimental diagnostic tool for engine combustion and propellant combustion flames.

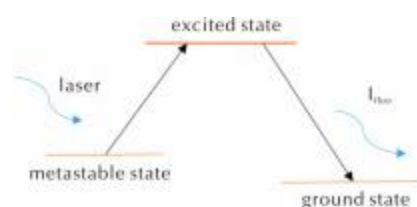


**Figure 1** Schematic diagram of the principle of laser-induced fluorescence

The application of LIF technology in the field of energetic material combustion was originally used by Edwards et al. to burn Octogen (HMX) and ammonium perchlorate/hydroxy-terminated polybutadiene (AP/HTPB) composite propellants at 3.5MPa. Experimental diagnosis. Later Parr et al[5] LIF was applied to other types of solid propellants, the LIF signals of several free radicals (such as CN, NH, NO, OH) were monitored, and the combustion characteristics of HMX/GAP/BTTN solid propellants were studied using OH-LIF and other technologies. The flame structure, combined with OH-LIF, UV/vis data and thermocouple measurements, more accurately corrects the burning surface temperature and flame zone temperature during solid propellant combustion. Before the LIF excitation light enters the combustion flow field, it is first formed into a sheet laser through the sheet light shaping system, which is developed into Planar Laser-Induced Fluorescence, (PLIF) technology, because PLIF technology can obtain two-dimensional information

parameters of the combustion environment, it is more widely used in energetic material combustion and flow field diagnosis research in engine combustion chambers.

Yan Zhiyu et al [6] Using OH-PLIF, NO chemiluminescence and high-speed photography methods, the self-luminescence process of RDX reaction and the OH inside the flame before and after focused ignition were studied. Two-dimensional concentration distribution of free radicals, RDX is briefly analyzed based on the results combustion mechanism. Ruesch et al. [7] used PLIF to study CN in hexanitrohexaazaisowurtzitane (CL-20) cocrystal and HMX/AP polycrystalline composite crystals. and OH concentration distribution and flame structure during the combustion process, and the obtained PLIF flame structure changes were used to explain the difference in combustion rates between HMX/AP physical mixtures and composite crystals. Kevin et al [8-9] This system was used to study the combustion process of gel propellant droplet jets. At a time resolution of 0.2ms, three different types of jets were observed. This two-dimensional visualization of the flame structure of gel jets based on PLIF enables Scholars have a more basic understanding of the combustion laws of gel fuel droplets.

The planar visualization technology provided by PLIF satisfies the diagnosis of flame structure at the two-dimensional level, but for the three-dimensional measurement of the complete structure of the flame in three-dimensional space, the development of new testing technology is still needed. Peterson et al. [10-11] used two sets of PLIF systems to study the flame propagation changes in the early stages of engine ignition through OH concentration distribution. The system realized the PLIF signal tomographic inversion of OH. three-dimensional spatial distribution. Yuan Xun et al. [12] designed and built a multi-plane 3DLIF system based on scanning galvanometers to meet the needs of supersonic flame combustion diagnosis and the limitations of high-frequency scanning technology, which can perform high-frequency scanning in the 20mm sheet light range and realize OH-3DLIF spatial visualization.

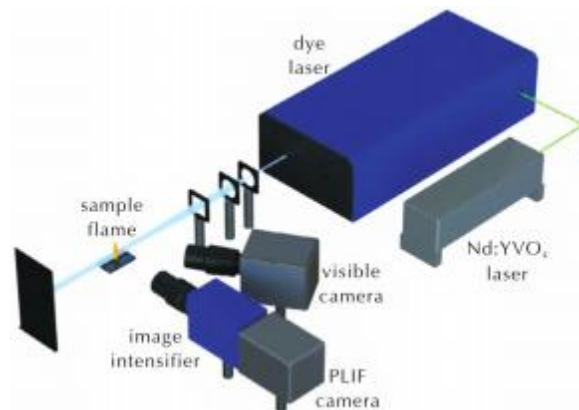


**Figure 2** Schematic diagram of PLIF test system [7]

In addition to the determination of combustion product concentration distribution and flame structure, LIF The technology is also widely used in combustion flow field temperature measurement. Currently, the most commonly used method for LIF temperature measurement is the double-line method. During temperature measurement, two laser beams of different wavelengths need to be used to excite two different rotational energies of a certain group at the same vibration energy level at the same time or within a very short time. level transition line, and then calculate the flame temperature through the ratio of the obtained fluorescence signal intensity at the two wavelengths. The test system is shown in Figure 3. This method can avoid the influence of free radical concentration and fluorescence quenching effect to a certain extent. Since OH contains abundant excitation spectral lines in the combustion reaction zone and high temperature zone, OH is often used as the laser action medium for temperature field measurement. Due to the strong dependence of OH concentration on temperature, OH-LIF temperature measurement is generally suitable for  $T > 1300\text{K}$  combustion environment [13].

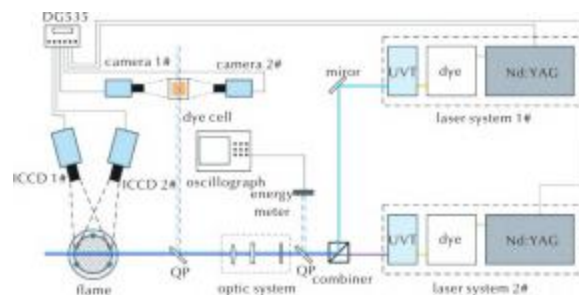


**Figure 3** Two-wire PLIF temperature measurement system

Foreign research on LIF dual-line temperature measurement was earlier. In 1984, Soloukhin et al. from Sandia Laboratories in the United States [14] First use to describe the density of absorption states [15] The Boltzmann population function relates the ratio of fluorescence signals to temperature, and uses the ratio of the two fluorescence

image intensities to determine the temperature distribution of the flame. This has also become a classic solution for LIF temperature measurement since then. Lu Yongxu[16] used dual-line OH-PLIF technology to measure the two-dimensional temperature distribution of the combustion flame of propellant samples, and combined with the results of thermocouple calibration experiments, determined Q2 (11) and P1 (7) The two excitation spectral lines are the best spectral line selection for the dual-line PLIF technology to measure the alcohol lamp flame and the combustion flame temperature of a certain type of propellant, which provides ideas for the testing method of formulated propellants. There is also dual tracer temperature measurement, which uses two tracers and tests with two different excitation frequencies or with lasers with the same excitation frequency. This method follows the principle of dual-line temperature measurement and uses the fluorescence intensity ratio to measure temperature. Measurement calculations.

Because aluminum atoms have strong fluorescence characteristic signal intensity, it produces a good signal-to-noise ratio [17-20], improves the LIF sensitivity in solid propellant flames, and the development of aluminum-based LIF enables a more accurate optical test method for measuring the combustion temperature of aluminum-containing solid propellants. Gas-phase AIO plane laser-induced fluorescence technology has been applied to single particle aluminum combustion temperature and AIO concentration [21] Under measurement. Chevalier [22] carried out a combustion experiment of aluminum-containing solid propellant at a pressure of 1.0MPa, using high-speed Al-LIF to detect the generated aluminum vapor, and using a one-dimensional quasi-steady state model to simulate the concentration and temperature of aluminum atoms around the combustion of aluminum droplets. distributed. The comparison shows that the experimental data and simulation results are consistent, indicating that the Al-LIF method can provide verification data for building a more accurate aluminum combustion model. Vilmart[23-24] AILIF is used in high temperature applications (1200K and 2600K) and medium to low pressure (100Pa to 0. 1MPa) environment, a model of the relationship between Al-LIF spectrum and temperature was established, and the model was used to estimate that the LIF signal of Al can still be detected under high temperature and high pressure conditions (3000K and 10bar), which is Al The application of LIF-based in higher temperature environments provides theoretical support. For solid propellants containing aluminum, the combustion of aluminum particles increases the temperature and makes the flame highly luminous. The radiation background interference makes it difficult to accurately measure the combustion temperature by passive spectroscopy methods such as optical emission and absorption, which also reflects the advantages of the LIF method. Advantage. In addition, in the current study, iron-containing catalysts (ferrocene derivative-type catalysts) present in solid propellants can also be studied using LIF. Current experiments show that iron atoms have high fluorescence yield and high sensitivity, and the fluorescence signal can be easily detected. Vilmart et al. [25] conducted a Fe-PLIF-based study on AP/HTPB propellant combustion and established an iron atom LIF signal model, which further confirmed the real-time diagnostic capability of iron atoms in solid propellant combustion. In the future, microscale flow and phase changes on the solid propellant combustion surface, and the impact of additives on combustion performance (velocity, propellant surface behavior) are expected to be realized relying on metal atom PLIF technology and high-speed PLIF technology.

As an active non-contact optical diagnostic technology, PLIF has received more and more attention in solid propellant combustion diagnosis. Compared with other flow field diagnostic technologies such as schlieren technology mentioned later, PLIF has higher spatial resolution and more Low laser scattering effect on the flow field surface and high fluorescence yield of key combustion intermediates. The introduction of PLIF tracer molecules enables it to participate in the study of supersonic and hypersonic boundary layers. And the above-mentioned combustion intermediates almost have a common optical feature: their spectral transitions from the ground state to the first several excited states are in the ultraviolet wavelength range, which can be easily achieved using dye lasers or optical parametric oscillators (OPO). However, energetic materials still face some challenges: such as the difficulty of extracting LIF signals from strong laser scattering of condensed matter particles, high-pressure environments and continuous background emission, the attenuation of strong laser beams and the capture of fluorescence signals in dense media., and how to solve the pressure-dependent quenching of the LIF signal of free radicals to obtain quantitative information. Currently, PLIF technology has developed to 100KHz~1MHz, which can meet the temperature measurement requirements of medium Reynolds number subsonic turbulence with spatial and temporal resolution. However, it is still difficult to capture the detonation or transient combustion of hypersonic (1500m/s) flow that may occur in energetic materials.. Considering the instability of the flame, current combustion wave diagnosis requires increasingly higher time resolution, which also requires PLIF to develop towards higher frequency technology to meet the transient diagnosis of ultrasonic flow fields.

## 2.2 Coherent Anti-Stokes Raman Scattering (CARS)

Coherent Anti-Stokes Raman Scattering (Coherent AntiStokes Raman Spectroscopy (CARS) technology is a nonlinear four-wave mixing process. The pump light ( $\omega_1$ ) and the Stokes light ( $\omega_2$ ) are selected according to the measured molecular Raman shift ( $\omega_R$ ). The two laser beams are phase matched. Incident into the flame area, the detection light ( $\omega_3$ ) produces coherent light ( $\omega_4$ ), which is the CARS signal, after mixing. Since the frequency difference between the pump light and the Stokes light is exactly equal to the Raman shift of the selected medium, the CARS signal intensity is greatly enhanced (see Figure 4). Due to the coherence properties, the CARS signal has laser-like characteristics and is almost unaffected by fluorescence and background light to obtain high spatial and temporal resolution and high-precision measurement results. This nonlinear optical scattering method will not interfere with the flame or flow field, and has played an important role in obtaining parameter information such as combustion field temperature [26-28] and component concentration [29-30]. Zhang Lirong et al. [31] used a self-developed integrated CARS system to measure

the temperature of the exit jet of the supersonic combustion chamber, and obtained the single-pulse nitrogen CARS temperature fitting results and the temperature change model with time. The integrated CARS diagnostic system has good anti-vibration performance and can match on-site test conditions in a targeted manner, realizing the flexibility of CARS temperature measurement.

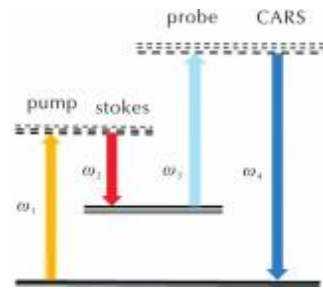


**Figure 4** Schematic diagram of the basic principles of CARS

CARS in energetic materials that do not contain metal components [32-33] Chinese applications are relatively mature, including RDX Decomposition[34], SGP-38 [35], nitramine [36-37] and hydrazine nitroformate [37] combustion under different pressure conditions.

Hu Zhiyun et al. [38] used single-pulse CARS technology to diagnose the transient temperature and nitrogen concentration of the solid propellant combustion field under normal pressure and high pressure, and combined the theoretical calculation and fitting values to give the transient temperature of the solid propellant combustion field (about 2250K). and the distribution of nitrogen concentration with flame height. The results show that the broadband CARS technology can be applied to real-time diagnosis of solid propellant combustion field temperature under normal pressure and high pressure.

Traditional CARS technology uses high-energy pulsed nanosecond lasers with a repetition rate of 10Hz. In recent years, with the development of optical technology, femtosecond (fs) CARS with a repetition rate of up to 5kHz has been widely used in laboratory burners. The high repetition rate provided by the fs-CARS system can directly measure the corresponding parameters in the high-speed transient combustion field without relying on conventional time-averaged statistical analysis. The use of detection pulses with a duration of picoseconds (ps) to detect Raman coherence constitutes a femtosecond/picosecond (fs/ps) hybrid CARS system. Using femtosecond/picosecond (fs/ps) purely rotating CARS system to measure combustion plume temperature and O<sub>2</sub>/N<sub>2</sub> of solid propellant containing aluminum particles under normal pressure The measurement was carried out, and Figure 5 is the schematic diagram of the CARS system used. The difference from propellants that do not contain metal components is that the combustion of metal-based propellants has strong background brightness and scattering of hot metal particles with a diameter of 102 μm, which constitutes an unfavorable environment for laser diagnosis. Traditional CARS or even nanosecond-level CARS pulse lasers are used in aluminum Particle combustion diagnosis is seriously affected by non-resonant background, and it has been confirmed that laser-induced breakdown plasma is generated in the process. The introduction of femtosecond/picosecond (fs/ps) laser pulses improves CARS detection by providing time gating to eliminate strong non-resonant background interference. The background-free spectrum obtained by delayed detection makes the temperature and relative oxygen content fitting values closer. This further proves the strong adaptability of the integrated fs/ps hybrid CARS system in detecting multi-phase environments and combustion of solid propellants containing large particles. fs/ Another obvious advantage of ps CARS is the non-collision nature of the measurement resulting from the ultra-short time scale of laser-matter interaction, within 300~ The measurement error within the 2400K temperature range is approximately ±8%. Improving the optical resolution of the detection system, extending the detection time, or taking other means can effectively enhance its low-temperature sensitivity.

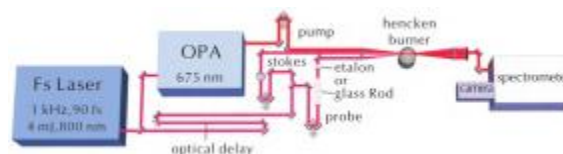


**Figure 5** fs/ps CARS temperature measurement system schematic diagram

To sum up, the current application of CARS technology in the field of energetic materials at home and abroad has developed from nanosecond CARS to fs/ps CARS. The reduction of laser pulses by several orders of magnitude allows it to overcome the traditional CARS technology, which is greatly affected by the collision effect. At the same time, high-frequency CARS provides more data in the same time, allowing CARS technology to accurately obtain rapidly changing combustion field information. For a series of problems such as the complex combustion environment and particle scattering of solid propellants containing metal materials, fs/ps CARS technology also provides suitable solutions. Compared with PLIF, a big drawback of CARS technology is that its single-point measurement requires simultaneous spatial and temporal alignment of multiple laser beams and spectral modeling, which may sometimes be difficult to achieve in the complex combustion environment of solid propellant applications, and is accompanied by low

spatial resolution. In addition, this technique is difficult to perform at high pressures due to the narrowing of the collision spectral lines.

### 3 OPTICAL EMISSION AND ABSORPTION

Optical emission and absorption are similar to the light scattering method and also belong to the category of spectroscopic analysis. It has the characteristics of non-contact, fast response, and can measure high temperature and component concentration. However, the disadvantage is that it can only measure thermal equilibrium and no self-absorption. The combustion zone is sometimes difficult to measure point by point, and the error is large. Optical emission and absorption include radiation, RS-FTIR and LIBS dominated emission spectra and LAS dominated absorption spectra.

#### 3.1 Radiation Method

The radiation temperature measurement method is a non-contact passive temperature measurement method. This method selects an appropriate detection period based on the radiation characteristics of the flame source itself to obtain the radiation information of the corresponding band of the field to be measured for temperature measurement. According to Planck's law, researchers have proposed flame temperature calculation methods such as radiation intensity method, single-wavelength method, dual-wavelength method, and multi-wavelength method. Since the emissivity of complex combustion flames is a function of wavelength, in order to eliminate the influence of changes in emissivity with wavelength and improve measurement accuracy, the dual-wavelength method and the multi-wavelength method are more suitable for application in energetic material combustion and solid rocket ramjet engine combustion flow field measurements. Mild.

Yang et al. used radiation spectroscopy to carry out online measurement of the combustion temperature of rocket solid propellant in the harsh environment of the engine and proposed its calibration method and spectral characteristics. Based on Planck's law and spectral fitting method, the corresponding solid propellant combustion was obtained temperature. In Rocketbasedcombined loop (Rocketbasedcombined cycle, RBCC) engine ground test, an online measurement system using a fiber spectrometer was used to obtain the relationship between the radiation spectrum from 200 to 1100nm and combustion efficiency. This method can effectively diagnose the quality of combustion through combustion temperature parameters and radiation rate parameters. That is, when the radiation rate in the 200~1100nm measurement band is close to 0 and relatively stable, it can be determined that the flame is in efficient and steady state combustion. In the combustion of composite solid propellant, a large number of solid metal particles burn and emit strong light, which causes great noise interference to laser diagnostic technology. However, there is still a radiation signal with a sufficient signal-to-noise ratio during the combustion process, so the radiation method can obtain Better temperature test results.

A dual-wavelength solid rocket motor plume temperature testing method based on flame radiation spectrum was proposed. A test system was built using a 350-1000nm band optical fiber spectrometer. The solid rocket motor plume radiation spectrum measurements of propellant formulas with different aluminum contents were carried out. Through The experimental data analyzed the effects of different aluminum content formulas on the radiation spectrum, plume temperature and emissivity, and provided experimental data support to guide the formula design of aluminum-containing solid propellants. The dual-wavelength method improves its time resolution and measurement accuracy by measuring the spectral radiation of two bands on the same optical path and using the ratio to eliminate interference from external factors such as optical path loss and vibration. However, this method requires that the wavelengths are close and The spectrum is single. In actual engineering measurements, it is difficult to achieve a single spectrum due to spectral diffusion, causing the dual-wavelength method to introduce errors. In order to avoid such problems, multi-wavelength temperature measurement methods that perform ratio processing at the same wavelength have been developed and applied. Pingli used the multi-wavelength radiation temperature measurement system shown in Figure 6 to study the radiation spectrum characteristics of aluminum particle combustion. A dual-machine simultaneous measurement method combining blue light backlight and radiation method was used to measure the combustion process of solid propellant aluminum particles, and analyzed the aluminum particles. The agglomeration process at the burning surface of solid propellants. In addition, three-dimensional temperature field reconstruction can also be performed through radiation temperature measurement and imaging methods. A dynamic combustion field three-dimensional radiation thermometry method based on multi-CCD synchronous coupling was used to measure the temperature of a certain model of fixed tail flame, and the three-dimensional temperature field of the tail flame was inverted. The error was within 8%, and the upper limit of temperature measurement could reach 2000~3000K. Dual-wavelength and multi-wavelength temperature measurement methods have shown good application prospects in real-time dynamic measurement of combustion temperatures of solid propellants, especially high-energy propellants in harsh combustion environments.

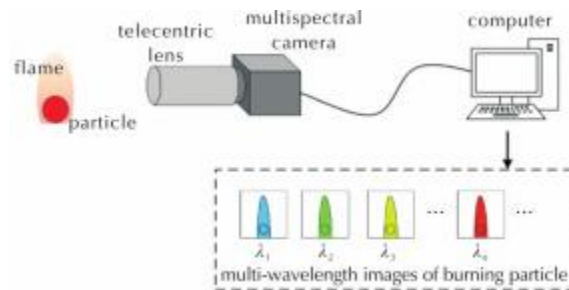


**Figure 6** Principle diagram of multi-wavelength radiation method temperature measurement

Compared with other non-contact active temperature measurement methods, the radiation method does not require emitting signals around the flame, making the measurement system relatively simple and easy to use. And because this method only obtains the flame temperature by measuring flame self-radiation, it provides direct heat transfer information and has good measurement stability in strong vibration environments. Even though the application of radiation method in energetic material combustion or engine combustion diagnosis is subject to measurement errors caused by smoke and combustion particles in the test environment, and the measurement accuracy is slightly lower, this method can simultaneously ensure spatiotemporal resolution and can still achieve high accuracy in extreme environments. It can achieve better results and is still one of the important methods for measuring the combustion temperature of aircraft tail flames and energetic materials.

### 3.2 Laser Absorption Spectroscopy (LAS)

Laser absorption spectroscopy is an absorption spectroscopy technology that uses laser as a light source. Absorption spectroscopy is a macroscopic manifestation of the material absorbing light and transitioning from a low energy level to a high energy level. Materials can be analyzed through the quantitative relationship between matter and light absorption described by molecular spectroscopy and Beer-Lambert's law. Microscopic components and concentration information. Because the laser is highly monochromatic and directional, it has good selectivity for the spectral lines of the measurement object, and because the laser is tunable, it also avoids the added structural complexity of optical devices such as gratings and prisms.

Different types of lasers are available for this diagnostic technique, the most widely used currently being Tunable Diode Laser Absorption Spectroscopy (TDLAS) using tunable diode lasers. TDLAS is a highly sensitive, non-contact combustion diagnosis method based on molecular absorption spectroscopy (the principle is shown in Figure 7). The controller changes the temperature and current to rapidly modulate the semiconductor laser, so that the laser reaches the absorption frequency domain of the target component, and realizes the absorption spectrum. Quickly scan and use Beer-Lambert's law to obtain the relevant parameters of the area to be measured by calculating the incident and projected light intensities.

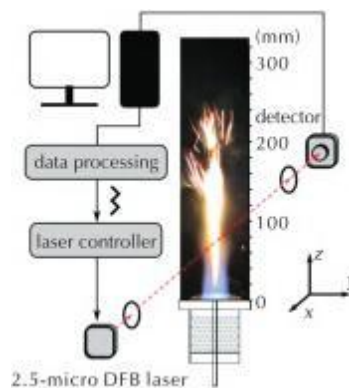


**Figure 7** Principle diagram of aluminum particle jet flame TDLAS diagnostic system

Since the wavelength range of the semiconductor laser covers H<sub>2</sub>O, CO<sub>2</sub>, O<sub>2</sub> The molecular absorption spectra of combustion products such as these are often used as probes to study the entire combustion process. Use 150 W Pulsed Arc Lamp vs. RDX The propellant was subjected to absorption spectrometry and the important combustion intermediate product CN was obtained. and NH component concentration. The absorption spectrum in the 307 ~ 311 nm region was used to measure the flame temperature and OH concentration of the double-base propellant under a high pressure of 69.1 atm. Although the flame temperature obtained at high pressure was in good agreement with the chemical equilibrium calculation, the measured OH concentration was lower than the calculated value. 40%, a difference the researchers attribute to the high sensitivity of OH concentration to local flame stoichiometry and temperature changes.

In recent years, TDLAS has been applied to high-pressure combustion flow field diagnosis in engines, which can provide detection of combustion process status, intermediate products, airflow velocity and other information for the combustion flow field of aviation, rocket and other engine combustion chambers. The TDLAS technology was used to measure the water vapor concentration and temperature at the combustion chamber outlet of the scramjet engine. The standard deviations between the measured values of temperature and water vapor concentration and the actual values were 4 respectively. 2% and 2.7%, which are generally similar to the CFD simulation results. The modulation parameters were used to calculate calibration constants, and the TDLAS second harmonic method was used to measure the transient supersonic flow field of the supersonic nozzle. The measured average temperature of the combustion chamber exceeded 1832K, with a standard deviation of 53K. After analysis, it was found that the source of the measurement error is the flame oscillation in the combustion process, and the system error is the deviation between the theoretical and actual values of the spectral line parameters.

In terms of propellant combustion, utilizing TDLAS Wavelength modulation spectroscopy technology measured the combustion flame zone temperature and CO concentration of AP/HTPB composite propellants containing aluminum particles of different particle sizes and without aluminum using mid-infrared wavelengths, while AIO emission spectroscopy technology was used to measure the temperature of the aluminum particle combustion zone. Experimental results show that on the basis of equal time, micron-sized aluminum particles burn in a diffusion-controlled state, while nano-aluminum particles burn in a kinetically controlled combustion state or close to a kinetically controlled combustion state. Subsequently, the gas temperature and HCl concentration in the flame during the combustion of metal-containing AP/HTPB composite propellant were studied. The results showed that the combustion temperature of aluminum-lithium propellant was 80~200K higher than that of aluminum propellant, and the combustion was more complete. It also confirmed the application of TDLAS technology. Effectiveness in measuring propellant combustion flame temperature and combustion product concentration. Research has found that combining TDLAS technology with the Doppler effect can measure the airflow velocity in a supersonic flow field. Select the absorption spectrum line of H<sub>2</sub>O at the center wavelength of 1391.7nm, and use TDLAS The direct absorption spectroscopy method was used to conduct static and dynamic measurements of the rocket skid solid propellant charge combustion plume velocity. The average flow velocity during the entire ignition process under static conditions was measured to be 1057.5m/s, and the average flow velocity under dynamic sliding conditions was 1249.8m/s, which confirmed the Applicability of TDLAS system in static and dynamic measurements of solid propellant charge combustion plume velocity.

In addition to TDLAS technology, the LAS-based method uses an ultrafast laser absorption spectroscopy (ULAS) diagnostic method to measure and characterize the combustion flame temperature and temperature of AP/HTPB and AP/HTPB/Al propellants under different pressures (1~40bar) at kHz. CO concentration. The results show that mid-infrared ULAS technology can provide high-fidelity, calibration-free temperature and gas concentration measurements with sub-nanosecond time resolution in a typical rocket engine high-pressure combustion environment.

For testing the flow field of aviation and rocket engine combustion chambers and the combustion flame of energetic materials, the optical absorption method has the same advantages as the light scattering method, which are non-contact and fast time response, and is suitable for measuring small molecules and free radicals in the combustion flame. and changes in the combustion flow field. However, for flames with large temperature gradients, optical measurement errors are often caused, and the resolution is lower than other optical methods; for macromolecules and their component concentrations, because it is difficult to measure point by point, the spectral peaks of macromolecules overlap at high temperatures. and other factors lead to inability to accurately measure. However, its advantage over technical methods such as CARS is that its cost is not high, and it can be flexibly applied to various combustion environments without complex operations. Based on the shared optical port, it can be combined with optical methods such as high-speed photography and radiation temperature measurement. achieve the purpose of measurement.

twenty three Remote sensing Fourier transform infrared spectroscopy (RS-FTIR)

Remote sensing Fourier transform infrared spectroscopy (RS-FT-IR) is a typical infrared emission spectrum testing method. Its principle is based on the Pin the fine structure of the rotating baseband established by Herget et al. or R-branch spectroscopy method of measuring the temperature of hot gases, based on absorption measurements along the atmospheric path between a radiation source and a spectrometer. Its advantage is that the path can be extended to tens of meters to several kilometers, and the temperature and product component concentration can be measured over long distances in dangerous combustion environments. RS-FTIR technology has been applied to the combustion temperature of energetic materials. Measurement.

A passive remote sensing Fourier transform infrared spectrometer was used to measure the combustion flame temperature of solid propellants mixed with nanoscale metal oxides, mixed with common metal oxides of the same material, and without adulterants. FTIR The instrument resolution is 1cm<sup>-1</sup>. The combustion flame temperature is calculated based on the baseband emission spectrum structure of the H<sub>2</sub>O molecule in the combustion product and the molecular vibration spectrum thermometry. The results show that doped with nanoscale CuO, Fe<sub>2</sub>O<sub>3</sub> and NiO particles The combustion flame temperatures of the solid propellant are 3089 and 3193 respectively. and 3183K. This temperature is not significantly different from the combustion flame temperature of ordinary metal oxides mixed with the same material and solid propellant without adulteration. The RS-FTIR technology was used to measure the radiant brightness of the solid propellant combustion flame, and the curves of the combustion integrated brightness (radiant energy) of the two propellants changing with time were obtained. propellant gas composition and combustion characteristics information. Using a RS-FTIR spectrometer combined with a telescope, the infrared emission of nitroguanidine/AP/PTFE solid propellant was collected from 30m away, and a spectrum between 800 and 4700cm<sup>-1</sup>

was obtained. Its different combustion was determined through the HF and HCl anti-vibration bands. Temperature of time, spectral resolution 2cm-1.

The results show that RS-FTIR emission spectroscopy is a fast and sensitive method for testing flame temperature and product concentration, which can be used to diagnose the combustion process of energetic materials.

Although RS-FTIR technology has been proven to be able to better measure the combustion temperature of solid propellant and the influence of components on combustion temperature in a wide band range, it has high signal-to-noise ratio, high sensitivity, fast detection speed, and can identify the emission source. Absolute energy spectrum and other advantages, but commercial FT-IR instruments are expensive and have limited time resolution. The measurement results are sight range and path averages and are difficult to quantify. Factors such as high-pressure conditions accompanied by unstable combustion are still the mainstay of RS-FTIR technology in solid propellants. Problems faced in combustion diagnosis.

twenty four Laser Induced Breakdown Spectroscopy (LIBS)

Laser-induced breakdown spectroscopy (LIBS) technology is an advanced detection method based on atomic emission spectrometry analysis technology. It is extremely useful in the fields of qualitative and quantitative measurement of intermediate product elements in various complex combustion flow fields such as solid, liquid, and gas combustion flames. Development potential. The basic principle of LIBS technology is to use a high-energy pulsed laser to focus on the sample surface and interact with the sample. The atoms and molecules in the laser focus area absorb energy to generate laser plasma. The ion begins to cool immediately after the laser pulse terminates, and is in an excited state during the process. Atoms and ions jump from high energy levels to low energy levels to release light with specific frequencies, that is, the characteristic spectral lines of the corresponding atoms and ions. The component elements of the analyte can be obtained by detecting the wavelength of the characteristic spectral line, and the calibrated intensity of the characteristic spectral line can reflect the concentration of the target element in the analyte and other related information (Figure 8). Because the laser pulse energy is high, it can penetrate deep into the flame, the pulse time is short, and the range of action is small. Related research has been devoted to the application of this technology in combustion diagnosis. Figure 8 is a schematic diagram of the LIBS combustion diagnosis system.

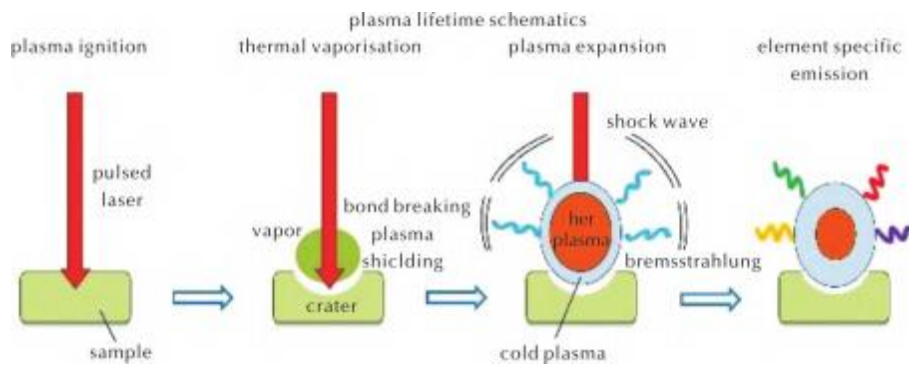


Figure 8 Schematic diagram of laser-induced breakdown spectroscopy

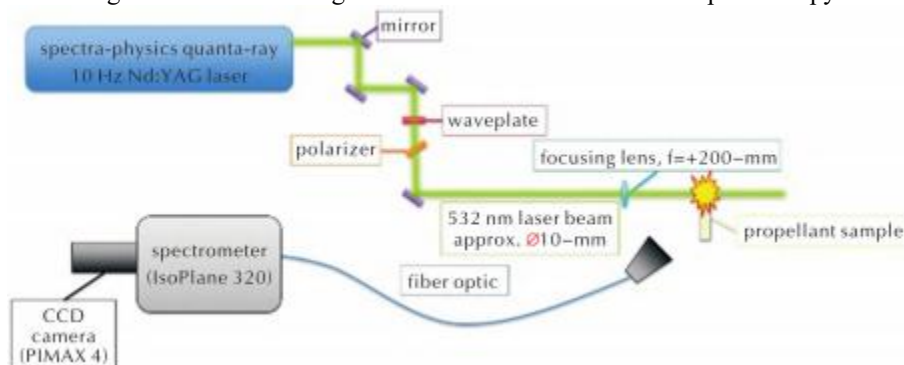
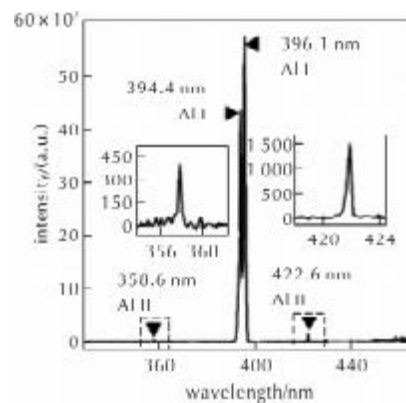


Figure 8 Schematic diagram of LIBS combustion diagnostic system

The most typical application of LIBS technology in the field of combustion is the quantitative measurement of flame equivalence ratio ( $\Phi$ ) to reflect the impact on the reaction process and the ratio of oxidizer and fuel to combustion products. The H/N peak intensity ratio and fuel equivalence ratio were calibrated, and a calibration curve of the H (656nm) spectral line half-height width and temperature was established for combustion jet flame detection. LIBS was used to detect the local carbon-to-hydrogen ratio in the ethylene partially premixed flame, and the relationship between the gas flow O/C peak intensity ratio and the concentration equivalence ratio was pre-calibrated, and then the distribution of carbon and oxygen atomic ratios in the flame axial height under different equivalence ratios was studied., which is consistent with the simulation results, confirming the effectiveness of LIBS technology in the combustion flow field.

In recent years, researchers have applied LIBS technology to the defense sector to characterize the release of heavy metal elements when energetic materials burn. In 2017, he first used a 10Hz solid laser as the excitation source to study the characteristic spectral lines of metal elements in the combustion flame of solid propellant containing trace amounts of metal. LIBS characteristic spectral lines were detected in solid propellant combustion plumes doped with known concentrations of aluminum, and the optimal energy for generating plasma was determined through studies of laser energy correlation, resulting in detection with a higher signal-to-noise ratio.. In order to reduce the impact of laser-plasma interaction and background noise interference on the experimental results, the above experiment was repeated using an ultrashort pulse laser with a pulse duration of 80fs at 1kHz (Figure 9 shows the peak spectrum of the solid propellant with an Al mass fraction of 16% Image), the result is a better linear relationship between the LIBS emission line intensity and the Al concentration initially present in the line beam (see Figure 10), confirming the superiority of ultra-short pulse LIBS technology and its application in aluminum-containing propellants Applicability in combustion diagnostics. Using a 10Hz Nd:YAG laser, the concentration of gas phase iridium was measured using LIBS technology for the first time. Iridium is one of the most commonly used catalysts in single propellants, and its damage and consumption during propellant combustion is one of the main factors affecting the life of single propellant. The significance of this work is to make LIBS technology have an important role in propulsion. Prospects for active monitoring of single propellant health by detecting propellant plumes during propellant combustion.



**Figure 9** LIBS spectrum of solid propellant with 16% Al mass fraction

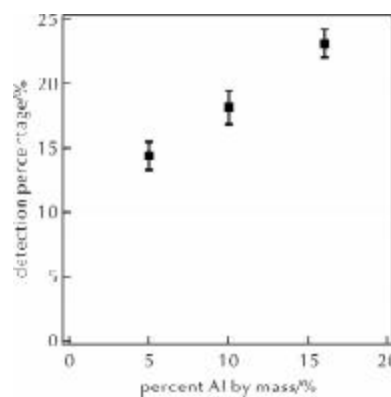


**Figure 10** Solid propellant signals with Al mass fractions of 5%, 10% and 16%

The relationship between intensity and mass concentration LIBS is widely used in in-situ rapid measurement of multiple types of products. It has high accuracy in measuring the gas fuel equivalence ratio and the concentration of metal atoms in solid fuel flames. It can also obtain non-metallic materials such as C, O, H, and N. Characteristic spectral lines of metal elements enable measurement of multi-product components and multi-characteristics. At the same time, LIBS has gradually developed combustion diagnosis near the wall of the liquid rocket combustion chamber to determine the relative concentration of the main combustion substances and reduce the uncertainty of CFD verification. It has only been developed and utilized in the field of energetic material combustion in recent years, mainly focusing on the quantitative detection of metal elements. The disadvantage of LIBS technology in this field is that it may be affected by factors such as the stability of the plasma signal of suspended particles in the gas, high-energy laser intrusion, and high pressure in the combustion chamber, resulting in large signal fluctuations.

#### 4 IMAGING METHOD

This type of method uses optical imaging principles such as interference to capture and image the results, often combined with high-speed photography and holography (DIH) technology, to measure the combustion flow field velocity and density gradient, and reflect the flame structure and changes over time. Compared with In terms of light

scattering and optical emission and absorption in the spectral range, imaging methods are more biased toward macroscopic measurements.

#### 4.1 Particle Imaging Velocimetry (PIV)

Particle imaging velocimetry (PIV) is a testing technology based on elastic scattering technology for instantaneous velocity spatial distribution, which can conduct plane and spatial testing of combustion flow fields. The basic principle of PIV is to continuously use laser pulses to take two spatial distribution images of fluid particles in a very short time. The images show the displacement size and direction of the flowing particles. The particle velocity vector is calculated through correlation analysis. Figure 11 is a schematic diagram of the PIV system. Compared with technologies such as single-point laser Doppler velocimetry (LDV) and phase Doppler particle analysis (PDPA), PIV is more inclined to test and study the overall flow field, and has been widely used in various engine combustion flow fields and liquid fuels. In the study of spray particle motion.

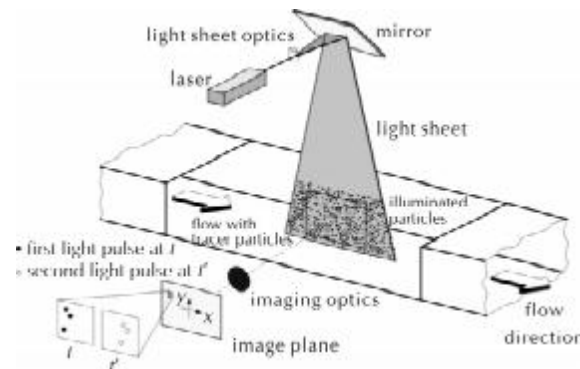


**Figure 11** Schematic diagram of particle imaging velocimetry system

PIV velocity measurements were carried out in the exhaust plume of a small solid rocket motor. The plume velocity in this environment reached 630m/s. Although the temperature exceeded 3000K and the heterogeneous particle distribution inside the plume caused a large amount of vector loss, the experimental results demonstrated it well. The applicability of PIV using jet particles as tracer particles in plume measurements was demonstrated. The small size of rocket engines makes optical access with shorter optical paths easier to achieve, however observing solid propellant plumes in larger rocket engines suffers from increased optical path lengths and reduced transparency due to increased particle scattering, and in larger devices The application of propellant combustion diagnostics is still the development direction of PIV technology. PIV was used to measure the flame flow field velocity under different total pressure losses in the cold state of the aeroengine recirculation combustor. MgO with an average particle size of 10  $\mu\text{m}$  was used as a tracer particle to fully mix with the airflow, and the pressure loss and combustion velocity in the recirculation combustor were obtained. Dynamic relationship. Using silicone oil particles with an average size of 1 $\mu\text{m}$  as tracer particles, PIV technology was used to observe the engine speed of 3500r/ The velocity field distribution at the center of the combustion chamber in the working cycle at min. In high-temperature and high-pressure environments, since PIV technology uses Mie scattering to be insensitive to high-pressure environments, and strong background light can be filtered by adding a filter, the test results are less disturbed and more accurate.

In recent years, PIV technology is developing to a multi-dimensional level in engine combustion flow field diagnosis. First of all, stereo PIV technology was developed, a single camera was replaced with a dual-camera group, and the test results of the three velocity components in the two-dimensional space of the combustion flow field were obtained, allowing researchers to have a more intuitive understanding of the spatial flow conditions of the complex flow field. Secondly, a tomographic PIV technology was developed, using 4 CCD cameras to simultaneously shoot the flow field at different spatial positions. Through the two-dimensional projection of the tracer particles, the tomographic algorithm was used to reconstruct the three-dimensional structure, thereby realizing the engine combustion chamber. Transient measurement of three velocity components in three dimensions near the tumble plane. In the body PIV part, a double-pulse YAG laser is used as the light source, and four CCD cameras are positioned in the vertical direction of laser irradiation to take pictures. Through high-resolution images (Figure 12 shows the PIV reconstruction results of the swirling flame body), the temperature and velocity coupling effect on the combustion flow field is obtained. The resulting influence patterns verify the feasibility of this quantitative, multi-dimensional, and visual comprehensive optical technology in diagnosing complex flame flow fields. This three-dimensional velocity vector field measurement technology (Tomo-PIV), which combines planar PIV and tomographic reconstruction algorithms, is a current research hotspot in the field of three-dimensional flow field velocity measurement. This method is suitable for high-density tracer particles, does not require coherent light illumination, and obtains flow The field spatial resolution is higher and the imaging quality is better, and it is expected to be widely used in three-dimensional velocity measurement research on complex turbulent flow fields of energetic materials and aerospace engines.

In terms of research on the combustion of energetic materials, we combined PIV, high-speed photography, FTIR and other technologies to conduct visual research on the flame flow field and temperature field of pyrotechnic powder

combustion. We used PIV technology to observe the gas-particle two-phase flow in the flame flow field, and analyzed the combustion reaction mechanism of this composite energetic material. In the study of muzzle flow field velocity measurement, in order to verify the applicability of PIV technology in this extremely challenging supersonic environment, comparative experiments with PIV, high-speed schlieren, optical particle counters, combustion chamber pressure sensors and other technologies were used. 300BLK ammunition propellant combustion flow rate. The test results show that PIV technology can accurately distinguish the main characteristics of the flow and the instantaneous velocity field. The sub-micron particles in the combustion products can follow the gas flow with high fidelity and serve as tracer particles. The solid ZrO<sub>2</sub> coated on the propellant pellets also have good flow fidelity and are suitable for combustion in subsonic conditions.

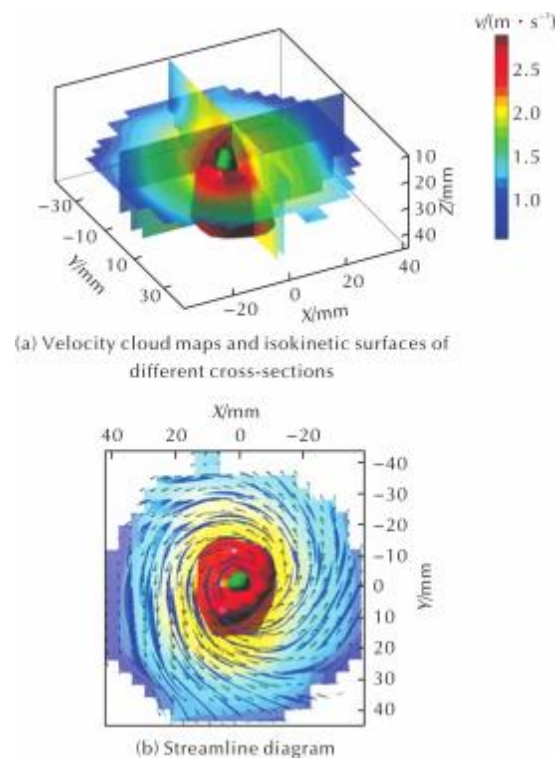


**Figure 12** PIV reconstruction results of swirling flame body

While PIV technology is developing towards high dimensions and high spatiotemporal resolution, the comprehensive diagnostic method combined with PLIF or PDPA, schlieren and other technologies further enriches the visual information of the combustion flow field and is useful in diagnosing complex combustion processes of energetic materials and engines. It provides more comprehensive image information in complex combustion environments and has great development potential.

## 4.2 Schlieren Method

Schlieren technology is a flow field display technology that was first proposed by Töpler in the 1880s. The schlieren method uses the principle that when a beam passes through a flow field with a density gradient, the beam will be deflected due to a change in the refractive index, and then the deflected beam is converged, and a knife-edge shield is used to form a stripe image after the beam diverges, and the light and dark areas of the image represent the density change of the flow field. Typical light paths of the schlieren method include Z-shaped and T-shaped light paths. The Z-shaped light path is the most commonly used light path for jet research, while the T-shaped light path is mostly used in burners such as engines with a single window. According to different combinations of light sources and holes, the schlieren method can also be divided into ordinary schlieren and laser schlieren. In recent years, with the help of high-frequency lasers and flash lamps, or combined with high-speed photography, the time resolution and brightness display of the schlieren method have been greatly improved, making it widely used in engine combustion flow fields and energetic material combustion diagnosis.

Combining the ignition delay and combustion characteristics of paraffin-based fuels with solid amine borane, chemiluminescence and high-speed schlieren imaging techniques were used to identify different steps of the combustion process. The reduction in ignition delay of the viscosity-modified rocket propellant was clearly observed, confirming that there is a clear correlation between ignition delay and higher polymerized  $\alpha$ -olefin concentration, which provides an effective research method for studying the comprehensive impact of other condition changes such as subsequent pressurization and addition of rheological additives on ignition delay. Focused schlieren technology was used to study the aluminum agglomeration mechanism on the burning surface of HTPB/AP/Al propellant. The flame structure information during propellant combustion was obtained (Figure 13), and the melting,

ignition and combustion during the evolution of the agglomerates were analyzed, and other microscopic processes, and statistics of parameters such as particle size distribution and velocity were used to verify the numerical simulation results of propellant combustion.

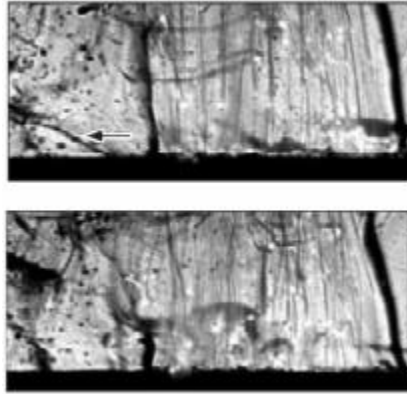


**Figure 13** HTPB/AP/Al propellant flame propagation image captured by focusing on schlieren technology

Research results show that schlieren technology can effectively display the structure and development process of solid propellant flames, and can also track and monitor the alumina particles generated by combustion. A new algorithm based on focused schlieren technology for solid propellant containing inert particles to burn surface particles and aggregates is proposed. Compared with the study of the aluminum agglomeration phenomenon on the burning surface of propellant, this method focuses more on detecting the protrusions of continuous one-dimensional curves. About 84% of the particle size detection of a certain type of propellant is close to the marked particle size, with an allowable deviation of 25%. When applied During the combustion of aluminum-containing solid propellants, particles and aggregates can be detected before they begin to coalesce. The newly developed background-oriented schlieren technology ( BOS) is the current research hotspot in schlieren imaging. BOS Correlation calculations applicable to the schlieren method can be performed on the image background. Although it is different in principle from the schlieren effect, it can still image the density gradient and obtain an image effect similar to the schlieren, so it is also used in sprays. Research.

Schlieren technology does not require complex optical paths and expensive laser light sources, the application conditions are relatively simple, and the measurement cost is relatively low. When studying the combustion of energetic materials, the thin combustion zone under high pressure reduces the resolution of the ordinary schlieren method. The reflection from the observation window may also interfere with the schlieren image. Similar to the direct optical photography method, there is a single focal plane and excessive depth of field. Narrow and other shortcomings reduce measurement efficiency. The use of laser monochromaticity and bandpass filters can largely solve the problem of flame self-illumination and interference, combined with high-speed photography and digital coaxial holography (DIH), it is also possible to obtain instantaneous surface schlieren patterns of energetic materials suitable for the working conditions of the schlieren method in combustion experiments.

## 5 CONCLUSION

Optical diagnostic methods play an important role in the experimental diagnosis of energetic material combustion. With their advantages of non-contact, no interference, and real-time monitoring, they have become a powerful tool for contemporary research on engine combustion flow fields and energetic material combustion phenomena. For engine flow, Provide guidance on field design and energetic material formulations and combustion mechanisms. As far as current research is concerned, optical diagnostic methods have been widely used in combustion diagnosis of energetic materials. However, due to the relatively harsh combustion environment of energetic materials and engines, different optical methods have their limitations and applicability. A single test There are certain deficiencies in the experimental parameters available through technology. Research should combine different diagnostic methods based on actual conditions and needs, and use their respective complementary advantages to achieve more accurate experimental research on multiple parameters of the combustion process. Based on the above issues, this article reviews the application of several optical diagnostic methods in the study of energetic material combustion and engine combustion chambers in recent years. It summarizes the measurement principles and objects of various methods, analyzes their respective advantages and disadvantages, and provides guidance for the future. Optical diagnostic methods for studying the combustion of energetic materials provide reference. The specific conclusions are as follows:

(1) Methods such as radiation method, LIF and LAS have great application potential in carrying out multi-dimensional temperature field measurement research. They can be widely used in measurement research on energetic material combustion and aerospace engine combustion chamber temperature fields, and further develop three-dimensional temperature field reconstruction, etc. Work.

(2) PLIF technology has superiority in testing combustion intermediate products and is sensitive to detecting concentration changes of free radicals and molecules such as OH, CH, CN, NO, HCO, CH<sub>2</sub> O, etc., as well as metal atoms such as Al and Fe during the combustion process. The above groups and atoms are also important tracer products

that characterize the flame structure of energetic materials. By studying the concentration distribution and changes of intermediate products, the reaction kinetic model of energetic materials can be further improved and verified, and microscopic data can be provided for the combustion reaction mechanism. support.

(3) Technologies such as radiation method, LAS and LIBS have development potential in terms of equipment miniaturization and portability, and LAS has a shareable optical port, which can combine radiation method and optical methods such as high-speed photography for simultaneous measurement. The optimization and improvement can carry out synchronous online diagnosis of the temperature field and flow field structure of the engine combustion chamber under more environmental conditions.

(4) Schlieren method and PIV have great development potential in multi-dimensional flow field display and multi-velocity component measurement research. They can be more applied in the testing of aviation engine combustion flow fields. By combining direct shooting with high-speed cameras and PLIF and other optical methods to build a more suitable and efficient optical diagnosis system to obtain more microscopic and rich multi-dimensional data information.

## COMPETING INTERESTS

The authors have no relevant financial or non-financial interests to disclose.

## REFERENCES

- [1] HEDMAN TD, CHO K Y, SATIJAA. Experimental observation of the flame structure of a bimodal ammonium perchlorate composite propellant using 5kHzPLIF. *Combustion and Flame*, 2012, 159(1): 427-437.
- [2] ISERTS, HEDMAN T D, LUCHTRP. Oxidizer coarse-to-fine ratio effect on microscale flame structure in a bimodal composite propellant. *Combustion and Flame*, 2016, 163: 406-413.
- [3] HEDMAN T D, REESE D A, CHO K Y. An experimental study of the effects of catalyst sonan ammonium perchlorate based composite propellant using 5 kHz PLIF. *Combustion and Flame*, 2012, 159(4): 1748-1758.
- [4] YANG Y, ZHU T, YAN Z. A study on combustion characteristics of insensitive triple-base propellant. *Applied Sciences*, 2023, 13(9): 5462.
- [5] PARR T, HANSON-PARR D. Cyclotetramethylene tetranitramine/glycidyl azide polymer/butanetriol trinitrate propellant flame structure. *Combustion and Flame*, 2004, 137(1/2): 38-49.
- [6] Yan Zhiyu, Wang Liangchen, Song Chen. Optical diagnosis of RDX focus ignition and reaction processes. *Journal of Explosives*, 2021, 44(4):468-473.
- [7] RUESCH M, POWELL M S, SATIJA A. Burning rate and flame structure of cocrystals of CL-20 and a polycrystalline composite crystal of HMX/AP. *Combustion and Flame*, 2020, 219: 129-135.
- [8] CHO K, POURPOINTT, SON S. High repetition rate OH planar laser induced fluorescence of gelled propellant droplet. 47th AIAA/ASME/SAE/ASEE Joint Propulsion Conference and Exhibit: New York: AIAA, 2011.
- [9] CHO K Y, POURPOINTTL, SON SF. Micro explosion investigation of mono methyl hydrazine gelled droplet with OH planar laser-induced fluorescence. *Journal of Propulsion and Power*, 2013, 29 (6): 1303-1310.
- [10] PETERSON B, BAUM E, BÖHM B. Spray induced temperature stratification dynamics in a gasoline direct-injection engine. *Proceedings of the Combustion Institute*, 2015, 35(3): 2923-2931.
- [11] PETERSON B, BAUM E, DREIZLER A. An experimental study of the detailed flame transport in a SI engine using simultaneous dual-plane OH-LIF and stereoscopic PIV. *Combustion and Flame*, 2019, 202: 16-32.
- [12] Yuan Xun, Yu Xin, Peng Jiangbo. Research on 3DLIF visualization technology of supersonic flame. *Experimental Fluid Mechanics*, 2022, 36(4): 30-36.
- [13] Liu Jingru, Hu Zhiyun. Application of laser-based measurement technology in combustion flow field diagnosis. *China Optics*, 2018, 11: 531-549.
- [14] SOLOUKHIN R I, OPPENHEIM A K, BOWEN J R. Two-dimensional imaging of flame temperature using laser-induced fluorescence. *Dynamics of Flames and Reactive Systems*, 1984: 714-721.
- [15] LAURENDEAU N M. Temperature measurements by light-scattering methods. *Progress in Energy and Combustion Science*, 1988, 14(2): 147-170.
- [16] Lu Yongxu. Research on propellant combustion temperature measurement method based on two-color plane laser-induced fluorescence technology. Mianyang: Southwest University of Science and Technology, 2022.
- [17] VILMART G, DORVAL N, ATTAL-TRETOUB. Detection of iron and aluminum atomic vapors by LIF technique: application to solid propellant combustion // 33rd AIAA Aerodynamic Measurement Technology and Ground Testing Conference. New York: AIAA, 2017.
- [18] VILMART G. Detection of vapors of metal atoms per induced fluorescence by laser (LIF): application has there propulsion solid. French: University Paris Saclay (Cam UE), 2017.
- [19] BUCHER P, YETTER R A, DRYER F L. Flames structure measurement of single, isolated aluminum particles burning in air. *Symposium on Combustion*, 1996, 26(2):1899-1908.
- [20] BUCHER P, YETTER R A, DRYER F L. PLIF species and radiometric temperature measurements of aluminum particle combustion in O<sub>2</sub>, CO<sub>2</sub> and N<sub>2</sub> O oxidizers, and comparison with model calculations. *Symposium on Combustion*, 1998, 27(2): 2421-2429.
- [21] Peng Jiangbo, Cao Zhen, Yu Xin. Application of time-resolved AIO-PLIF imaging technology. *Solid Rocket Technology*, 2021, 44(1):106-111.

- [22] CHEVALIERPH, DORVALN, DEVILLERSR W. Investigation of aluminum drop let combustion in solid propellant flames: Al-PLIF experiments and numerical simulation // AIAA Propulsion and Energy 2021Forum: American Institute of Aeronautics and Astronautics. New York:AIAA, 2021.
- [23] VILMART G, DORVAL N, ATTALTRETOUTB. Detection of aluminum vapors b y laser-induced fluorescence for solid propellant combustion //33<sup>rd</sup> AIAA Aerodynamic Measurement Technology and Ground Testing Conference. New York: AIAA, 2017.
- [24] VILMART G, DORVAL N, DEVILLERS R. Imaging aluminum particles in solid-propellant flames using5kHzLIF of Al atoms. Materials, 2019, 12 (15): 2421.
- [25] VILMARTG, DORVALN, ORAIN M. Detection of iron atoms by emission spectroscopy andlaser-induced fluorescence in solid propellant flames. Applied Optics, 2018, 57(14): 3817.
- [26] GRASSER, THOMAS W, KEARNEY. CARS thermometry in a 2 -m-Diameter methanol poolfire//AIAA Aerospace Sciences Meeting and Exhibit. New York: AIAA, 2013.
- [27] TEDDERS A, DANEHY P M, MAGNOTTI G. CARS temperature measurements in a combustion heated supersonicjet //47thAIAA Aerospace Sciences Meeting and Exhibit Including the New Horizons Forum and Aerospace Exposition. New York: AIAA, 2009.
- [28] Tian Ziyang, Zhao Huijie, Wei Haoyun. Dynamic high-temperature combustion field temperature measurement based on hybrid femtosecond/picosecond coherent anti-Stokes Raman scattering. Acta Physica Sinica, 2021, 70(21): 214203.
- [29] O'BYRNES, DANEHYP M, CUTLERA D. Dual-Pump coherent anti-stokes Raman scattering measurements in a supersonic combustor. AIAA Journal, 2012, 45(4): 922933.
- [30] THARIYAN M, ANANTHANARAYANAN V, BHUIYAN A. Dual-pump CARS temperature and major species concentration measurements in laminar counter flow flames and inagasturbine combustor facility //AIAA Aerospace Sciences Meeting Including the New Horizons Forum & Aerospace Exposition. New York: AIAA, 2006.
- [31] Zhang Lirong, Hu Zhiyun, Ye Jingfeng. Mobile CARS system measures supersonic combustor exit temperature. China Laser, 2013, 40 (4): 0408007.
- [32] Li Chunxi, Zhao Ming, Zhang Rui'e. CARS measurement technology of dual-base propellant combustion flame temperature. Journal of Explosives and Explosives, 2003, 26(1): 65-67.
- [33] Fan Chuanxin. A review of the radiation characteristics of solid rocket plume and its temperature measurement technology. Solid Rocket Technology, 2004, 27(3): 238-242.
- [34] ARON K, HARRISLE. CARS probeof RDX decomposition. Chemical Physics Letters, 1984, 103 (5): 413-417.
- [35] HARRIS L E. Coherent anti-Stokes Raman (CARS) temperature measurements in a propellant flame. Combustion and Flame, 1982, 48: 97-100.
- [36] HARRIS L E. Hydrogen coherent antistokes Raman spectra from CH<sub>4</sub>-N<sub>2</sub> O and nitramine composite flames. Journal of the Chemical Society Faraday Transactions, 1986, 82(12): 2129-2141.
- [37] STUFFLEBEAM JH, ECKBRETHAC. CARS diagnostics of solid propellant combustion at elevated pres-sure. Combustion Science and Technology, 1989, 66 (46): 163-179.
- [38] Hu Zhiyun, Liu Jingru, Zhang Zhenrong. Application of broadband CARS in diagnosing solid propellant combustion fields. Journal of Explosives, 2009, 32(2): 52-55.

# DESIGN OF A DISPOSABLE WOODEN TABLEWARE PACKAGING INSPECTION DEVICE

JianWu Hou, TianYue Jiang\*, JiBo Li, HaoJun Zhao

*College of Information and Electronic Technology, Jiamusi University, Jiamusi 154007, China.*

*Corresponding Author: TianYue Jiang, Email: 13704503245@163.com*

**Abstract:** This paper addresses the shortcomings of traditional manual sorting methods in the field of packaged tableware by proposing a novel disposable wooden tableware packaging inspection mechanism. Through analysis and comparison of existing technologies, a design scheme was determined, and the structural design and working principles were elaborately described. This mechanism utilizes the principle of buoyancy to stratify water and employs devices such as drive motors and rotating screws to achieve batch inspection of packaged tableware. Its advantages include scientifically reasonable structural design, safe and convenient operation, and efficient separation of intact and damaged wooden tableware, thereby enhancing inspection efficiency. This mechanism provides a solution for packaging quality inspection, with the potential to play a significant role in reducing pollution, minimizing resource wastage, enhancing product quality, and maintaining brand image. It is expected to make a positive contribution to the industry's development.

**Keywords:** Disposable wooden tableware; Packaging inspection mechanism; Structural design; Working principle

## 1 INTRODUCTION

In recent years, with the continuous implementation of "plastic-restriction" policies worldwide[1], traditional disposable plastic tableware is gradually being replaced by disposable wooden tableware, which is favored by more and more consumers as an environmentally friendly and healthy choice[2]. However, improper packaging during the production process may lead to the rupture and leakage of packaging bags, exposing wooden tableware to the air and causing secondary pollution by breeding a large number of bacteria. This not only potentially threatens the health of consumers but also affects the reputation of companies. Therefore, quality inspection of packaged tableware to remove defective items contributes to improving the overall quality of batched products and ensures the personal health and safety of users. Currently, to prevent damaged packaged tableware from entering the market, manufacturers mainly rely on visual inspection by human eyes for quality sorting, requiring substantial number of workers to manually select them one by one beside the conveyor belt of the tableware production line. However, this manual inspection method suffers from low efficiency, high costs, and the possibility of human error leading to misjudgments and omissions[3], resulting in some damaged packaged tableware still potentially entering the market and affecting product quality and corporate image. To address these issues, this paper aims to design a disposable wooden tableware packaging inspection mechanism (referred to as the packaging inspection mechanism hereafter) to enhance the controllability and accuracy of packaging quality inspection, ensuring that product quality meets standards. This is intended to meet consumer demand for health and safety while enhancing the competitiveness and sustainable development capabilities of enterprises in the market[4].

## 2 MECHANICAL STRUCTURE DESIGN

As illustrated in Figures 1 to 5, the packaging inspection mechanism features the following enhanced mechanical structural design:

(1) Parallel tracks are installed on the top sides of the mounting plate, with mobile seats mounted on the top of the tracks. Electric wheels are installed at the bottom of the mobile seats, engaging with the tracks to ensure stable movement of the mechanism during operation. By engaging the electric wheels with the tracks, the power of the electric wheels is effectively transmitted to the entire mechanism, enabling it to move steadily along the track trajectory. This design ensures stable speed and trajectory of the mechanism during the inspection of packaged tableware.

(2) The top center of the mobile seat is equipped with a lifting cylinder, and a mounting platform is installed on the top of the lifting cylinder. One side of the mounting platform is fitted with a supporting sliding rod, while the top is installed with a drive motor. The input end of the drive motor is electrically connected to the external power output end, and its output end is connected to one end of the rotating screw. The purpose of the drive motor is to control the movement of the mechanism, allowing it to operate according to the designed program and path, thereby achieving automated detection of the packaged tableware.

(3) The outer side of the supporting sliding rod is fitted with an extendable sleeve rod, inside of which a groove is provided for supporting the sliding rod's movement. The supporting sliding rod is located inside the groove, with both its outer surface and the inner wall of the groove being smooth to reduce relative friction between them, facilitating smoother movement of the extendable sleeve rod on the supporting sliding rod. This helps control the position of the

filtering hole plate, achieving effective stratification and separation of the packaged tableware. The top of the extendable sleeve rod is connected to the rotating screw, so when the drive motor starts and rotates the rotating screw, the threaded connection between the rotating screw and the screw seat causes the extendable sleeve rod to move on the supporting sliding rod. The extendable sleeve rod then extends or retracts according to the movement of the rotating screw, allowing the filtering hole plate to move up and down in the water tank. With the assistance of the extendable sleeve rod, the position of the filtering hole plate can be accurately controlled.

(4) At one end of the extendable sleeve rod's top, a screw seat is welded, and the other end of the rotating screw is connected to the screw seat through threads. The screw seat serves as a fixed support for the rotating screw, supporting and maintaining the stable position of the rotating screw. The threaded connection between the rotating screw and the screw seat enables the rotating screw to maintain a stable axis of rotation during operation, ensuring the accuracy of the movement and positioning of the extendable sleeve rod. The rational design of the screw seat directly affects the stability and efficiency of the entire mechanism.

(5) At the bottom of the extendable sleeve rod, an electric cylinder is installed, with its input end electrically connected to the external power output end. The electric cylinder controls and adjusts the position of the moving parts. At the top end bottom of the extendable sleeve rod, a first rotating seat is welded, which connects the connecting rod and the filtering hole plate, and tilts the filtering hole plate when necessary. The bottom of the first rotating seat is rotatably connected to the connecting rod, which serves to connect the first rotating seat and the second rotating seat. The connecting rod is located at the bottom of the first rotating seat, connected to the first rotating seat by welding, and extends to the second rotating seat. When the extending end of the electric cylinder retracts, the connecting rod rotates together with the first rotating seat, causing the first rotating seat to tilt, thereby tilting the filtering hole plate. This action discharges the damaged utensils into the discharge pipe and sends them to the collection box. Therefore, the connecting rod plays a crucial role in connecting and transmitting motion in the packaging detection mechanism, ensuring the accurate movement of the filtering hole plate and effectively handling the packaged tableware.

(6) The outer side of the connecting rod is welded with the second rotating seat, which is rotationally connected to the extending end of the electric cylinder. The second rotating seat serves as the rotational pivot of the other end of the connecting rod, and it is rotationally connected to the extending end of the electric cylinder. When the extending end of the electric cylinder retracts, the second rotating seat rotates accordingly, transmitting the tilting action to the first rotating seat and the filtering hole plate through the connecting rod. This function enables the discharge of damaged packaged tableware from the discharge pipe and their collection in the collection box. Therefore, the second rotating seat plays a role in rotating and transmitting motion in the packaging detection mechanism, working in conjunction with other components to handle and collect packaged tableware.

(7) At the bottom of the connecting rod, there are connecting ears, which ensure that two filtering hole plates can be tightly fitted together without interference from the ears affecting their fit. The longitudinal cross-section shape of the connecting ear is "L" shaped, which allows the connecting ear not to hinder their fitting when the two filtering hole plates are closely adhered. The design of the connecting ears helps maintain the sealing between the filtering hole plates, ensuring the effective isolation of packaged tableware stratified in water. Therefore, the connecting ears play a role in maintaining the fitting and sealing of the filtering hole plates in the packaging detection mechanism, ensuring the smooth progress of the detection process.

(8) At the bottom of the two connecting ears located on the same track, filtering hole plates are welded, and the function of the filtering hole plates is to isolate and filter the stratified packaged tableware in the water. The packaging detection mechanism utilizes buoyancy to stratify the packaged tableware, with the filtering hole plates playing a crucial role. When the two filtering hole plates come into contact, they separate the stratified packaged tableware in the water, allowing intact utensils to float on the water surface while damaged ones are trapped in the space between the filtering hole plates. Consequently, the filtering hole plates effectively separate intact packaged tableware from damaged ones, facilitating subsequent discharge and collection tasks. Therefore, the filtering hole plates play a critical role in screening and separating packaged tableware in the packaging detection mechanism, ensuring the accuracy and efficiency of the detection process.

(9) Between the installation boards, there are reservoirs, and on the top of both sides of the reservoirs, there are movable grooves. The longitudinal cross-section of the movable groove is equal in size to that of the filtering hole plate. When the filtering hole plate is inside the movable groove, it can seal the movable groove to prevent water from overflowing from the joint. One side of the reservoir bottom is perforated and connected to a discharge pipe, which has a parallelogram-shaped cross-section with a sloping bottom surface to facilitate the discharge of unsuitable packaged tableware. The ends of the discharge pipe are rotated by the spindle, one of which is connected to the output end of the rotating motor, while the input end of the rotating motor is electrically connected to an external power source. One side of the shaft is welded with a sieving hole plate, located at the bottom inside the reservoir. The outer side of the sieving hole plate tightly adheres to the inner wall of the reservoir to prevent utensils from leaking from the connection between the sieving hole plate and the inner side of the reservoir. At the bottom of the discharge pipe, there is a hinged sealing door to prevent water or residual objects from leaking out of the discharge pipe, ensuring a clean and tidy discharge process. One side of the reservoir bottom is perforated and connected to a drainage pipe for draining water from the reservoir.

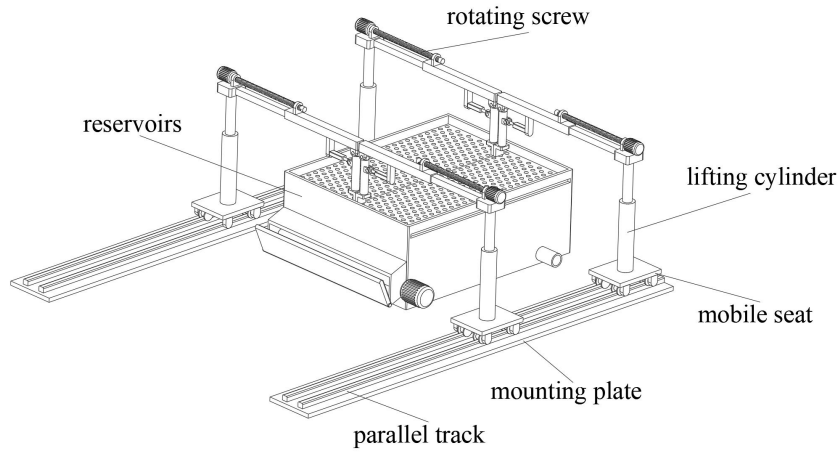


Figure 1. Schematic diagram of the three-dimensional structure

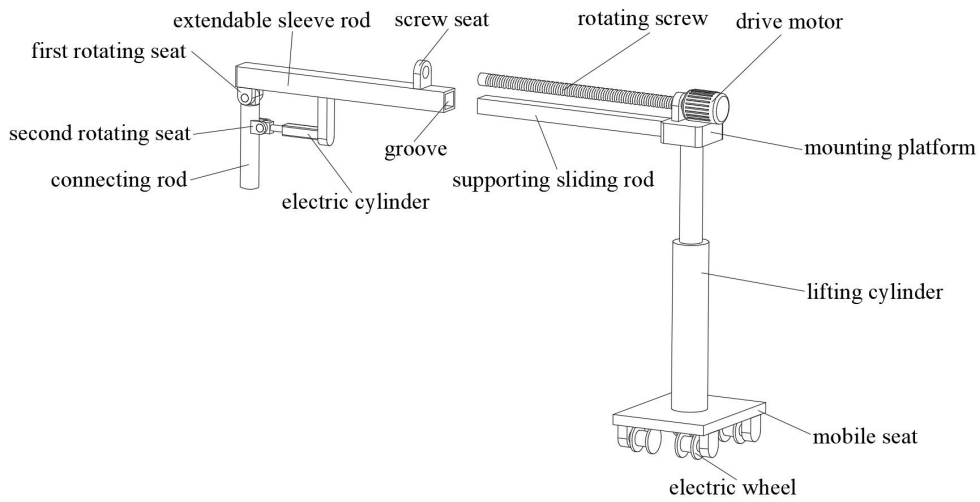


Figure 2. Schematic diagram of the installation structure of the moving seat

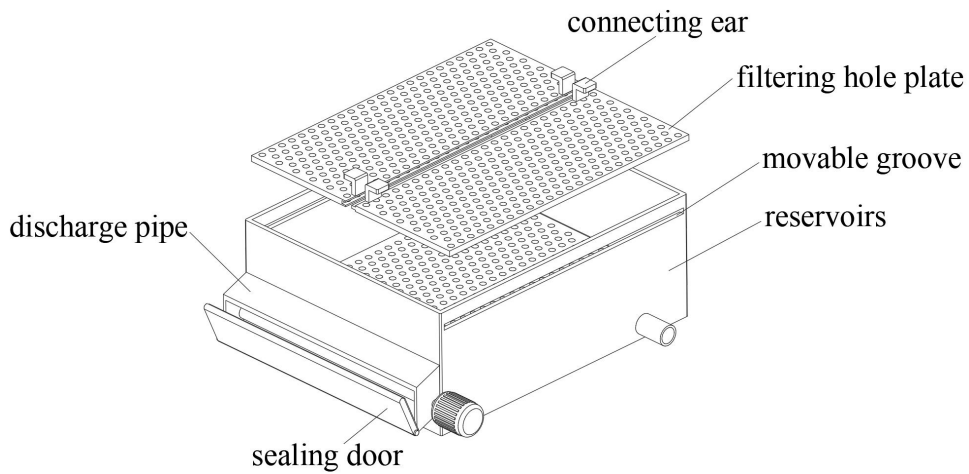
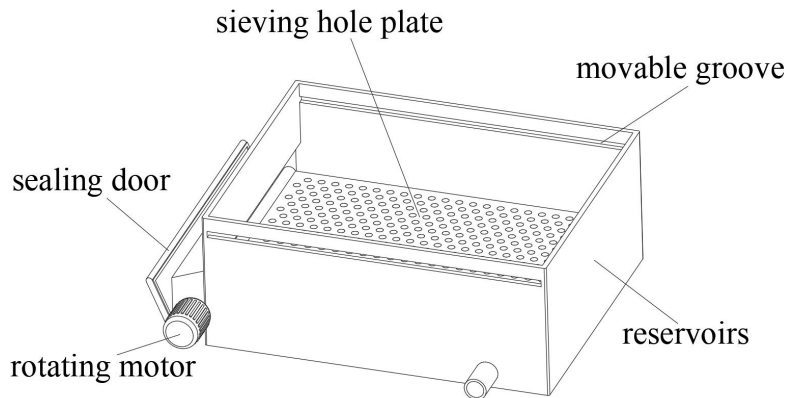
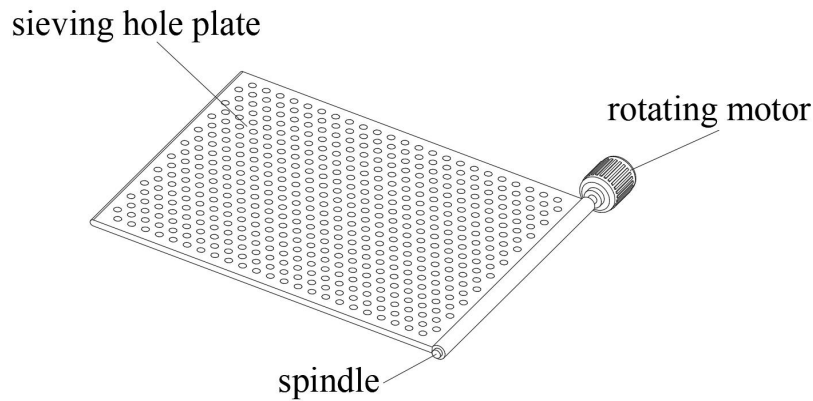


Figure 3. Schematic diagram of the filter plate installation structure



**Figure 4.** Schematic diagram of the selection hole plate installation structure



**Figure 5.** Schematic diagram of the installation structure of the rotating motor

### 3 DESIGN ADVANTAGES

The packaging detection mechanism presented herein offers significant advantages compared to existing technologies. Its specific strengths are outlined as follows:

#### 3.1 Scientific and Rational Structural Design

This packaging detection mechanism incorporates components such as tracks, movable seats, electric wheels, lifting cylinders, support rods, rotating screws, telescopic rods, electric cylinders, connecting rods, and filtering hole plates. The structural design has been meticulously considered and planned, ensuring functional complementarity and coordination.

#### 3.2 Convenient and Safe Operation

During usage, the operation is convenient, safe, and reliable. With the operation of the driving motor, the rotation of the screw rod, and the isolation of the filtering hole plates for stratifying water, the opening of the drainage pipe and the lifting operation of the lifting cylinder can be easily controlled by the operator, thereby enhancing the convenience and safety of the operation.

#### 3.3 Improved Inspection Efficiency

Batch inspection of packaged utensils is achieved through automated equipment operation[5]. The movement of the filtering hole plates and the arrangement of the collection box enable the rapid collection of damaged packaged utensils, thereby enhancing inspection efficiency.

#### 3.4 Prevention of Damaged Utensils Entering the Market

The efficient operation of the equipment effectively prevents damaged packaged utensils from entering the market, thereby avoiding damage to brand reputation and ensuring a dual safeguard of product quality and consumer interests[6].

### **3.5 Resource Recycling**

The design of components such as the collection box and drainage pipe in this packaging inspection mechanism enables the recycling of damaged utensils, aligning with environmental protection and resource conservation principles[7].

In summary, this packaging inspection mechanism not only demonstrates significant advantages in terms of convenient operation, high safety, and efficiency improvement but also contributes to safeguarding product quality and brand reputation. This underscores its innovation and practicality within existing technology.

## **4 THE WORKING PRINCIPLE AND OPERATIONAL PROCEDURE**

The working principle and operational procedure of this packaging inspection device are described as follows:

### **4.1 Preparation Stage**

Prior to operation, the filtering plates are positioned within the movable slots, with the connecting ears tightly fitted against the inner walls of the water reservoir on both sides. The filtering plates are in a horizontal position. The water reservoir is filled with water using an external water pump, and batches of packaged disposable wooden utensils are poured into the water reservoir.

### **4.2 Stratification in Water**

Intact wooden utensils, buoyed by buoyancy, float on the surface of the water, while damaged ones sink due to water ingress into the packaging, resulting in a stratified configuration within the water.

### **4.3 Filtration and Separation**

The driving motor initiates operation, causing the rotation of the rotating screw. The rotating screw is threaded into the screw seat, and as it rotates, the telescopic rod gradually moves away from the support rod. The filtering plates progressively move towards the center of the water reservoir until they make contact. When the two filtering plates come into contact, the driving motor ceases operation, and the filtering plates isolate the stratified wooden utensils within the water.

### **4.4 Drainage and Removal**

The drainage pipe is opened, allowing a portion of the water in the reservoir to be discharged. This causes intact wooden utensils floating on the water surface to fall onto the surface of the filtering plates. The discharged water can be collected for recycling. The lifting cylinder ascends, detaching the filtering plates from the water reservoir. The electric wheel starts, driving the moving seat to move along the track, removing the filtering plates from the top of the water reservoir.

### **4.5 Collection and Recycling**

After the filtering plates are removed from the top of the water reservoir, a collection box can be placed at the bottom of the filtering plates. Then, the electric cylinder is activated to retract its extending end. With the rotational connection between the first and second rotating seats, the filtering plates tilt, causing the packaged utensils on them to fall into the collection box, completing the collection process. Once collection is finished, the electric cylinder returns the filtering plates to a horizontal position and then to their initial state. External water pumps replenish the water in the water reservoir, awaiting the next batch of packaged utensils for inspection. Repeat these steps to complete the mass inspection of packaged utensils.

### **4.6 Conclusion Phase**

After all batches of packaged utensils have been inspected, open the drainage pipe to discharge all the water from the water reservoir, causing damaged utensils to fall onto the surface of the filtering plates. Open the sealing door, activate the rotary motor, and the rotary motor drives the shaft to rotate. Rotation of the shaft tilts the filtering plates, causing damaged packaged utensils to be discharged from the discharge pipe. Place a collection box at the bottom of the discharge pipe to collect the damaged packaged utensils for further recycling.

Through the above process, this packaging inspection mechanism can effectively conduct rapid and accurate inspections of the packaging of disposable wooden tableware, ensuring that the product quality meets the standard requirements.

## **5 CONCLUSION**

China is the world's largest producer and consumer of takeaway food packaging, with a growing demand for disposable wooden packaging tableware[8]. In response to the issues of low efficiency, high cost, and the inability to meet actual production needs associated with traditional manual sorting methods, this paper proposes a disposable wooden tableware packaging inspection mechanism to address the current pain points in production. The advantages of this inspection mechanism lie in its scientifically reasonable structural design, convenient and safe operation, and effective separation of intact and damaged packaged tableware, thereby enhancing inspection efficiency and ensuring product quality meets standards. Furthermore, against the backdrop of increasingly stringent environmental policies, this mechanism offers multiple advantages such as reducing environmental pollution, improving product quality, and maintaining brand image. However, despite the significant progress made by this mechanism, there is still room for improvement. For example, further optimization of structural design and the introduction of more advanced technologies are needed to meet the growing demands and standards of the market. In summary, this mechanism provides a practical and feasible solution for packaging quality inspection for manufacturers of disposable wooden tableware, with the potential for wide application in actual production. It aims to drive sustainable development within the industry while promoting the protection and sustainable utilization of environmental resources.

## COMPETING INTERESTS

The authors have no relevant financial or non-financial interests to disclose.

## FUNDING

This article was supported by the National General Project: Heilongjiang Province University Students' Innovation and Entrepreneurship Training Program Project, Project Title: IntelliEye Defect Recognition - Visual Inspection System for Surface Imperfections on Disposable Wooden Tableware (Project Number: 202310222068).

## REFERENCES

- [1] Chen, X., Chen, F., Wang, G., Ma, X., Wang, J., Deng, J. Eco-friendly, disposable bamboo fiber dishware: Static and dynamic mechanical properties and creep behavior. *Industrial Crops and Products*, 2022, 187, 115305.
- [2] Li, L., Li, Z., Han, H., Yang, L., Feng, X., Roli, F., Xia, Z. Wooden spoon crack detection by prior knowledge-enriched deep convolutional network. *Engineering Applications of Artificial Intelligence*, 2023, 126, 106810.
- [3] Golkar, E., Patel, A., Yazdi, L., Prabuwno, A. S. Ceramic tile border defect detection algorithms in automated visual inspection system. *Journal of American Science*, 2011, 7(6), 542-550.
- [4] Safin, R. R., Talipova, G. A., Galyavetdinov, N. R. Design of packaging materials based on polylactide and wood filler. *International Journal of Engineering and Technology (UAE)*, 2018, 7(4.36), 1089-1091.
- [5] Judal, A., Bhadania, A. G. Role of machine vision system in food quality and safety evaluation. *International Journal of Advance Research and Innovation*, 2015, 3(4), 611-615.
- [6] Wandel, M., Bugge, A. Environmental concern in consumer evaluation of food quality. *Food quality and preference*, 1997, 8(1), 19-26.
- [7] Chen, X., Zhong, T., Jiang, H., Wang, J., Chen, F., Wang, G. Recyclable cellulose nanofibrils composite film derived from bamboo fiber tableware waste. *Industrial Crops and Products*, 2023, 205, 117539.
- [8] Semple, K. E., Zhou, C., Rojas, O. J., Nkeuwa, W. N., Dai, C. Moulded pulp fibers for disposable food packaging: A state-of-the-art review. *Food Packaging and Shelf Life*, 2022, 33, 100908.

# RESEARCH ON THE LAUNCH AND RECOVERY METHODS OF UAV

JinHui Ge, RenJun Zhan\*

*Engineering University of PAP, Xi'an 710086, Shanxi, China.*

*Corresponding Author: RenJun Zhan, Email: zhanrenjun@aliyun.com*

**Abstract:** With the continuous progress of science and technology, the UAV launch and recovery method has also undergone an iterative update. Stable and reliable launch and recovery technology determines whether the UAV can play its due operational effectiveness in a modern war. Around the study of UAV launch and recovery, the research status of domestic and abroad is introduced, analyses the corresponding technical principles and gives typical cases. Meanwhile, the advantages and disadvantages of different methods are compared and analysed to provide choices for the methods of UAV launch and recovery. This paper discusses the lack of universality of launch and recovery methods, low cluster launch capability and low technology integration in practical application, and gives suggestions and prospects for technological development, hoping to achieve the further purpose of promoting UAV launch and recovery technology.

**Keywords:** UAV; Launch technology; Recycling technology; Cluster operations; Weaponry

## 1 INTRODUCTION

Unmanned Aerial Vehicle, or UAV, is a kind of aircraft that can fly independently, be driven by its own power and can be used repeatedly [1]. Because it breaks through the physical limitations of human and aircraft pilots, it has gained a broad space for development in the military field, and is widely used in rescue, intelligence gathering, communication interference and reconnaissance and early warning. Compared with the traditional manned aircraft, the UAV has the advantages of small size, simple operation, low production and maintenance cost, and low requirements for combat environment [2-4].

With the update and development of UAV technology, the supporting launch and recovery technology is also constantly innovating. Whether the UAV can be launched safely is directly related to the survival ability, the reuse ability, the combat area adaptability and the flexible response ability of the whole UAV system in the battlefield. The complex and changeable battlefield environment will affect the launch of the UAV, so the safe launch capability is regarded as one of the important indicators to evaluate the UAV [5]. On the other hand, the landing and recovery stage of the UAV occupies a small workload, but in the process of performing the mission, once the failure occurs, it will cause great damage to the UAV. According to statistics, the faults caused by recovery accounted for more than 50% of the total drone failure. Therefore, UAV recovery technology has become one of the key technologies related to the development of UAV. Whether the recovery task can be completed safely is an important indicator to evaluate the performance of UAV [6-7].

The problems existing in the current launch and recovery technology greatly restrict the efficiency of release UAV in combat operations. In order to solve the problems existing in the current UAV launch and recovery device and improve the combat effectiveness of UAV, proposing new launch and recovery technology solutions becomes a key step.

## 2 UAV LAUNCH TECHNOLOGY

Nowadays, the domestic and foreign UAV launch methods are generally divided into the following types: hand throw launch, roll off launch, rocket-booster launch, catapult launch, air launch and vertical take-off launch.

### 2.1 Hand Throw Launch

The hand throw launch method is very simple, just by the operator in a certain direction, like a paper throwing plane to throw the drone to take off. Due to the use of human mode, it is only suitable for small micro or lightweight drones, such as the "Big crow" in the United States, China's "Rainbow" -902, etc.

### 2.2 Roll off Launch

The take-off mode means that the UAV with landing gear takes off along the runway under the thrust of its own engine [8]. Such as the "Global Eagle" of the United States, Australia's "Jindivik" and so on. The advantages of this take-off mode are the simple and reliable structure, mature technology and low ground support pressure; the landing gear increases the weight and volume of the UAV and requires a runway in good condition with poor mobility.

### 2.3 Rocket-Booster Launch

A rocket booster launch is the way that uses the chemical energy generated by the booster to convert it into kinetic energy [9]. Such as "RQ-2" in Israel and "ASN-206" in China. The method generally adopts zero-long emission or short-range guide rail emission [10]. Therefore, it has the advantages of low cost, strong mobility and good environmental adaptability, but the disadvantages of noise, strong light and smoke restrict the large-scale promotion of this method.

## 2.4 Catapult Launch

Ejection take-off launch is the method of converting different forms of energy into kinetic energy to accelerate the UAV to take-off in a certain length of orbit. The source of emission kinetic energy can be divided into elastic potential energy, gas / hydraulic energy and electromagnetic energy. The elastic potential energy emission [11]. With the use of the elastic potential energy of the elastic element to "bounce" into the air, its simple structure and low cost, only suitable for launching micro, light drones, such as the British "cone"; air / hydraulic ejection. It refers to the use of pneumatic / hydraulic pressure catapult to launch the UAV, with a relatively mature and flexible launch technology, such as the British "undead bird"; electromagnetic ejection [12-13]. It refers to the electromagnetic energy generated by electromagnetic field, which has high launch efficiency and is suitable for different types of UAV, but the equipment has high technical requirements and expensive cost, such as China's "HK-5000G".

## 2.5 Air Launch

Air launch refers to the use of aircraft, missiles and other carriers to carry drones into the air in the way and separate the launch. For example, the "MQ-9" Reaper UAV of the United States launched the "Sparrow Eagle" UAV in the air, and the Israeli F-4 hanger carried the "Dille" unmanned, bait aircraft. The simple operation of air delivery reduces the probability of the UAV being intercepted, but the flight carrier should be equipped with ground support facilities, with high maintenance cost and poor mobility.

## 2.6 Vertical Take-off Launch

The vertical take-off launch is different from the above launch method, and the launch direction is perpendicular to the runway and can hover in the air. The power sources of this launch mode can be divided into two categories, one is to take off vertically, the other is to rely on the lift generated by its own rotor, such as "Dragonfly" and "Dragon Warrior" in the United States. This launch method requires no runway and can meet the needs of hover tasks [14], But it only applies to specific types of drones and is not popularized.

Through a comprehensive analysis of the basic principles of the above UAV launch methods, most of them need to power the take-off speed and altitude through different ways at a certain launch site, to make its successful launch. The following Table 1 summarizes the advantages, disadvantages, and typical models of existing launch methods.

**Table 1** Summary of launch methods

Method	Advantage	Disadvantage	Typical models
Hand throw launch	Extremely simple	Only suitable for micro drones, difficult to control during operation	"Big crow" in the United States, China's "Rainbow" -902
Roll off launch	Simple structure, no need for ground support	High runway requirements and large takeoff weight	"Global Eagle" of the United States, Australia's "Jindivik"
Rocket-booster launch	Low cost, strong mobility, and good environmental adaptability	Fuel is difficult to store and transport, and the emission process produces sound, light, and smoke	"RQ-2" in Israel and "ASN-206" in China
Catapult launch	Mature technology, low cost, and good universality	Emission quality is limited	the British "undead bird", China's "HK-5000G"
Air launch	Easy to operate, reducing the probability of drone interception	The carrier needs to be equipped with ground support facilities, resulting in high maintenance costs	the United States launched the "Sparrow Eagle" UAV in the air, and the Israeli F-4 hanger carried the "Dille" unmanned bait aircraft
Vertical take-off launch	No runway required, low launch environment requirements	Only applicable to specific types of drones	"Dragonfly" and "Dragon Warrior" in the United States

### 3 UAV RECOVERY TECHNOLOGY

With the increase of dispatch missions, the UAV is required to be recycled to improve the utilization of a single UAV. Minimal failures in the recovery process can cause damage to the entire drone, so the ability to stabilize the landing and recovery becomes critical. The existing recovery technology mainly includes parachute recovery, recovery of buffer air cushion, interception net recovery, intercept rope recovery, roller run recovery, vertical landing recovery and air recovery [15].

#### 3.1 Parachute Recovery

Parachute recovery refers to the recovery method in which the UAV opens its own parachute after receiving the command and uses the generated air resistance to slow down and land [16-17]. The technology is relatively mature and simple structure, easy to operate, so it is used in light UAV on a large scale. Such as the "fire bee" of the United States, China's "long arrow" and so on. Although the whole recovery is completed by the UAV, without the assistance of ground personnel, its own parachute increases the load of the fuselage, and the landing stage is easy to be affected by the environmental wind, which has a certain risk of failure. According to the landing site, the parachute recovery can be divided into land recovery, water recovery and high-altitude recovery.

#### 3.2 Recovery of Buffer Air Cushion

Buffer air cushion recovery refers to the recovery method of using the airbag carried by the belly position of the UAV machine to form the air cushion when near the ground or water [18], to avoid the violent impact with the contact surface. The recovery method is simple and easy to install, not limited by terrain conditions and the size and weight of the UAV, with strong environmental adaptability, high mobility and low cost; but the structure and material selection of the air cushion will also affect the uncertainty of the recovery success.

#### 3.3 Intercept Net Recovery

Interceptor recovery refers to the use of elastic materials to intercept the UAV in flight and slow it down to zero in a very short period of time, such as the "silver fox" and "killer eagle" in the United States. The interceptor network recovery system usually consists of the interception network, the energy absorption buffer device and the end guide device [19]. This method can be regarded as zero long recovery, which is suitable for fixed recovery in a limited area. The recovery process is stable; but the interception network area is narrow, and the UAV enters the interception network, so the implementation of the method is complicated, with high requirements on operators and is susceptible to environmental factors.

#### 3.4 Intercept Rope Recovery

The interception rope recovery can be divided into horizontal recovery and vertical recovery according to the direction of the rope placement [20], the former needs to install an interception hook in the belly or tail of the UAV, and adjust the flight altitude to buffer the interceptor rope; the latter needs to install the interception hook on the wing tip of the UAV, and recycle it after taxiing operation, such as the "scanning Eagle" in the United States. The two modes are simple in structure, easy to arrange, suitable for narrow areas, and the vertical recovery mode requires low requirements and higher fault tolerance; but they have high buffer performance requirements and high requirements for the control level of the UAV.

#### 3.5 Roller Run Recovery

Roller run recovery is similar to manned landing, which refers to the recovery method of running landing by using the friction between the landing gear and the ground. At the same time, the tail hook can be installed at the tail, and the blocking rope and blocking net can be used to shorten the running distance. Such as Israel's "pioneer", the American's "X-47B" and so on. The runway of this method has low requirements, the UAV bears small overload, and the working process is reliable, but the recovery distance is still long, and the mobility is poor.

#### 3.6 Vertical Landing Recovery

Vertical landing recovery is only suitable for rotor drones or special fixed-wing drones, which use the rotor as a power source, such as China's Red Dragon 850; the latter uses engine thrust to counteract gravity, such as Israel's Hermes-450. This method is not limited by terrain, mobile and flexible, but it is very difficult to develop the thrust vector technology with special fixed wing, and the input cost is high.

#### 3.7 Air Recovery

Air recovery refers to the way for the UAV to slow down and open the hook umbrella and sling while lowering the height after receiving the command, waiting for the manned to approach for recovery [21]. For example, the United

States successfully recovered the "elf" drone in the air on October 29, 2021. The only advantage of this approach is that it does not damage the drone; but the recovery process requires manned pilot proficiency and vulnerability to weather and wind, causing high cost and low success rate.

To sum up, there are many recovery methods for UAV, and the most appropriate methods should be further selected according to the specific requirements to increase the success rate of recovery. The advantages and disadvantages of recycling methods and representative models are summarized in the Table 2 below.

**Table 2** Summary of recovery methods

Method	Advantage	Disadvantage	Typical models
Parachute recovery	The technology is relatively mature and the structure is simple, making it easy to operate	Increase the load on the aircraft body, making it susceptible to environmental wind during the landing phase	"fire bee" of the United States, China's "long arrow"
Recovery of buffer air cushion	Not limited by terrain conditions and the size and weight of drones, with strong environmental adaptability	Uncontrollable inflation process of air cushion	Australia's "Jindivik"
Intercept net recovery	Zero length recycling, suitable for fixed-point recycling in limited areas, with a smooth recycling process	Difficulty in interception and susceptibility to environmental factors	"silver fox" and "killer eagle" in the United States
Intercept rope recovery	Simple structure, easy to arrange, suitable for narrow areas	High requirements for aircraft control capability	"scanning Eagle" in the United States
Roller run recovery	Drones can withstand minimal overload and operate reliably	The recycling distance is still relatively long, and the mobility is poor	Israel's "pioneer", the American's "X-47B"
Vertical landing recovery	Unrestricted by terrain, flexible and maneuverable	Applicable only to specific drones, difficult to develop thrust vector technology	China's Red Dragon 850, Israel's Hermes-450
Air recovery	Will not damage the drone	High cost, requires skilled driver skills, and is susceptible to environmental impact	"elf" in the United States

#### 4 PROSPECT OF UAV LAUNCH AND RECOVERY TECHNOLOGY

With the continuous progress and development of UAV technology, its functions and uses have been continuously expanded, especially the emergence of the concept of cluster operations in the military field makes it a reality to replace the UAV as the main fire point, and the successful launch and recovery has become an important index to evaluate its performance. In recent years, military powers have attached great importance to the research and development of air-launched drones and related testing work. Since 2013, the U.S. Navy has gradually carried out technical research and experimental verification work on launching the Unmanned Targeting Air System (UTAS) based on the P-8A anti-submarine patrol aircraft platform. The Perdix drone cluster project, led by the U.S. Department of Defense, completed demonstration tests of aerial cluster flight and reconstruction in 2016. The Defense Advanced Research Projects Agency (DARPA) of the United States is advancing the concept of distributed air combat and launching the Gremlins air-to-air UAV project. In October 2021, it completed demonstration and verification tasks based on transport aircraft for air launch and recovery, and has preliminary combat application capabilities. Under the guidance of the "Air Launch Effect" project, AERA-I Corporation of the United States has developed the "Agile Launch, Tactically Integrated, Unmanned System" (ALTIUS), an integrated unmanned system. In recent years, it has successively carried out test launch and flight missions on platforms such as helicopters and loyal wingmen. However, in China, this aspect is still in its early stages, and there is relatively little research and literature on it.

Summarize the existing launch and recovery technology, although some methods have been widely used, there are still the following technical problems at this stage [22], need for further research and development.

(1) Lack of universal applicability. Since the emergence of drones, the research on the corresponding launch and recovery methods has been put on the agenda. So far, there are various kinds of UAV launch and recovery methods, each of which has its own applicable model. According to the corresponding launch and recovery methods according to the types of drones, the final results can only be applied to the model, while the complex UAV models lead to the complex launch and recovery methods. Up to now, there is still no launch and recovery method that is generally applicable to various models and meets the requirements of different environments, far from reaching the unity and universal applicability of technology.

(2) The cluster emission level is low. With the wide application of small drones in the military field, how to launch large cluster drones in a short time has become a research hotspot. Most of the existing launch and recovery methods are carried out for a single UAV, and there is more support equipment, long layout time and poor mobility, which greatly reduces the combat efficiency of the UAV. Due to the lack of large-scale launch and high frequency rapid recovery, the progress of UAV group integration is greatly restricted.

(3) The technology integration degree is not high. UAV launch recovery technology is often divided into two areas, the existing launch recovery technology mostly needs two sets of independent device use, greatly increased the drone launch load, and even occupies part of the task load space, reduces the efficiency of the drones, is not only a waste of space, more improve the development cost.

As the UAV tends to high altitude timing, stealth, air combat and swarm, based on the limitations of the existing launch recovery technology, the direction of future technology development is as follows.

(1) In view of the complex and changeable battlefield combat environment in the future, higher requirements are put forward for the adaptability of the launch and recovery environment. Therefore, the development of zero-long launch and precise fixed-point recovery technology has become the key.

(2) According to the requirements of UAV cluster technology, the capacity of large-scale mass launch and high-frequency rapid recovery is taken as the design index requirements, and devices that can continuously launch and achieve rapid recovery are vigorously developed.

(3) In view of the low integration degree of launch and recovery technology, we are required to highly integrate the two technologies, strengthen the integrated design, reduce the waste of UAV space and cost, and promote the development and progress of UAV.

## COMPETING INTERESTS

The authors have no relevant financial or non-financial interests to disclose.

## REFERENCES

- [1] Tao Y J, Li P F. Overview of UAV system development and key technologies. *Aeronautical Manufacturing Technology*, 2014, 20: 34-39.
- [2] Xiao N Z. Analysis of military application of UAV swarm technology. 2020 3rd International Conference on Unmanned Systems (ICUS), 2020, IEEE: 1200-1204.
- [3] Kapustina L, Izakova N, Makovkina E, et al. The global drone market: main development trends. *SHS Web of Conferences*. EDP Sciences, 2021, 129: 11004.
- [4] Jackman A. Consumer drone evolutions: Trends, spaces, temporalities, threats. *Defense Security Analysis*, 2019, 35(4): 362-383.
- [5] Zou X F, He Q H, He J L. UAV development status and related technologies. *Flying missile*, 2006.
- [6] Cui M H, Zhou J J, Chen C. Discussion on key technologies for UAV shipborne applications. *Aeronautical Science and Technology*, 2004, 5: 31-33.
- [7] Kuang S G, Liu D C. An Overview of the development of shipborne UAVs. *Flying missile*, 2003, 2: 16-19.
- [8] Siddiqui B A, Rahman H U, Kumar C, et al. Computer aided modeling and simulation of pneumatic UAV catapult mechanism. 7th International Mechanical Engineering Congress, 2017, 24-25.
- [9] Li H, Xiao Q G, Hu S S. Modeling and simulation of the take-off and launch section of the rocket-propelled UAV. *Journal of Southeast University*, 2010, 40 (9): 136-139.
- [10] Bao C M, Liu C L, Sun Y. UAV launch technology and its development. *Flying missile*, 2012.
- [11] Yang C S, Yin X S, Jiang H N, et al. Research on UAV launching system based on rubber tendon rope ejection. *Modern Manufacturing Technology and Equipment*, 2017, 11: 67-68.
- [12] Bolyukh V F, Kocherga A I, Shchukin I S. Electrodynamic Catapult for Unmanned Aerial Vehicle. 2020 IEEE KhPI Week on Advanced Technology, 2020, IEEE: 159-164.
- [13] Mikhail V S. Drone Launched Short Range Rockets. *Aerospace*, 2020, 7(6).
- [14] Wang G L, Wu Z. Vertical take-off and landing technology and its application in UAV. *Flying navigation missile*, 2006, 06: 20-25.
- [15] Cao L, Geng B B, Zhou L, et al. Research on the development of UAV cluster launch and recovery technology. *Space and Space Defense*, 2019, 2 (02): 68-72.

- [16] Wu H, Wang Z, Zhou Z, et al. Research on dynamics behaviours of small UAV parachute recovery system. *International Journal of Mechatronics and Automation*, 2020, 7(3): 156-164.
- [17] Wu H, Wang Z, Zhou Z, et al. Modeling of small UAV parachute recovery system based on lagrangian method. *2019 IEEE International Conference on Mechatronics and Automation*. 2019, IEEE: 1127-1132.
- [18] Li X B. Air cushion landing system scheme design and landing simulation analysis. 2017, Nanjing: Nanjing University of Aeronautics and Astronautics.
- [19] Pei J H. UAV collision network recovery technology. *Journal of Nanjing University of Aeronautics and Astronautics*, 2009, 12: 6-8.
- [20] Skitmore A. Launch and Recovery System for Improved Fixed-Wing UAV Deployment in Complex Environments. *Unmanned Aerial Remote Sensing*, 2020, 303-316.
- [21] Jorgensen D S, Haggard R A, Brown G J. The Past, Present, and Future of Mid-Air Retrieval. *AIAA* 2005-1673.
- [22] Liu Y B, Xue K, Wang C K. Research on UAV development trend abroad. *Engineering and Testing*, 2020, 60 (03): 41-42,64.

# AIRLINE INTERNATIONAL CREDIT CARD PAYMENT RISK CONTROL SYSTEM

XiangNan Li, DouDou Li\*, LingNan Meng, HaoRan Sun, WeiMing Yi, WeiDong Meng  
*Jiamusi University, Jiamusi 154002, Heilongjiang, China.*  
*Corresponding Author: DouDou Li, Email: ldd@jmsu.edu.cn*

**Abstract:** The article focuses on the theme of "Airline International Credit Card Payment Risk Control System," analyzing the feasibility and advantages of such a system. Based on the discussion of the challenges faced by airlines in international credit card payment risk control, the article proposes an airline international credit card payment risk control system. It provides a detailed description of the system's structure, operational value, and application prospects, aiming to promote the adoption and implementation of the airline international credit card payment risk control system.

**Keywords:** International credit card; Risk control; Airline payments; Fraud prevention; Transaction security; Financial management

## 1 INTRODUCTION

Challenges in Payment Risk Management Faced by Airlines in Global Business Expansion. As the airline industry develops internationally, airlines have increasingly accepted international credit cards as one of the primary payment methods. However, the introduction of international credit card payments brings a series of risks, including but not limited to credit card fraud, transaction disputes, and liquidity risks. These risks pose challenges to the financial security and operational stability of airlines. To effectively manage these risks, airlines need to develop a risk control system for foreign card acquiring. The purpose of this system is to ensure the security of transactions, reduce the occurrence of fraud, and improve liquidity.

## 2 FEASIBILITY OF THE AIRLINE INTERNATIONAL CARD PAYMENT RISK CONTROL SYSTEM

Developing an airline international credit card payment risk control system can improve the efficiency of handling international credit card transactions and reduce fraud risks. This system can help airlines better comply with international payment regulations to ensure transaction security and provide real-time transaction monitoring and analysis to identify and prevent potential fraud.

### 2.1 Technical Aspects

Airlines can leverage existing risk control platforms and integrate the latest security technologies such as artificial intelligence, big data analysis, biometrics, and blockchain to build a comprehensive risk control system. AI and machine learning algorithms can help the system automatically identify abnormal transaction patterns, big data analysis can assess transaction risks, biometrics can enhance identity verification, and blockchain can improve data security and transparency[1].

### 2.2 Regulatory Compliance

The risk control system needs to align with the payment regulations and standards of various countries, such as complying with PCI DSS (Payment Card Industry Data Security Standard)[2]. This ensures that airlines can accept credit card payments from around the world while protecting consumers' financial information. Compliance with regulations and standards can also enhance the airline's credibility and increase consumer trust.

### 2.3 User Experience

The design of the risk control system should simplify processes and minimize unnecessary steps to ensure a fast and convenient payment experience. The system should offer an intuitive and user-friendly interface, enabling users to complete payments easily. Airlines can also provide multilingual customer service support to cater to the needs of consumers from different countries and regions, thereby enhancing user satisfaction and loyalty.

### 2.4 Collaboration and Sharing

Airlines can establish partnerships with payment service providers, banks, and security experts to jointly develop and optimize the risk control system, improving its overall performance and reliability. Through these measures, airlines can offer safer and more convenient payment services to meet the growing demands of international business.

### **3 ADVANTAGES OF THE AIRLINE INTERNATIONAL CARD PAYMENT RISK CONTROL SYSTEM**

#### **3.1 Global Service Support**

The airline International Card Payment risk control system is dedicated to providing global service support. This not only means supporting credit card payments from multiple countries and regions but also deeply adapting to the payment habits, laws, regulations, and financial infrastructures of different countries and regions. The system can handle multiple currencies and provide a multilingual user interface, allowing travelers from different cultures to make payments seamlessly. Additionally, the system is backed by a robust technical support team to ensure 24/7 online service, providing convenient and reliable payment services to travelers regardless of their location[3].

#### **3.2 Real-Time Risk Monitoring**

Real-time risk monitoring is one of the core functions of the system. By integrating a risk management system, it performs in-depth analysis of each transaction, including transaction amount and frequency, location, time, and payment method. This multidimensional analysis helps the system accurately identify fraudulent behavior and take immediate action, such as issuing alerts or intercepting suspicious transactions, to protect the interests of both the airline and travelers.

#### **3.3 Intelligent Decision Engine**

The intelligent decision engine is the heart of the system. It uses advanced algorithms and AI technology to analyze transaction patterns, self-learn, and optimize to improve fraud detection accuracy and efficiency. The system can make automatic decisions to reduce reliance on manual intervention and predict potential risk points by analyzing vast amounts of historical and real-time data, achieving preventive risk management. This proactive risk management approach helps airlines control risks more effectively and reduce potential losses.

#### **3.4 Customized Risk Control Strategies**

Airline businesses are diverse, with a broad customer base, necessitating a system capable of tailoring risk control strategies based on specific characteristics. This includes risk management for different flights or passenger classes and addressing the personalized risk control needs of frequent flyers and corporate clients. The system should offer advanced configuration tools, allowing airlines to adjust risk control rules and thresholds according to actual conditions, ensuring the precision and flexibility of risk management strategies.

#### **3.5 User-Friendly Interface**

To enhance operational efficiency and user satisfaction, the system should feature an intuitive and easy-to-use interface. The interface should provide clear operation guides and prompts, enabling users to complete various operations effortlessly and reduce errors and misunderstandings. The system should also support a multilingual interface to cater to users from different countries and regions, enhancing the overall user experience. The design should consider the varying technical proficiency levels of users, offering simplified operation processes to ensure that even non-technical users can easily master and use the system.

### **4 CHALLENGES IN AIRLINE INTERNATIONAL CREDIT CARD PAYMENT RISK CONTROL**

#### **4.1 High Transaction Fees**

When airlines use international credit card payment services, they typically need to pay a certain percentage of transaction fees, which may vary depending on the card type, transaction amount, and acquiring institution's policies. These fees often increase the airline's costs. For instance, some credit card companies may charge higher fees for international transactions, posing an additional financial burden for airlines operating across borders. Since these costs are unavoidable, airlines may choose to pass these fees onto consumers, potentially raising ticket prices and affecting consumer purchasing decisions.

#### **4.2 Long Settlement Cycles**

The settlement cycle for international credit card payments is usually long, which can negatively impact an airline's cash flow management. After a transaction occurs, airlines must wait for a period before receiving the funds, during which their capital is tied up and cannot be used for other potentially rewarding activities. A long settlement cycle can also lead to difficulties in financial planning, such as shortages when paying suppliers, employee salaries, and other operating costs.

### 4.3 Exchange Rate Uncertainty

Issues related to exchange rates can create uncertainty for airlines. When converting foreign currencies amidst fluctuating exchange rates, airlines may face exchange rate losses[4]. Additionally, different acquiring institutions may have varying exchange rate policies, making it difficult for airlines to predict and control conversion costs. This uncertainty affects cost control and can influence ticket prices, affecting consumer purchase decisions.

### 4.4 Insufficient International Credit Card Payment Capabilities

Some airlines may not have direct access to international credit card networks, limiting their ability to accept international credit card payments. This limitation can result in lost potential customers, especially in scenarios requiring convenient payment methods. A lack of international credit card payment capabilities can also affect an airline's competitiveness in the market.

### 4.5 Risks of Card Theft and Chargebacks

Despite having certain risk assessment and management systems, airlines still face risks of card theft and chargebacks. Credit card fraud can lead to financial losses for airlines and erode consumer trust. Chargeback situations may result in airlines being unable to recover sales revenue, impacting their financial health. To mitigate these risks, airlines must continuously update and optimize risk management strategies to ensure transaction security and reliability.

## 5 COMPOSITION OF THE AIRLINE INTERNATIONAL CREDIT CARD PAYMENT RISK CONTROL SYSTEM

### 5.1 Integration with Airline Information Systems

Constructing an airline international credit card payment risk control system requires deep integration with the airline information system to meet the risk management needs of domestic airlines when accepting international credit card payments. The airline information system, developed by China Civil Aviation Information Group Corporation, includes functions such as flight sales, reservations, departures, and operational control but lacks support for international credit card payment controls. To effectively operate the risk control system, professionals need to conduct secondary development of the airline information system to add international credit card payment risk management and control functions.

This integration project combines the risk control system with the airline information system to enhance the security and efficiency of handling international credit card transactions. By introducing international credit card payment controls, the system can effectively monitor and manage payment process risks, including preventing credit card fraud and managing transaction chargebacks and theft. Additionally, integrating the risk control system can optimize the payment process, improve transaction processing speed, reduce manual operation errors, and enhance overall service quality. Achieving this goal requires cooperation with professional payment service providers to jointly develop and refine international credit card payment controls. This involves technical adjustments and upgrades to the airline information system to support new international credit card payment functions. The risk control system also needs to have real-time monitoring and transaction data analysis capabilities to take timely action when issues arise.

By implementing this integration, airlines can establish a comprehensive international credit card payment risk control system to effectively reduce payment process risks and protect the interests of both the company and consumers. This also helps enhance the airline's brand image and competitiveness in domestic and international markets.

### 5.2 Integration with Acquiring Bank's 3D Verification System

In the airline international credit card payment risk control system, the acquiring bank's 3D verification system is a key component. Its primary function is to verify the authenticity of credit card transactions and the cardholder's identity. By sending the credit card number, expiration date, and security code (typically CVV2/CVC2) to the issuing bank or relevant authentication center for verification, it ensures that the transaction is authorized by the cardholder. The 3D verification system usually adopts industry-standard security protocols, such as ISO/IEC 8785-2:1999, which defines standardized methods for data exchange in an Open Systems Interconnection (OSI) environment.

During the transaction process, the airline's risk control system will transmit key credit card information to the acquiring bank's 3D verification system, which then forwards this information to the issuing bank or authentication center for verification. The verification process includes checking the card information and may also involve further authentication of the cardholder's identity through SMS verification codes, one-time passwords (OTP), or other methods. This process helps ensure transaction security and reduces the chargeback rate due to unauthorized transactions.

By incorporating the 3D verification system, airlines can significantly reduce the risk of credit card transactions and improve transaction success rates.

### 5.3 Integration with Acquiring Bank's Payment System

The integration of the acquiring bank's payment system with the risk control system is a critical aspect of the airline international credit card payment risk control system. This process involves sending key information such as credit card numbers, expiration dates, and transaction types to the acquiring bank's payment system. This step requires accurate information transmission and ensuring the security and efficiency of the data transfer.

During the integration process, the risk control system communicates with the acquiring bank's payment system through a series of interfaces, which may include XML-based API calls, JSON-format data transmission, or other communication protocols suitable for the payment industry. The risk control system packages the collected transaction information into an appropriate format and sends it to the acquiring bank's payment system through these interfaces.

Upon receiving the information, the acquiring bank's payment system processes it, including verifying the credit card's validity, checking if the transaction amount exceeds the credit card's limit, and identifying any suspicious transaction behavior. The payment system also handles the authorization request for the transaction, confirming whether sufficient funds are available to complete the transaction and generating an authorization code. This process may also involve the issuing bank.

The risk control system waits for the payment system's response and uses callback interfaces to determine whether the transaction is successful. If the transaction is successful, the risk control system records the relevant transaction information and continues monitoring the transaction to prevent potential fraud. If the transaction fails, the risk control system processes accordingly, such as notifying the airline's customer service department, recording abnormal transaction information, or taking other risk control measures.

The smooth operation of this integration is crucial to the entire risk control system, directly affecting the transaction's security, efficiency, and customer experience. Therefore, airlines need to ensure that the integrated payment system is stable, reliable, and capable of timely updates to adapt to the ever-changing payment security standards and regulatory requirements.

#### **5.4 Internal Verification Module of the Risk Control System**

The internal verification module is a core component of the airline international credit card payment risk control system. It establishes and maintains a blacklist mechanism through various means and uses artificial intelligence technology to dynamically analyze the security of the user's payment environment, identifying and blocking potential fraudulent transactions.

The blacklist mechanism is one of the fundamental defense measures in the risk control system. It constructs a database of common transaction characteristics used by fraudsters by collecting and updating information such as bad IP addresses and stolen user card BINs (Bank Identification Numbers). When user transaction information matches this blacklist data, the system immediately issues a warning, takes further verification measures, or directly blocks the transaction.

The internal verification module also employs AI and machine learning technologies to conduct real-time analysis and pattern recognition of user payment behavior. These technologies help the system better understand the differences between normal transactions and fraudulent activities, effectively identifying potential fraud risks even without obvious blacklist information.

The system dynamically analyzes the user's payment environment, including the geographical location of the IP address, device fingerprint information, and abnormal transaction times, to assess transaction security. For example, if a user suddenly conducts transactions from an IP address in another country or initiates transactions on a device that does not usually use electronic payments, these could be considered signs of fraud.

When the internal verification module identifies potential fraud risks during the initial transaction stage, it takes corresponding measures, such as delaying the transaction, sending additional verification information to the user, or directly blocking the transaction, preventing financial losses for the airline and protecting consumers' payment security.

### **6 OPERATION MECHANISM AND PROSPECTS OF THE AIRLINE INTERNATIONAL CREDIT CARD PAYMENT RISK CONTROL SYSTEM**

#### **6.1 Operation Mechanism of the Airline International Credit Card Payment Risk Control System**

This project is based on secondary development on the Travelsky GDS platform. When airlines conduct international credit card payment business, they call this system's payment interface, transmit payment amounts, acquiring methods, and passenger information to the system, and input card numbers, expiration dates, security codes, and cardholder names through a web page. In the North American region, international credit cards support postal code verification, so for this region, additional verification of billing address and postal code is required. Once verification is passed, it proceeds to the next step.

The system performs multifactor portrait analysis of the IP address and network environment. If the risk verification level is low, it sends the card number, expiration date, and security code information to the acquiring bank interface, redirecting to the issuing bank's 3D verification page for 3D verification. If the risk verification level is medium, the system performs 3D verification and then returns the information to the airline system for secondary manual review to determine if on-site card verification at the airport is necessary. If the risk verification level is high, the transaction is rejected, and the risk control system returns a result of REJECT.

After passing 3D verification, the system sends an authorization command to the acquiring bank. If authorization is successful, the system returns the card number, authorization code, and expiration date information to the airline system. After ticketing, the system modifies the Form of Payment section in the ticket information to CC (credit card) and indicates the card number and expiration date. For medium risk levels, the system writes the ticket information into the PNR as a REMARK. When the passenger checks in at the airport, the departure system displays the REMARK information for further verification.

## 6.2 Prospects of the Airline International Credit Card Payment Risk Control System

The application prospects of the airline international credit card payment risk control system are very promising. With the continuous advancement of globalization and digitalization, airlines and various travel service providers will increasingly rely on electronic payment methods, especially international credit card payments. Therefore, an efficient and reliable risk control system becomes a necessary tool to ensure transaction security, safeguard enterprise interests, and enhance customer experience. In the future, the application of the airline international credit card payment risk control system will be further promoted and applied in the following aspects:

- **Cross-Border Transaction Security Assurance:** With the internationalization of the aviation industry, airlines will face more transactions from different countries and regions, bringing various security risks. The risk control system can help airlines effectively identify and prevent fraudulent activities in cross-border transactions, ensuring fund security.
- **Personalized and Intelligent Services:** Utilizing big data analysis and AI technology, the airline international credit card payment risk control system can not only prevent fraud but also provide personalized payment services based on customer behavior patterns, further enhancing customer experience.
- **Risk Management and Loss Control:** Through real-time monitoring and analysis of transaction data, the airline international credit card payment risk control system can help airlines better manage risks, promptly identify abnormal behaviors, and reduce fraud losses.
- **Adaptation to Emerging Payment Methods:** With the rise of mobile payments, digital currencies, and other emerging payment methods, the airline international credit card payment risk control system must continuously update and optimize to adapt to these new payment trends, ensuring airlines are not left behind by advancements in payment technology.

## CONCLUSION

The airline international credit card payment risk control system is not only essential for current business security but also a critical tool for addressing future challenges in the payment sector. As technology continues to advance and application scenarios expand, such risk control systems will play an increasingly important role in the aviation industry and other sectors.

## COMPETING INTERESTS

The authors have no relevant financial or non-financial interests to disclose.

## REFERENCES

- [1] Zheng Xin. Research on the Issues of Passenger Fund Settlement and Clearing Management in Chinese Airlines Based on E-commerce. University of International Business and Economics, 2015.
- [2] Tian Yuan. Research on Risk Control of Online Payment for International Credit Cards by Domestic Airlines. Shandong University, 2024-06-13.
- [3] Zhao Xuwei. Analysis and Prevention Strategies of Credit Card Business Risks. 2024-06-13.
- [4] Ji Xiaojie. Exploration and Reflection on Digital Transformation of Credit Card Risk Control Empowered by UnionPay Data. China Credit Card, 2022(7): 21-26.

# INVESTIGATION ON THE REMOVAL OF SE(IV) FROM AQUATIC SYSTEMS USING ORGANIC AND INORGANIC SORBENTS

CaiYu Liu<sup>1</sup>, ZhongShan Zhao<sup>1,\*</sup>, Yue Sun<sup>1</sup>

<sup>1</sup>College of Chemistry and Chemical Engineering, Qingdao University, Qingdao 266000, Shandong, China.

\*Corresponding Author: ZhongShan Zhao, Email: 1454320732@qq.com

**Abstract:** Among various selenium (Se) species in water, Se(IV) poses a greater toxicity due to its unique structural characteristics. To address the contamination issue posed by Se(IV) more effectively, this study employed a hydrothermal synthesis method to create an inorganic metal material, specifically a Mg–Al layered double hydroxide (Mg–Al–CO<sub>3</sub> LDH). Meanwhile, the organic material, silk fibroin (SF), was synthesized via a lithium bromide approach. Scanning electron microscopy (SEM) was utilized to characterize the morphology and structure of the fabricated materials, confirming the successful preparation of both Mg–Al–CO<sub>3</sub> LDH and SF as adsorbents. Through adsorption experiments, their efficacy in removing Se(IV) was investigated, with results revealing that both Mg–Al–CO<sub>3</sub> LDH and SF demonstrate notable adsorption capacities for Se(IV). Specifically, the adsorption capacity of LDH towards Se(IV) was measured at 29 mg/g, while SF exhibited a capacity of 16 mg/g. Notably, the two adsorbents synthesized in this research offer significant advantages: they are environmentally friendly, low cost and their synthesis procedures are straightforward, thereby showcasing high potential for the remediation of Se(IV) in its anionic form from contaminated aqueous environments.

**Keywords:** Mg–Al–CO<sub>3</sub> LDH; Silk fibroin; Se(IV); Removal performance

## 1 INTRODUCTION

In recent years, the advancement of industrialization has led to frequent occurrences of Se overloads in industrial wastewaters, posing a severe threat to human health. Excessive exposure to Se not only inflicts damage to the respiratory system but also elevates cancer risks, leading to grave health consequences. Consequently, the hazardous nature of Se has garnered global attention. Classified as a metalloid element, Se shares similarities with sulfur and exists in four principal forms in aquatic environments. Among these, Se (IV) exhibits the most toxicity due to its unique molecular structure. Hence, developing an effective, economical, safe, eco-friendly, and efficient method for Se removal is of paramount importance. Various techniques have been explored for this purpose, including coprecipitation, ion exchange, coagulation, electrochemical methods, membrane separation, and adsorption, among which adsorption stands out due to its simplicity, technological maturity, energy efficiency, making it a pivotal technology in water purification. [1] Central to the adsorption process is the identification of a suitable adsorbent material. [2] An ideal adsorbent must not only demonstrate high adsorption efficiency but also be economically viable, sustainable, and environmentally benign.

In recent times, researchers have been incessantly exploring and fabricating diverse types of adsorbents to tackle the challenges presented by heavy metals and metalloid contaminants in water treatment. Adsorbent materials can broadly be categorized into two classes: organic and inorganic adsorbents. Organic adsorbents, SF standing out among them. Owing to its excellent properties, wide availability, low cost, good biocompatibility, and biodegradability, SF has emerged as a promising eco-friendly material, attracting substantial attention in recent years. The abundance of functional groups on the surface serves as efficacious adsorption sites, has great application potential its potential in water purification. Inorganic adsorbents such as LDH, it's a class of uniquely structured anionic clay materials. LDH boast simple synthesis procedures, high specific surface areas, ordered porous structures, good biocompatibility, strong anion exchange capabilities, and exceptional stability and regenerability, [3] positioning them as efficient,

environmentally friendly, and cost-effective adsorbents.[4]

In alignment with the aforementioned context, our research utilized readily available and inexpensive raw materials, adopting green and safe preparation methods to synthesize two distinct types of adsorbents, SF and Mg-Al-CO<sub>3</sub> LDH. SEM was employed to examine the microstructures of both materials, with images vividly illustrating the anticipated structural features, thereby validating the efficacy of our synthesis methodologies. Ultimately, the adsorptive performance of these two materials towards Se(IV) was evaluated.

## 2 EXPERIMENT SECTION

### 2.1 Materials and Equipment

Lithium bromide (LiBr, 99%, Shanghai Hushi Chemical Co., Ltd.), sodium carbonate (Na<sub>2</sub>CO<sub>3</sub>, 99.5%, Shanghai Hushi Chemical Co., Ltd.), sodium selenite (Na<sub>2</sub>SeO<sub>3</sub>, 99.5%, Shanghai Hushi Chemical Co., Ltd.), Aluminum nitrate hexahydrate (AlCl<sub>3</sub>·6H<sub>2</sub>O, 99.99%, Aladdin reagent Co., Ltd.), magnesium chloride hexahydrate (MgCl<sub>2</sub>·6H<sub>2</sub>O, 98%, Aladdin reagent Co., Ltd.), sodium hydroxide (NaOH, 96%, Aladdin reagent Co., Ltd.). The concentration of Se(IV) in supernatant was determined by inductively coupled plasma emission spectrometry (ICP-OES, Avio 200). Scanning electron microscopy (SEM) images were taken on the Quanta 250 FEG (SEM).

### 2.2 Preparation of Organic Material

The process of synthesis of SF aqueous solution is shown in Figure 1. Firstly, the chopped silkworm cocoons was boiled in 0.5wt% Na<sub>2</sub>CO<sub>3</sub> solution for degumming, during which time it was constantly stirred for 30 minutes and repeated twice. The cooked silk was then rinsed several times in a beaker filled with deionized water to remove sericin and residual ions. After the degumming, the SF were pulled loose and dried at 50°C to get the degumming silk.

After the above operation, the degumming silk was dissolved by lithium bromide, and 0.5g deglumed silk was put into a centrifuge tube, and 9.3 M lithium bromide solution was added, and then heated and stirred in a water bath at 60°C for 4h to obtain a transparent and viscous SF solution. The obtained SF solution was centrifuged at low speed, and the insoluble matter and bubbles in the solution were removed and put into a dialysis bag for dialysis with ultra-pure water for three to four days. The supernatant was centrifuged and freeze-dried to obtain the regenerated SF.



**Figure 1** Diagram for preparation process of SF aqueous solution

### 2.3 Preparation of Inorganic Materials

The synthesis of the Mg-Al-CO<sub>3</sub> LDH adsorbent was carried out via a widely-employed and straightforward hydrothermal method. A series of Mg-Al-CO<sub>3</sub> LDH nanomaterials with varying molar ratios of Mg<sup>2+</sup>/Al<sup>3+</sup> ranging from 1 to 5 were fabricated in the experiment. Initially, quantified amounts of MgCl<sub>2</sub>·6H<sub>2</sub>O and AlCl<sub>3</sub>·6H<sub>2</sub>O were mixed in deionized water at molar ratios of 1.0, 2.0, 3.0, 4.0, and 5.0 to form a mixed metal salt solution. Under vigorous magnetic stirring at room temperature, a combined solution of Na<sub>2</sub>CO<sub>3</sub> and NaOH was gradually added to the above mixture until the pH of the reaction mixture was maintained above 10. Subsequently, after continuous stirring for two hours at room temperature, the mixture was transferred to a reaction kettle and heated at 170°C for 17 hours. Upon cooling to room temperature, the resultant white precipitate was collected by centrifugation, washed several times with deionized water and ethanol, and finally dried in an oven at 50°C.

## 2.4 Microstructure of SF

The microscopic morphology of SF was analyzed by SEM, and the observation results were shown in Figure 2. The SEM image clearly reveals the fine structure inside the SF material. SF is composed of numerous interwoven and connected filament fibers, which presents a complex winding state. In particular, some areas showed that SF had been successfully stripped to form SF nanofibers, indicating that degumming and subsequent treatment effectively exposed the nanoscale structure of fibroin. However, a certain degree of heterogeneity in the length of SF nanofibers was also observed, suggesting that there may be some randomness or control challenges in the process of fiber dissociation or preparation.

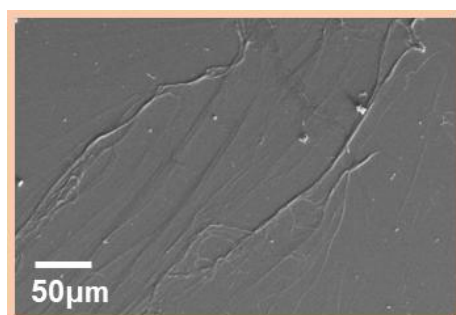


**Figure 2** SEM images of SF

## 2.5 Microstructure of Mg-Al-CO<sub>3</sub> LDH

The microstructure and structure of Mg-Al-CO<sub>3</sub> LDH with Mg<sup>2+</sup>/Al<sup>3+</sup> ratio of 3 were investigated by scanning electron microscopy (SEM), and the observed results were shown in Figure 3. It can be clearly seen in the figure that the prepared LDH material presents a typical hexagonal sheet structure with regular edges and intact structure, which directly confirms the success of LDH material synthesis. Each layer structure is evenly distributed, showing good crystallinity and order, which is crucial for understanding the interaction mechanism of LDH materials and its application properties in adsorption, catalysis and other fields.

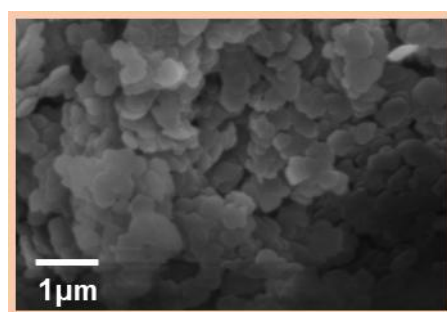


**Figure 3** SEM mages of Mg–Al–CO<sub>3</sub> LDH

## 2.6 Se(IV) Concentration Determination

The concentration of Se(IV) in water was quantitatively analyzed using ICP-OES to establish an accurate standard curve, with standard solutions prepared over a concentration range of 0-80.00 mg/L. As illustrated in Figure 4, the tested standard curve was obtained with a correlation coefficient reaching 0.999, indicating excellent linearity.

During the adsorption process, Na<sub>2</sub>SeO<sub>3</sub> powder was dissolved in deionized water to prepare a stock solution of 1000 mg/L Se(IV). Thereafter, this stock solution was utilized for conducting adsorption experiments to attain an initial Se(IV)

concentration of 50 mg/L. Upon completion of each experiment, samples of the supernatant were taken for determining the residual Se(IV) concentration.

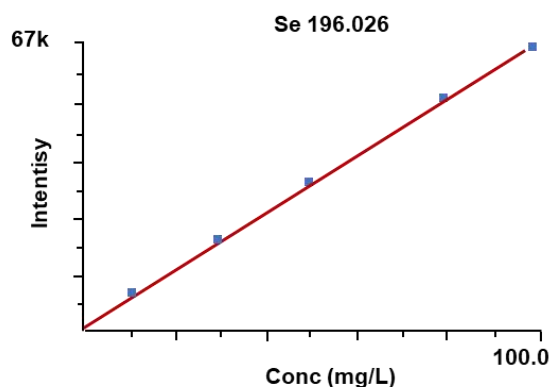


**Figure 4** Standard curve of Se(IV) concentration

## 2.7 Adsorption Experiment

It was discovered that pure SF exhibited an adsorption capacity of 16 mg/g for Se(IV). As depicted in Figure 5, the influence of varying  $Mg^{2+}/Al^{3+}$  molar ratios on the adsorption performance of Se(IV) was investigated. The findings revealed that as the molar ratio of  $Mg^{2+}/Al^{3+}$  increased from 1.0 to 5.0, there was a corresponding ascending trend in the adsorption capacity, followed by a decline as the ratio continued to increase beyond 3. Notably, when the  $Mg^{2+}/Al^{3+}$  molar ratio was precisely 3, the highest adsorption capacity of 29 mg/g was observed. This observed trend is potentially attributed to the fact that with an increment in the molar ratio, the formation of a more orderly structured LDH leads to an increased exposure of adsorption sites, thus enhancing the overall adsorption capacity.

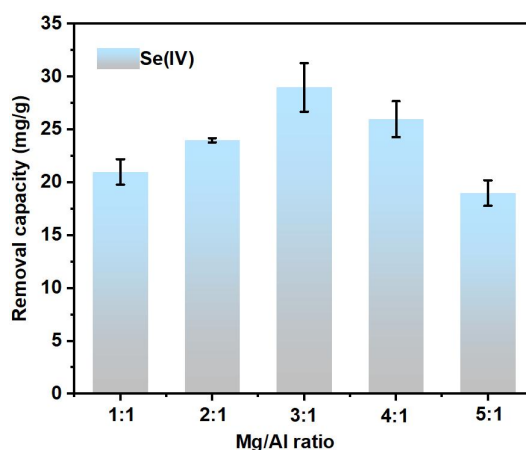


**Figure 5** Influence of Varied Mg/Al ratios on the adsorption performance of Se(IV)

## 3 CONCLUSION

This study successfully developed two adsorbent materials, SF and Mg-Al-CO<sub>3</sub> LDH, for the removal of Se(IV) from aqueous solutions. SF exhibited an adsorption capacity of 16 mg/g for Se(IV), while the Mg-Al-CO<sub>3</sub> LDH demonstrated a higher capacity of 29 mg/g when the molar ratio of  $Mg^{2+}/Al^{3+}$  was set at 3. The inherent nature and structural characteristics of SF contribute to its favorable adsorption performance. Meanwhile, the unique layered structure of Mg-Al-CO<sub>3</sub> LDH facilitates the effective adsorption of Se(IV). Both synthesis processes are characterized by simplicity, environmental friendliness, and economic viability, thereby presenting novel strategies for the mitigation of Se(IV) contamination.

Through comprehensive experimental evaluations and meticulous analyses, the adsorption efficiency of these materials was validated, establishing their potential application in water treatment. Future research endeavors can delve deeper into the adsorption mechanisms, refine operational conditions, and facilitate the practical application of these materials, thereby addressing the challenge of selenium pollution in the environment.

### COMPETING INTERESTS

The authors have no relevant financial or non-financial interests to disclose.

### REFERENCES

- [1] Taka A L, Klink M J, Mbianda X Y, et al. Chitosan nanocomposites for water treatment by fixed-bed continuous flow column adsorption: A review. *Carbohydrate Polymers*, 2021, 255: 117398.
- [2] Keshvardoostchokami M, Majidi M, Zamani A, et al. A review on the use of chitosan and chitosan derivatives as the bio-adsorbents for the water treatment: Removal of nitrogen-containing pollutants. *Carbohydrate polymers*, 2021, 273: 118625.
- [3] Goh K H, Lim T T, Dong Z. Application of layered double hydroxides for removal of oxyanions: a review. *Water research*, 2008, 42(6-7): 1343-1368.
- [4] Guan X, Yuan X, Zhao Y, et al. Application of functionalized layered double hydroxides for heavy metal removal: A review. *Science of The Total Environment*, 2022, 838: 155693.

# RESEARCH ON TALENT CULTIVATION IN CYBERSECURITY UNDER THE BACKGROUND OF NEW ENGINEERING DISCIPLINES

Xiong Wei, BangChao Wang\*, Hang Luo, YingKai Yuan

*School of computer Science and Artificial Intelligence, Wuhan Textile University, Wuhan 432022, Hubei, China.*

*Corresponding author: BangChao Wang, email: 576728902@qq.com*

**Abstract:** In the current rapid and stable economic operation, network security is an important cornerstone to safeguard national security and the interests of the people. The rapid development of new technologies and applications such as blockchain, virtual reality, smart IoT, and artificial intelligence has spawned a series of new formats and models. In the context of the new engineering disciplines, there exist problems in the cultivation of talents in the field of network security, such as insufficient integration of disciplines, lack of teaching staff, and insufficient cultivation of comprehensive qualities. This paper explores the cultivation methods of talents in the field of network security under the background of the new engineering disciplines from three aspects: strengthening the practical ability of interdisciplinary integration, expanding international perspectives and continuous learning ability, and cultivating teamwork and social responsibility.

**Keywords:** New engineering disciplines; Interdisciplinary integration; Network security

## 1 INTRODUCTION

President Xi's speech at the first meeting of the Central Leading Group on Cyber Security and Informatization in February 2014 stated that without cyber security, there would be no national security, no stable economic and social operations, and it would be difficult to protect the interests of the broad masses of the people [1]. President Xi pointed out in the "Speech at the National Symposium on Cyberspace Security and Informatization Work" in April 2018 that "cyberspace security and informatization are strategic issues for national security and development, a new field of military struggle, and an opportunity to win." , New means of winning from the commanding heights "The importance of cyberspace security has become increasingly obvious in today's digital society. With the popularization of the Internet and the rapid development of information technology, the network has become the core infrastructure in various fields such as business, government, education, and social networking. Cultivating and possessing high-quality cyberspace security talents is crucial. These professionals can ensure the security of network systems and prevent and respond to various network threats.

### 1.1 Cyberspace Security

Cyberspace security is a discipline dedicated to the study and practice of protecting the security of network systems, data and communications. It covers many aspects, including network security, information security, computer security, cryptography, etc. Students majoring in cyberspace security usually need to learn computer science, network technology, information security regulations, risk management and other related knowledge. After graduation, they can work as network administrators, information security analysts, security engineers, risk management experts and other positions in various organizations, providing network security protection services for enterprises and government agencies [1]. There are certain differences between the three majors of cyberspace security, information security and network security. The foothold of cyberspace security lies in space, namely the four major areas of sea, land, air and space. The foothold of information security lies in information, the security of information during transmission, that is, the security of the information itself, uninterrupted, not tampered with, intercepted, and generally refers to various information and data. The foothold of network security lies in the entire network, ensuring the normal operation and security of the network.

### 1.2 Importance of Cyber Security

The importance of cyberspace security has become increasingly apparent in today's digital society. Especially its importance to individuals, organizations and society is becoming more and more obvious:

First, individuals generate a large number of digital footprints on the Internet, including personal information, social media activities, financial transactions, etc. The importance of cyberspace security lies in ensuring that personal privacy is not illegally accessed and abused. Secondly, cyberspace security ensures the safety of online banking, electronic payment, financial fraud, and e-commerce activities, and prevents the theft and abuse of financial information. Enterprises and organizations store and transmit a large amount of sensitive information on the Internet, including business plans, research and development results, customer data, etc. The maintenance of cyberspace security ensures that these business secrets are not accessed and leaked without authorization [1].

In the digital economy era, enterprises and countries rely on the Internet for business activities. Maintaining cyberspace security helps create a safe, stable and trustworthy network environment, promoting economic development and business activities. In cyberspace, the integrity of information is crucial. Cyberspace security ensures that information is not tampered with during transmission and storage, and maintains the credibility of information[4][5]. The country's critical infrastructure, government agencies and military systems all rely on the Internet. Maintaining cyberspace security is crucial to national security and can prevent threats such as cyber attacks and information warfare. The importance of cyberspace security lies in preventing all kinds of cyber crimes, including online fraud, telecommunications fraud, and malware propagation. This helps protect individuals, businesses and society from criminals.

Maintaining cyberspace security helps prevent and respond to various types of cyber attacks, including malware, ransomware, distributed denial of service attacks, etc. As a global network, the importance of cyberspace security is related to cooperation and exchanges between countries. Ensuring the security of cyberspace helps promote global connectivity, international cooperation and information sharing.

Cyberspace security is vital to individuals, businesses and society as a whole, and its maintenance involves many aspects of technology, regulations and awareness. With the continuous development of science and technology, the importance of cyberspace security will continue to increase.

### 1.3 The Importance of Cultivating Cyberspace Security Professionals

Talent is the key to the competition in cybersecurity. The key to a clean and clear cybersecurity space lies in people and relies on people. My country has a huge population of 710 million people on the cyber front, and the construction of a security protection network cannot be separated from professional core talents[3]. During the 2019 National Cybersecurity Publicity Week, General Secretary President Xi made important instructions to adhere to the integrated development of cybersecurity education, technology, and industry, and to form a benign ecology of talent training, technological innovation, and industrial development[4]. In the current global cyberspace competition, cyberspace security technology and talents are the red line of absolute discourse power and sovereign security.

According to the Internet Security Report, my country's major industries currently need about 700,000 cybersecurity talents of all kinds, with a gap of 95%. It is estimated that by 2027, there will be a gap of 3.27 million cybersecurity personnel in my country, while the talent training scale of colleges and universities is 30,000 per year. Many industries are facing a serious shortage of cybersecurity talents[1]. In this sense, instead of calling for "talents in all kinds of ways", it is better to "cultivate talents in all kinds of ways". Although there are some "hackers", this requires systematic professional training under the background of new engineering. There is a serious lack of truly original and systematic high-level talents. "The training of cyberspace security talents in the teaching and scientific research system is a key move to occupy the high ground of cybersecurity[6].

In 2016, my country awarded a large reward to cybersecurity talents for the first time, which shows that the country attaches great importance to professional, leading and compound talents in the field of cybersecurity. Cyberspace is the fifth territory to be explored after land, sea, air and space. If we take the lead in occupying the talent high ground and building a talent echelon, the cyber world will return to rationality and order, and the vast dream will be more smoothly reflected in reality.

## 2 TRAINING OF CYBERSPACE SECURITY TALENTS AT HOME AND ABROAD

According to the White Paper on the Practical Capabilities of Cybersecurity Talents issued by the Ministry of Education, by the end of 2021, 215 universities in my country have opened cybersecurity majors, more than 60 universities have established cyberspace security colleges, 11 universities have been approved as national first-class cybersecurity colleges, 37 universities have been approved as first-level doctoral programs in cyberspace security, and 16 universities have established cyberspace postdoctoral research stations [8][9][14]. The cyberspace security major of Beijing Institute of Technology cultivates high-quality engineering and technical talents who are oriented towards the field of cyberspace security, can serve national strategies, meet the needs of economic and social development, have lofty ideals and beliefs, excellent professional knowledge, sound physical and mental personality, profound humanistic qualities, broad international vision, can propose, analyze and solve complex engineering problems with a systematic perspective, and are competent for scientific exploration, technical research, product development, education and teaching, and management work in this professional field and related fields. Beihang University has signed strategic cooperation agreements with 18 cybersecurity companies, including 360 Technology, Qi'anxin, Tencent, Venusstar, and Sangfor, to cooperate deeply with cybersecurity companies, jointly educate talents, and jointly tackle key problems. Focusing on the four directions of discipline construction, we have made great progress in talent training goals, curriculum setting, textbook compilation, and practice. Strengthen cooperation in teaching, research and other aspects.

The 2023 Corporate Cybersecurity Compliance Survey Report released by the UK Department of Science and Technology shows that 32% of small and medium-sized enterprises have suffered data leaks and security attacks in the past 12 months. The average cost of corporate network application violations is £1,100, and the average cost for large and medium-sized enterprises is £4,960. In order to deal with cyberspace security, the British government has taken a series of measures to establish a certification training program to improve the professional level of professionals engaged in cybersecurity and information assurance; strengthen postgraduate education and expand the pool of experts

with cyberspace security expertise; and establish a cybersecurity research institute to conduct research to confirm the model, nature and extension of cybersecurity skills [10][11]. The demand for cybersecurity talents in the government, public sectors and industry is still growing [4]. The United States has a very mature management and talent training system and has established a high-level cybersecurity talent training system. For example, it has classified and formulated a standardized framework for the training of cyberspace security professionals in accordance with various knowledge and ability spectrums in the field of cybersecurity, and focused on practical ability training. In addition, in order to meet the needs of the government and society for urgently needed cybersecurity talents, the United States has broken through the obstacles in the management mechanisms of powerful departments and some public sectors. For example, the U.S. Department of Defense's Cyber Special Operations (CES) and the Department of Homeland Security, which is responsible for civilian critical infrastructure, have begun to play a role in setting up similar personnel sequences.

### 3 DEFICIENCIES IN THE TRAINING OF CYBERSPACE SECURITY TALENTS

Although both China and foreign countries have increased their efforts in the training of cyberspace security professionals, due to some reasons, the training of cyberspace security talents faces a series of defects, which may affect students' actual abilities and their ability to adapt to industry needs.

- (1) Outdated curriculum. The cybersecurity curriculum of some colleges and universities lags behind industry demand and cannot reflect emerging technologies and threats in a timely manner, resulting in students lacking the latest practical application knowledge after graduation[7][8].
- (2) Insufficient practical experience. Some training institutions and universities lack sufficient practical operation and experience in the process of cybersecurity professional training, which makes students feel uncomfortable when facing practical problems [8].
- (3) Lack of comprehensive quality training. In the process of cybersecurity talent training, sometimes too much emphasis is placed on the technical level, while the cultivation of students' comprehensive qualities, such as communication skills and teamwork skills, is neglected [9].
- (4) Insufficient teaching staff. The teaching staff of cybersecurity majors in some schools is relatively weak, resulting in the inability of teaching level and teaching resources to meet students' needs.
- (5) Insufficient cross-disciplinary integration. There is a lack of cross-disciplinary integration with journalism, law, intelligence and communications [7][8][9].
- (6) Lack of industry-recognized certificate training: Some schools and training institutions have failed to fully integrate industry needs and lack relevant certification courses. Students face competitive pressure in the job market after graduation [14].

### 4 DESIGN AND IMPLEMENTATION OF TRAINING MODEL

In the context of New Engineering, we should strengthen interdisciplinary and cross-border integration, and focus on cultivating engineering talents with innovative ability, practical ability and teamwork spirit. Cybersecurity talent training should also have a series of new characteristics and comprehensive abilities. Cyberspace security talent training under the background of New Engineering should be strengthened in the following aspects:

- (1) Strengthening the improvement of interdisciplinary integration and practical ability. New Engineering emphasizes the interdisciplinary training model. Cybersecurity talents should have multi-field knowledge. They should not only understand computer science and network technology, but also have knowledge of related fields, such as law, psychology, management, etc. Cybersecurity talents should improve their ability to solve practical problems through actual projects, experiments and drills. Practical training can include activities such as simulated network attack and defense, vulnerability mining, and emergency response. New Engineering focuses on cultivating innovative ability. Cybersecurity talents should have innovative thinking to discover new vulnerabilities and propose new security defense mechanisms. Students are encouraged to participate in scientific research projects in the field of security to cultivate independent thinking and problem-solving abilities.
- (2) Broadening international vision and continuous learning ability: Cross-internationalization is one of the goals of New Engineering training. Cybersecurity talents need to understand the latest international security threats, technologies and standards. Students are encouraged to participate in international security competitions and cooperation projects to enhance their international competitiveness. The field of cybersecurity is changing rapidly. New engineering disciplines should cultivate students' awareness and ability of continuous learning, encourage them to participate in industry certification, seminars, training and other activities, and continuously improve their professional level.
- (3) Cultivate teamwork and social responsibility. Cybersecurity issues usually require teamwork to solve. The training of cyberspace security talents in new engineering disciplines should emphasize teamwork and communication skills. Cultivate students to play different roles in the team, The ability to solve complex problems. New engineering advocates that engineering talents have a sense of social responsibility. Cybersecurity talents should understand the importance of their work to society, pay attention to the impact of information security on society, and their social responsibility in ensuring cybersecurity.

Through the characteristics of these new engineering disciplines, we can strengthen the integration of knowledge with fields such as journalism, law, and psychology, enhance the improvement of interdisciplinary practical capabilities,

broaden international perspectives and continuous learning capabilities, and cultivate teamwork and social responsibility. In the context of new engineering disciplines, we can cultivate more comprehensive talents with strong innovation capabilities and better adaptability to future cyberspace security.

## COMPETING INTERESTS

The authors have no relevant financial or non-financial interests to disclose.

## FUNDING

This article is supported by a grant of National Natural Science Foundation of China (Major Program) (program 92367201).

## REFERENCES

- [1] Li Qiang. Review meeting of "Planning Scheme for Urban Internet of Things Key Management System Based on Domestic Cryptographic Algorithms" was held in Beijing. *China Construction Informatization*, 2019(3): 2. DOI: CNKI:SUN:ZGJS.0.2019-03-022.
- [2] Yuan Sheng. Training of network security talents for practical combat. *China Information Security*, 2023(3): 47-48.
- [3] Wu Jianping. Cyberspace security is actually a competition for high-level talents. *China Education Network*, 2016(10): 1.
- [4] Wang Xing. Research on the construction system of network security talent team in the UK. *China Information Security*, 2015(11): 101103. DOI: 10.3969/j.issn.1674-7844.2015.11.038.
- [5] Yin Libo. Pay attention to Cybersecurity talent training. *China Information Security*, 2014(12): 1. DOI: 10.3969/j.issn.16747844.2014.12.038.
- [6] Li Xueying. Optimizing cybersecurity budget management mechanism and promoting cybersecurity talent training. *China Information Security*, 2023(4): 52-54.
- [7] Wang Xing. Prospects of Biden administration's cybersecurity talent strategy. *China Information Security*, 2023(3): 43-46.
- [8] An Shuzhao, Wan Xiaoyan. Research on cybersecurity talent training mechanism in the new era. *Internet Weekly*, 2023(7): 36-38.
- [9] Wang Lei, Xu Zijing, Zhu Ge, et al. Exploration of generative artificial intelligence empowering cybersecurity talent training. *China Audio-visual Education*, 2023(9): 101-108.
- [10] Yin X. Research on Training Strategies of High-level Practical Skills of Network Security Talents. *ICEMBE 2023*. DOI: 10.23977/ICEMBE2023.069.
- [11] Buttyán L, Félegyházi M, Pék G. Mentoring Talent in {IT} {Security-A} Case Study//2016 USENIX Workshop on Advances in Security Education (ASE 16). 2016.
- [12] Liu Z, Wang N. A New Experiment Teaching Mode for Network Security & Law Enforcement Major to Meet the Need of New Engineering Talent Training//2019 3rd International Conference on Education, Economics and Management Research (ICEEMR 2019). Atlantis Press, 2020: 214-217.
- [13] Yamin M M, Erdodi L, Torseth E, et al. Selecting and Training Young Cyber Talent: A Recurrent European Cyber Security Challenge Case Study//International Conference on Human-Computer Interaction. Cham: Springer International Publishing, 2022: 304-321.
- [14] Xiang Jizhi. Strengthening industry-university cooperation to improve the quality of cybersecurity talent training: An interview with Feng Huamin, Secretary General of the Ministry of Education's Higher Education Cyberspace Security Professional Teaching Committee. *China Information Security*, 2023, (03): 27-30.

# TRUXENONE AND ISOTRUXENONE-BASED POROUS ORGANIC POLYMERS AS METAL-FREE, HETEROGENEOUS PHOTOCATALYSTS FOR VISIBLE-LIGHT-PROMOTED REDUCTION OF LUNG CANCER A549 CELLS

YongLi Tan\*, YeMu Zhu, HaiFeng Duan

*The Affiliated Changsha Central Hospital, Hengyang Medical School, University of South China, Changsha 410004, Hunan, China.*

*Corresponding author: YongLi Tan, E-mail: 37330604@qq.com*

**Abstract:** While porous materials have been widely employed in numerous fields ranging from gas adsorption and separations, light emittance, sensing to energy storage, their applications in reducing respiratory morbidity are limited. In particular, the products obtained in a controlled manner using porous materials and thus applied to limit lung cancer cells multiplication are very rare. Here we report the synthesis of two new truxenone and isotruxenone-based porous organic polymers (POPs) via Friedel-Crafts alkylation/oxidation starting from truxene and isotruxene. These networks are thermally and chemically stable, and demonstrated as the first metal-free, heterogeneous photocatalysts for visible-light-induced tunable benzylic functionalization. Moreover, both POPs can be easily recovered and reused for at least 15 times without any apparent decrease in their photocatalytic activity. The synthetic utility of this newly-developed methodology is demonstrated in the value-added functionalization of chemical feedstocks such as xylenes and mesitylene, the resulting product can be used to reduce the number of lung cancer A549 cells.

**Keywords:** A549 cells; Heterogeneous photocatalysis; Metal-Free; Porous polymers; Visible-Light

## 1 INTRODUCTION

Visible-light photocatalysis has developed into an attractive and powerful platform to promote a variety of organic transformations over the past decades.[1,2] Since most organic compounds do not absorb visible light, these synthetic manifolds largely rely on the utilization of exogenous photocatalysts to facilitate the generation of reactive intermediates. Among them, transition-metal catalysts such as ruthenium- and iridium-polypyridyl complexes are the most frequently used due to their strong absorptions, long-lived excited states, and rich photoredox properties.[3] However, the intrinsic drawbacks regarding toxicity and residue of metals impose a limit for sustainable synthesis. On the other hand, organic dyes offer a more environmental benign opportunity by harvesting solar energy for organic synthesis in a metal-free fashion.[4] Nevertheless, the corresponding reactions suffer from severe postreaction removal problems. In this regard, the development of new photocatalysts that are free of metals, recoverable and reusable with high stability, and productively form bonds is highly desirable.

To this end, porous organic polymers (POPs) that built up from organic building units have emerged as promising alternatives for photocatalysts because these materials are non-metal in nature, synthetically versatile, thermally stable and chemically robust to organic solvents, acids and bases.[5-8] More importantly, the insoluble character, permanent porosity, and tunable electrical and optical properties render them very attractive for recyclable photocatalytic heterogeneous processes.[9-21] Despite these advantages, the utilization of POPs as sustainable photocatalysts for visible-light-driven switchable organic synthesis remains previously elusive.

Given the ability in enhancing lipophilicity, metabolic stability, and receptor binding affinity, fluorine substituents are becoming increasingly prevalent in pharmaceuticals, agrochemicals, and materials.[22,23] It is thus appealing to develop efficient methodologies for the selective incorporation of fluorine into organic molecules. On the other hand, aryl ketones and aldehydes are popular structures in pharmaceuticals and biologically relevant molecules, as exemplified by commercial drugs including Bupropion, Donepezil, (S)-Ketoprofen, and Pitofenone.[24-28] Due to the abundance of C-H bonds in organic compounds, benzylic C-H functionalization constitute a practical and straightforward strategy towards these targets, thereby arousing broad interest. A variety of transition-metals as well as organic catalysts have been adopted to promote each transformation.[29-34] However, the divergent catalytic protocols that allow the synthesis of both classes of products from the same starting materials, especially with a metal-free and recyclable heterogeneous catalyst, are challenging and unknown.

Owing to the unique structures, truxene and its derivatives have found applications in a wide range of research areas, particularly in the field of organic electronics, such as organic field-effect transistors (OFETs), organic photovoltaics

(OPVs), organic light-emitting diodes (OLEDs).[35,36] Recently, they are also exploited as building blocks in the construction of porous polymers,[37-40] which serve as heterogeneous photocatalysts to promote organic transformations including oxidative coupling of benzylamine, oxidative hydroxylation of arylboronic acids, etc.[14,18,41,42] Although impressive progresses have been achieved, the known examples mainly restricted with aerobic oxidation reactions that involve the transformations of oxidative labile substrates. It is of prominent interest to discover new reactivity of (iso)truxene-based scaffolds to broaden the reaction types, particularly those allow the direct functionalization of unactivated alkyl arenes such as chemical feedstocks xylenes. Here we show modification of (iso)truxene-based porous organic polymers enables recyclable photocatalysis for metal-free and tunable benzylic functionalization of alkylarenes under visible-light irradiation. By merely changing the solvents, either benzylic fluorination or benzylic oxidation is directed, allowing the facile synthesis of fluorinated compounds and functionalized ketones or aldehydes with high efficiency. The recycling capabilities with well-retained photoactivity of both POPs over fifteen times is also illustrated. Furthermore, this method is applicable to the value-added functionalization of chemical feedstocks including xylenes and mesitylene, the resulting product can be used to reduce the number of lung cancer A549 cells.

## 2 MATERIALS AND METHODS

### 2.1 Synthesis of TRO-POP and IsoTRO-POP

FeCl<sub>3</sub> (2.13 g, 13.14 mmol, anhydrous) was added to a solution of (iso)truxene (1.5 g, 4.38 mmol) in 20 mL 1, 2-dichloroethane (DCE). After being stirred at room temperature for 15 min, dimethoxymethane (1.16 mL, 13.14 mmol) was added. Then the resulting mixture was stirred at 85 °C for 60 h (TRO-POP) or 36 h (IsoTRO-POP) to complete the cross-linking. Afterwards, the reaction mixture was cooled to room temperature and the obtained precipitate was washed with water, acetone, ethanol, ethyl acetate, dichloromethane and petroleum ether, respectively. The product was collected and dried under vacuum as brown powders (TX-POP: 1.29 g, 69% yield; IsoTX-POP: 1.38 g, 74% yield).

To a 100 mL flask were added (Iso)TX-POP (1.0 g, 2.34 mmol), CrO<sub>3</sub> (3.51 g, 35.10 mmol), and acetic acid (20 mL). The reaction mixture was refluxed for 24 h. Then, the mixture was cooled to room temperature and ethanol (15 mL) was added. After stirring for 30 min, water (15 mL) was added and the reaction mixture was stirred for additional 30 min. Further, the obtained precipitate was washed with water, acetone, ethanol, ethyl acetate, dichloromethane and petroleum ether, respectively, and then extracted in a Soxhlet extractor with acetone. The product was collected and dried under vacuum as yellow powders (TRO-POP: 0.95 g, 79% yield; IsoTRO-POP: 0.90 g, 75% yield).

### 2.2 General Procedure for Visible-Light-Induced Benzylic Fluorination

To a sealed tube were added the substrate **1** (0.2 mmol, 1.0 equiv), Selectfluor (0.24 mmol, 1.2 equiv), TRO-POP or IsoTRO-POP (5 mol%), and acetonitrile (2 mL). The reaction mixture was degassed via freeze-pump-thaw for 3 cycles. After the mixture was thoroughly degassed, the vial was sealed and positioned approximately 2~3 cm from a 12 W CFL. The mixture was stirred at room temperature for the indicated time (monitored by TLC) under nitrogen atmosphere. Afterwards, the catalyst was separated by microcentrifuge and washed with dichloromethane. Then the filtrate was concentrated by rotary evaporation and the residue was purified by silica gel flash column chromatography using methylene chloride/petroleum ether or ethyl acetate/petroleum ether as the eluent to afford the desired products **2**.

### 2.3 General Procedure for Visible-Light-Induced Benzylic Oxidation

To a sealed tube were added the substrate **1** (0.2 mmol, 1.0 equiv), Selectfluor (0.24 mmol, 1.2 equiv), TRO-POP or IsoTRO-POP (5 mol%), acetonitrile (1 mL) and H<sub>2</sub>O (1 mL). The reaction mixture was degassed via freeze-pump-thaw for 3 cycles. After the mixture was thoroughly degassed, the vial was sealed and positioned approximately 2~3 cm from a 12 W CFL. The mixture was stirred at room temperature for the indicated time (monitored by TLC) under nitrogen atmosphere. Afterwards, the catalyst was separated by microcentrifuge and washed with dichloromethane. The filtrate was diluted with H<sub>2</sub>O, and extracted with dichloromethane. Then the organic phase was concentrated by rotary evaporation and the residue was purified by silica gel flash column chromatography using methylene chloride/petroleum ether or ethyl acetate/petroleum ether as the eluent to afford the desired products **3**.

## 3 RESULTS AND DISCUSSION

### 3.1 Synthesis and Characterizations of Tro-Pop and Isotro-Pop

The synthetic routes for TRO-POP and IsoTRO-POP have been shown in Figure 1. Truxene and isotruxene were synthesized according to known procedures.[43,44] With truxene and isotruxene as the starting materials, the polymerization firstly occurs by FeCl<sub>3</sub>-promoted Friedel-Crafts alkylation with formaldehyde dimethyl acetal (FDA) as electrophile providing TX-POP and IsoTX-POP with methylene linkers. Upon treatment with super stoichiometric amount

of  $\text{CrO}_3$  and under reflux condition, TX-POP and IsoTX-POP undergo subsequent oxidation to afford truxenone and isotru xenone-based POPs as yellow and orange powders, respectively. Both POPs were insoluble in all common solvents such as *N,N*-dimethylformamide (DMF), acetonitrile, and water. Thermogravimetric analyses (TGA) showed that TRO-POP and IsoTRO-POP were stable up to 405 and 365 °C, respectively (10% weight loss, Figure 5).

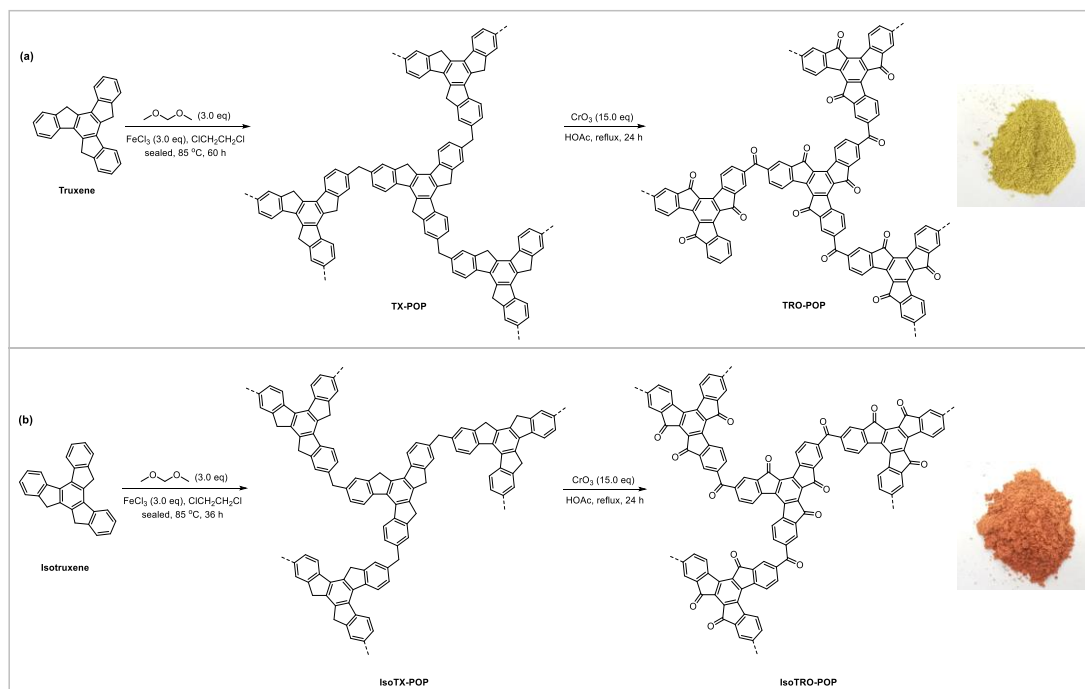


**Figure 1** Synthetic routes and idealized structures of TRO-POP and IsoTRO-POP.

The chemical structures of both POPs were elaborated by Fourier transform infrared (FTIR) analysis and  $^{13}\text{C}$  crosspolarization/magic angle spinning solid-state nuclear magnetic resonance (CP/MAS ssNMR) spectroscopy. In FTIR spectra, the peaks at  $1730\text{--}1715\text{ cm}^{-1}$  correspond to  $\text{--C=O--}$  stretching mode, supporting the existence of ketone moieties in the networks. The signals at  $1615\text{--}1610$  and  $1455\text{--}1450\text{ cm}^{-1}$  could be attributed to the vibrations of the truxenone and isotru xenone skeletons (a, Figure 2). Consistently, the CP/MAS ssNMR spectra show the signals at  $\sim 190$  ppm assigned to ketone moieties, and  $122$  to  $146$  ppm originated from the aromatic carbons of truxenone and isotru xenone (b, Figure 2). As a support, X-ray photoelectron spectroscopy (XPS) measurements disclosed that both POPs consist of carbon and oxygen elements (Figure 6). Furthermore, energy dispersive X-ray spectroscopy (EDS) and elemental analysis once again confirmed the presence of carbon and oxygen elements (Figure 8 and Table 1).

The porous feature of both POPs has been characterized by  $\text{N}_2$ -physisorption analysis (Figure 2). The  $\text{N}_2$  adsorption and desorption isotherms of both POPs indicated the presence of high percentage of micropores and minor proportion of mesopores (c and d, Figure 2). The Brunauer-Emmett-Teller (BET) specific surface areas of TRO-POP and IsoTRO-POP were measured to be  $1018$  and  $1156\text{ m}^2/\text{g}$ , with an average pore volume of  $1.43$  and  $1.44\text{ cm}^3/\text{g}$ , respectively (Figure 1). The pore diameter and distribution were determined using density functional theory (DFT) methods, revealing the majority are micropores with dimensions ranging from  $0.6$  to  $1.7\text{ nm}$  (both TRO-POP and IsoTRO-POP). Scanning electron microscopy (SEM) images demonstrated both POPs have irregular morphology (e and f, Figure 1). The amorphous structures were further confirmed by powder X-ray diffraction (PXRD) profiles, which did not exhibit any assignable peaks (Figure 10).

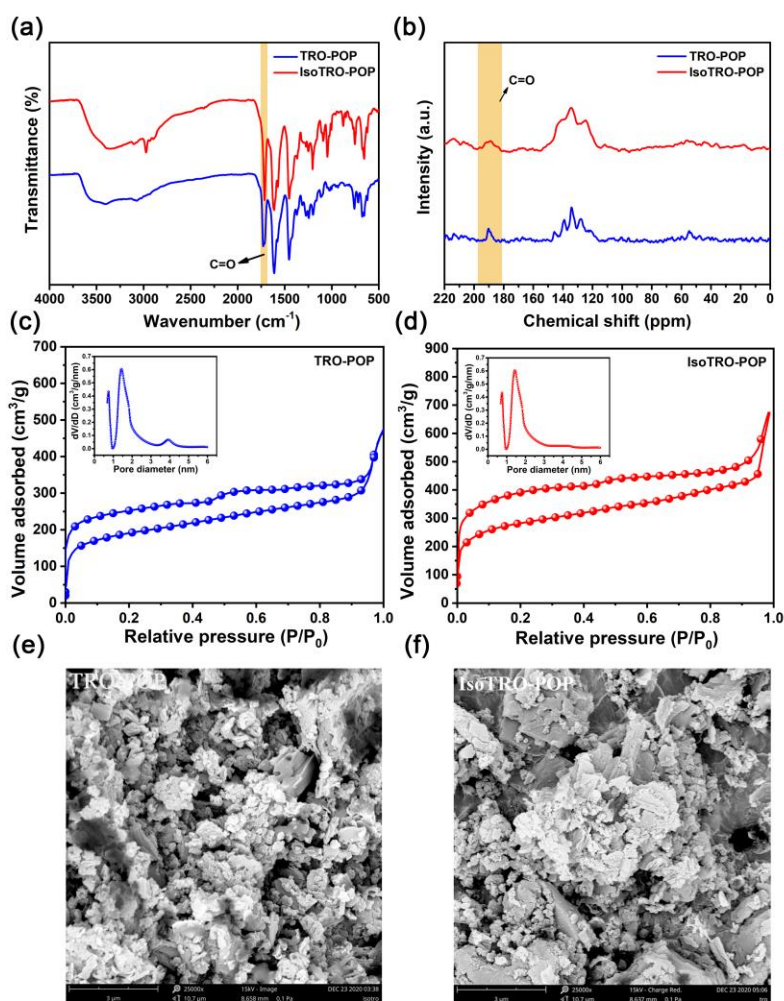


**Figure 2** (a) FTIR spectra of TRO-POP and IsoTRO-POP. (b) Solid-state  $^{13}\text{C}$  CP/MAS NMR spectra of TRO-POP and IsoTRO-POP. (c)  $\text{N}_2$ -physisorption isotherms and pore size distribution curve (inset) of TRO-POP. (d)  $\text{N}_2$ -physisorption isotherms and pore size distribution curve (inset) of IsoTRO-POP. (e) SEM images of TRO-POP. (f) SEM images of IsoTRO-POP.

Next, the optical and electronic properties of TRO-POP and IsoTRO-POP were probed. UV/vis diffuse reflectance spectra (DRS) of both POPs showed broad absorption bands from ultraviolet to visible light regions ( $\sim 800$  nm), which are crucial for their behavior as visible-light photocatalysts (a and b, Figure 3). It is worth noting that IsoTRO-POP exhibited an obvious redshift and enhanced absorption band compared to TRO-POP, indicating their stronger light-harvesting capability. The band gap of TRO-POP and IsoTRO-POP were calculated to be 2.36 and 2.11 eV from a Tauc plot. The conduction band minimum (CBM) of TRO-POP and IsoTRO-POP were established as -0.41 and -0.18 V via Mott-Schottky electrochemical measurements (c and d, Figure 3). On the basis of CBM and optical band gap, the valence band maximum (VBM) of TRO-POP and IsoTRO-POP were calculated to be 1.95 and 1.93 V, respectively (vs Ag/AgCl) (Figure 4).

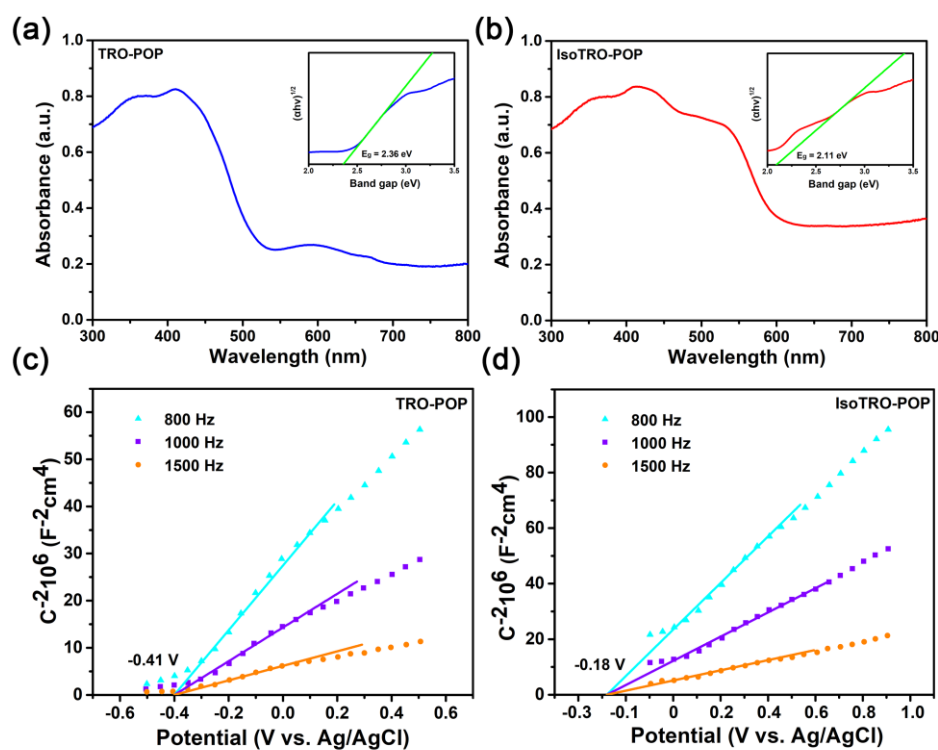


**Figure 3** (a) UV-vis diffuse reflectance spectra (DRS) and Tauc plot calculating the optical band gap (inset) of TRO-POP. (b) UV-vis diffuse reflectance spectra (DRS) and Tauc plot calculating the optical band gap (inset) of IsoTRO-POP. (c) Mott-Schottky plots of TRO-POP at frequencies 0.8, 1.0, and 1.5 kHz in a 0.2 M Na<sub>2</sub>SO<sub>4</sub> solution (pH = 7). (d) Mott-Schottky plots of IsoTRO-POP at frequencies 0.8, 1.0, and 1.5 kHz in a 0.2 M Na<sub>2</sub>SO<sub>4</sub> solution (pH = 7).

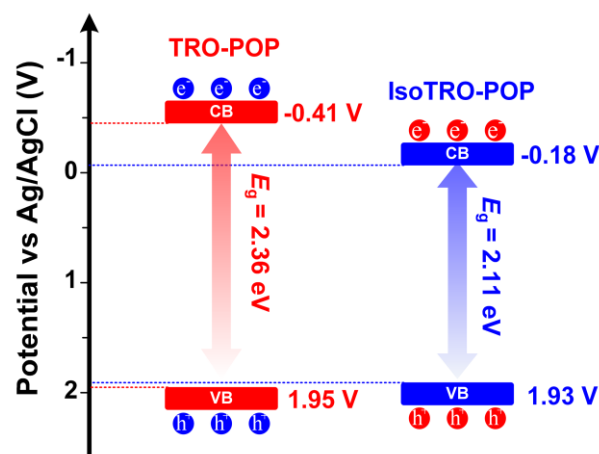


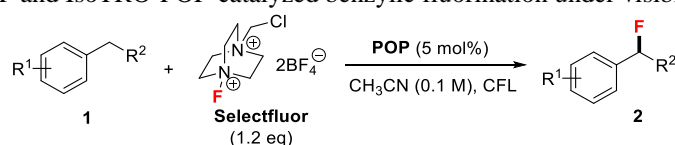
**Figure 4** Band energy diagram of TRO-POP and IsoTRO-POP.

### 3.2 Visible-Light-Promoted Benzylic Fluorination

We went on to explore the photocatalytic activity of TRO-POP and IsoTRO-POP in benzylic C-H fluorination. Gratifyingly, by using Selectfluor as the fluorine donor, benzylic fluorination of 4-ethylbiphenyl occurred smoothly in the presence of TRO-POP or IsoTRO-POP upon irradiation with a 12 W household compact fluorescent lamp (CFL), affording benzylic fluoride **2a** in 82% and 84% yield, respectively (entries 1-2, Table 1). Notably, truxene, isotruxene, TX-POP, and IsoTX-POP could not promote this reaction at all (entries 3-6, Table 1). Besides, the monomeric truxenone and isotruxenone gave poor yields under standard conditions (23-26% yield, entries 7-8, Table 1). Control experiments verified that both POPs and

visible light are essential (entries 9-11, Table 1). Then, the substrate scope was evaluated regarding both TRO-POP and IsoTRO-POP. In general, IsoTRO-POP led to better yields in a shorter reaction time compared to TRO-POP. Specifically, the ethylbenzene bearing a free carboxyl group was readily tolerated with both POPs, leading to **2b** in 78% and 82% yield, respectively (entries 12-13, Table 1). In addition to the methylene group, the methyl group could also participate in monofluorination efficiently, with good yields (88-94%) being obtained for **2c** and **2d** (entries 14-17, Table 1). The substrates possessing a variety of functionalities including a carboxylic acid, carboxylic ester, ketone, or tertiary alcohol underwent benzylic fluorination smoothly, affording the corresponding fluorinated products **2e-2h** in good yields (78-90%, entries 18-25, Table 1). Notably, the catalyst loading of both POPs could be further decreased to 0.5 mol% and 0.1 mol%, respectively, in which comparable results were achieved with a relatively prolonged reaction time (Figure 5).

**Table 1** TRO-POP and IsoTRO-POP-catalyzed benzylic fluorination under visible-light irradiation<sup>a</sup>



entry	substrates ( <b>1</b> )	products ( <b>2</b> )	catalyst	yield <sup>b</sup>
1			TRO-POP	82% (3.5 h)
2			IsoTRO-POP	84% (1.2 h)
3			Truxene	0
4			Isotruxene	0
5			TX-POP	0
6			IsoTX-POP	0
7			Truxenone	23% (1.2 h)
8			Isotruxenone	26% (1.2 h)
9 <sup>c</sup>			/	0
10 <sup>d</sup>			TRO-POP	0
11 <sup>d</sup>			IsoTRO-POP	0
12			TRO-POP	78% (21.2 h)
13			IsoTRO-POP	82% (16.2 h)
14			TRO-POP	92% (5.5 h)
15			IsoTRO-POP	94% (3.2 h)
16			TRO-POP	88% (4.3 h)
17			IsoTRO-POP	90% (2.2 h)
18			TRO-POP	82% (67.3 h)
19			IsoTRO-POP	88% (64 h)
20			TRO-POP	78% (69.3 h)
21			IsoTRO-POP	79% (65 h)
22			TRO-POP	83% (20.2 h)
23			IsoTRO-POP	86% (16 h)
24			TRO-POP	84% (22.5 h)
25			IsoTRO-POP	90% (15.3 h)

<sup>a</sup>General conditions: **1** (0.2 mmol), **Selectfluor** (0.24 mmol) in CH<sub>3</sub>CN (2.0 mL, 0.1 M) were stirred at room temperature under the irradiation with a 12 W CFL. <sup>b</sup>Isolated yield. <sup>c</sup>In the absence of TRO-POP or IsoTRO-POP. <sup>d</sup>In dark.

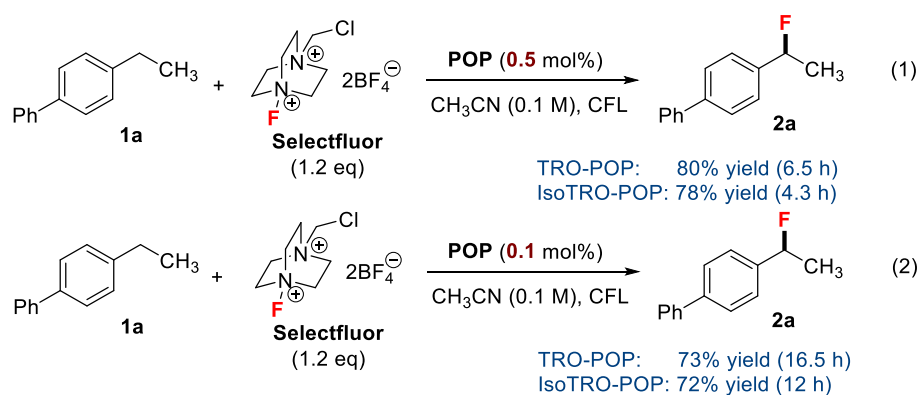
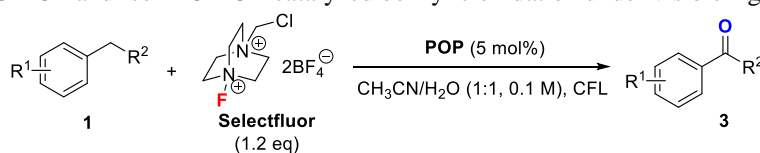


**Figure 5** Investigation of decreased catalyst loading for benzylic fluorination.

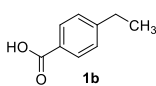
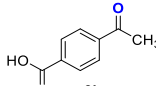
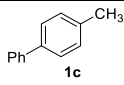
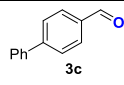
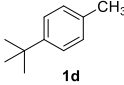
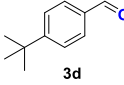
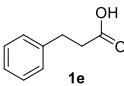
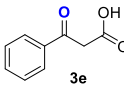
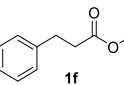
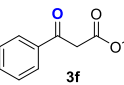
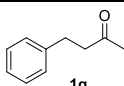
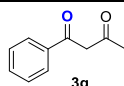
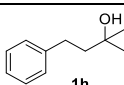
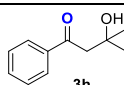
### 3.3 Visible-Light-Promoted Benzylic Oxidation

Interestingly, the fluorination products were completely switched to oxidation products when the solvent was changed to the mixture of acetonitrile and water. This result encouraged us to explore the generality of visible-light-promoted benzylic oxidation as two sets of completely different compounds can be obtained from the same starting materials under superficially similar conditions but in a controllable fashion. With TRO-POP and IsoTRO-POP as the catalysts and the mixture of acetonitrile and water as the solvent, 4-ethylbiphenyl proceeded effectively to afford the expected aryl ketone **3a** in 79% yield and 81% yield, respectively (entries 1-2, Table 2). Similarly, truxene, isotruxene, TX-POP, IsoTX-POP, truxenone, and isotruxenone proved less effective in promoting benzylic oxidations compared to that of TRO-POP and IsoTRO-POP (0-21% yields, entries 3-8, Table 2). Control experiments indicated that light and photocatalysts were indispensable for the formation of the benzylic oxidation product (entries 9-11, Table 2). Besides, the arene could be easily modified with electron-withdrawing and -donating groups (-COOH, -<sup>t</sup>Bu) (entries 12-17, Table 2). Methylbenzenes **1c** and **1d** are also good substrates, delivering the corresponding aldehydes **3c** and **3d** in 80-90% yields under the catalysis of each POP. Gratifyingly, the compounds bearing a variety of functionalities such as carboxylic acid (**1e**), carboxylic ester (**1f**), ketone (**1g**), or tertiary alcohol (**1h**) were well tolerated (entries 18-25, Table 2). The resultant 1,3-dicarbonyl compounds and  $\beta$ -hydroxyketones, which are common building blocks in organic synthesis could be constructed in a concise manner by directly editing C-H bond. When lowering the catalyst loading of both POPs to 0.5 mol% and 0.1 mol% respectively, the benzylic oxidation reactions proceeded smoothly to give the desired aryl ketone **3a** in good yields albeit with an extended reaction time (Scheme 3).

**Table 2** TRO-POP and IsoTRO-POP-catalyzed benzylic oxidation under visible-light irradiation<sup>a</sup>



entry	substrates ( <b>1</b> )	products ( <b>2</b> )	catalyst	yield <sup>b</sup>
1			TRO-POP	79% (15 h)
2			IsoTRO-POP	81% (12 h)
3			Truxene	0 (24 h)
4			Isotruxene	0 (24 h)
5			TX-POP	0 (24 h)
6			IsoTX-POP	0 (24 h)
7			Truxenone	19% (12 h)
8			Isotruxenone	21% (12 h)
9 <sup>c</sup>			/	0 (24 h)
10 <sup>d</sup>			TRO-POP	0 (24 h)
11 <sup>d</sup>			IsoTRO-POP	0 (24 h)

12			TRO-POP	75% (24 h)
13			IsoTRO-POP	79% (20 h)
14			TRO-POP	86% (10 h)
15			IsoTRO-POP	90% (8 h)
16			TRO-POP	80% (9 h)
17			IsoTRO-POP	85% (5 h)
18			TRO-POP	76% (76 h)
19			IsoTRO-POP	83% (70 h)
20			TRO-POP	70% (72 h)
21			IsoTRO-POP	76% (67 h)
22			TRO-POP	80% (26 h)
23			IsoTRO-POP	85% (19 h)
24			TRO-POP	79% (27 h)
25			IsoTRO-POP	86% (18 h)

<sup>a</sup>General conditions: **1** (0.2 mmol), **Selectfluor** (0.24 mmol) in CH<sub>3</sub>CN/H<sub>2</sub>O (1:1, 0.1 M) were stirred at room temperature under the irradiation with a 12 W CFL. <sup>b</sup>Isolated yield. <sup>c</sup>In the absence of TRO-POP or IsoTRO-POP. <sup>d</sup>In dark.

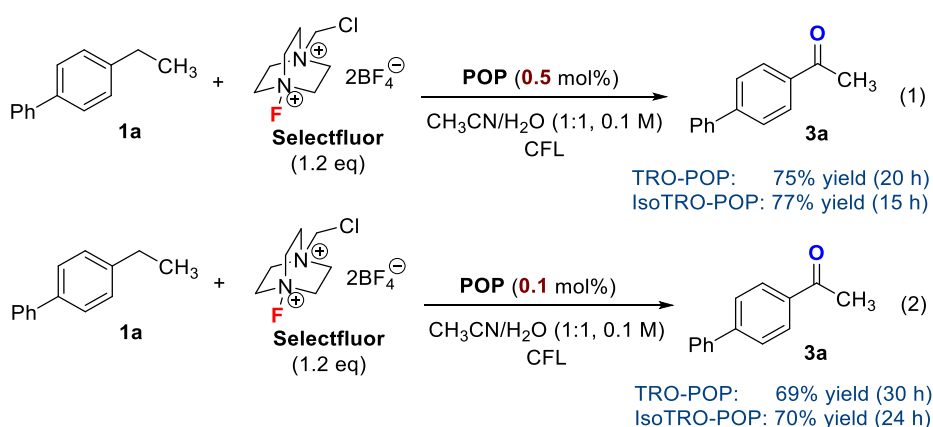
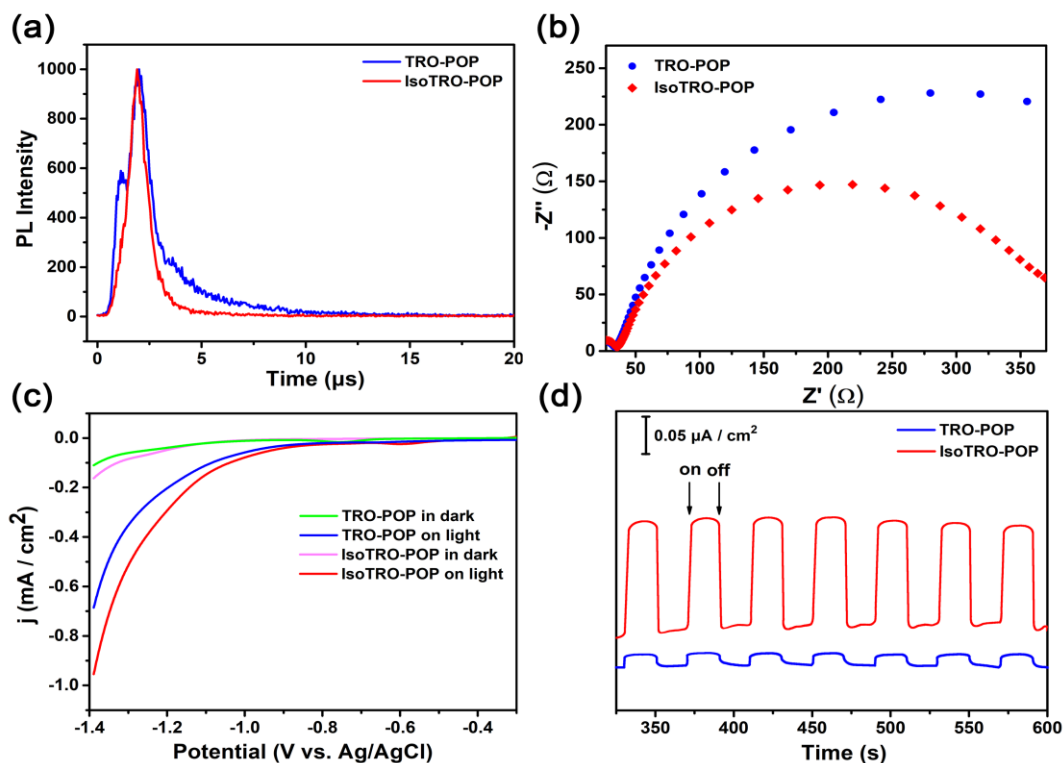


**Figure 6** Investigation of decreased catalyst loading for benzylic oxidation.

### 3.4 Mechanistic Investigation

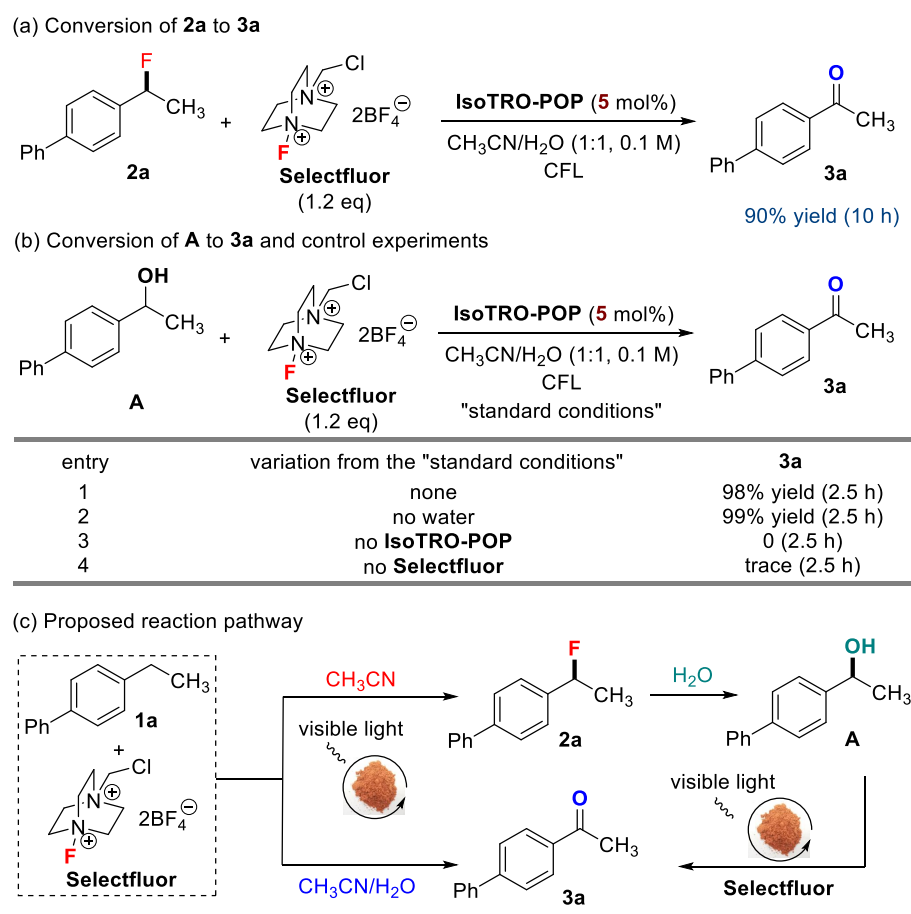
After examining the scope with respect to both benzylic fluorination and benzylic oxidation reactions, it was discovered IsoTRO-POP gave superior results in comparison with TRO-POP. To gain insights into the photocatalytic activity of both materials, the separation efficiency of photogenerated electron-hole pairs was evaluated (Figure 7). The time-resolved fluorescence spectra (TRPL) disclosed the average TRPL lifetime of IsoTRO-POP ( $\tau = 0.613 \mu\text{s}$ ) was shorter than that of TRO-POP ( $\tau = 2.017 \mu\text{s}$ ), implying that IsoTRO-POP had a more prominent non-radiative rate (a, Figure 7). The electrochemical impedance spectroscopy (EIS) indicated IsoTRO-POP had a smaller radius of a semicircular Nyquist plot compared to that of TRO-POP, which manifested a lower resistance in charge transfer for IsoTRO-POP (b, Figure 7). The linear sweep voltammetry (LSV) curves of TRO-POP and IsoTRO-POP showed the photocurrents under light irradiation were much higher than that in the dark, and meanwhile the current of IsoTRO-POP was higher than that of TRO-POP regardless of light illumination (c, Figure 7). These results suggested a better photo-electric activity of IsoTRO-POP. Consistently, IsoTRO-POP displayed a significantly enhanced photocurrent response compared to TRO-POP as shown in

Figure 7 d. Based on these studies, IsoTRO-POP bearing oligofluorene skeletons is believed to be more favored in photo-induced charge generation, transfer and separation, which can be explained for its better performance in photocatalysis.



**Figure 7** (a) Time-resolved PL spectra for TRO-POP and IsoTRO-POP. (b) EIS Nyquist plots of TRO-POP and IsoTRO-POP. (c) LSV curves of TRO-POP and IsoTRO-POP under visible-light irradiation and in the dark. (d) Photocurrent tests.

The second concern arises from the phenomenon that the product distribution can be diverted completely by simply changing the solvents. To probe the process, the reaction between **1a** and **Selectfluor** employing IsoTRO-POP as the catalyst and the mixture of acetonitrile and water as the solvent was monitored. It was observed that fluorination product **2a** was formed at the very beginning and gradually disappeared. Meanwhile, 1-([1,1'-biphenyl]-4-yl)ethan-1-ol (**A**) was detected. These insights suggested that **1a** might undergo nucleophilic substitution in the presence of water and serve as an intermediate in a sequential approach to benzylic oxidation. Accordingly, both **2a** and **A** were subjected to the standard conditions. As expected, the oxidation product **3a** was obtained in each case (Figure 8 a and entry 1 of Figure 8 b). Notably, the control experiments verified both IsoTRO-POP and **Selectfluor** were required for the subsequent oxidation (entries 2-4, Figure 8 b). Based on these observations, a plausible reaction pathway for the divergent synthesis was proposed, as depicted in Figure 8 c. By using acetonitrile as the solvent, TRO-POP and IsoTRO-POP-catalyzed benzylic fluorination occurs to afford fluorination product **2a** exclusively. When water is added as the co-solvent, a sequence including benzylic fluorination/nucleophilic substitution with water/oxidation takes place instead.



**Figure 8** Preliminary mechanistic studies. (a) Conversion of **2a** to **3a**. (b) Conversion of **A** to **3a** and control experiments. (c) Proposed reaction pathway.

### 3.5 Recyclability Tests

Next, the recycling experiments for the divergent reactions were performed by using centrifugation to recover the catalysts. It was found that both TRO-POP and IsoTRO-POP could promote the benzylic fluorination and oxidation for at least 15 recycling times without a significant drop in the yields (Figure 9 and Tables 2). And there is no apparent change in the FTIR spectra or UV/vis DRS of the spent TRO-POP and IsoTRO-POP after 15 cycles. As such, both POPs serve as highly efficient, robust, stable, recyclable, and low-cost pure organic heterogeneous photocatalysts for visible-light-induced tunable benzylic functionalization.

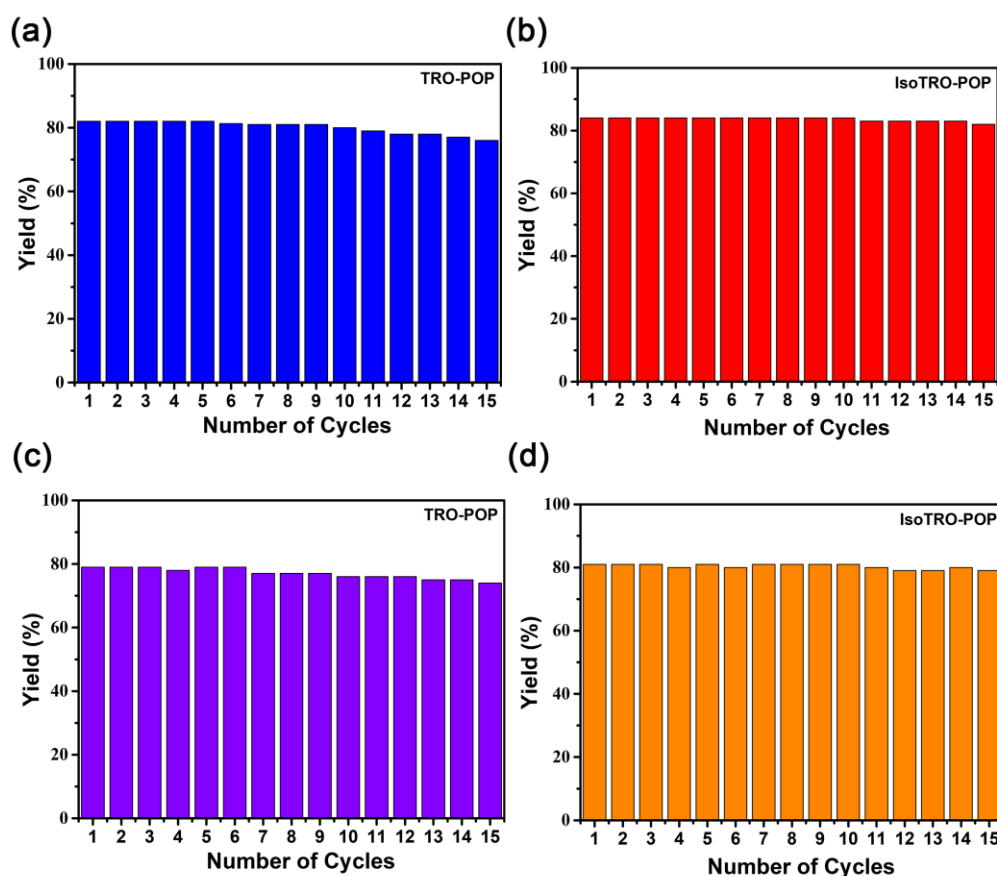


**Figure 9** (a) and (b) Recyclability tests of TRO-POP and IsoTRO-POP in the benzylic fluorination reaction. Reaction conditions: 1a (0.2 mmol), Selectfluor (0.24 mmol) in CH<sub>3</sub>CN (2.0 mL, 0.1 M) were stirred at room temperature under the irradiation with a 12 W CFL. (c) and (d) Recyclability tests of TRO-POP and IsoTRO-POP in the benzylic oxidation reaction. Reaction conditions: 1a (0.2 mmol), Selectfluor (0.24 mmol) in CH<sub>3</sub>CN/H<sub>2</sub>O (1:1, 0.1 M) were stirred at room temperature under the irradiation with a 12 W CFL.

### 3.6 Synthetic Utility

To demonstrate the amenability of this divergent strategy for value-added functionalization of chemical feedstocks, we subjected *o*-xylene, *m*-xylene, *p*-xylene, and mesitylene to standard conditions (Figure 10 a and Figure 10 b). In all cases, the fluorine and ketone moieties were introduced selectively using different solvents, leading to the corresponding multi-fluorinated derivatives and polyaldehydes in good yields, respectively. Notably, both types of products are of importance in the areas of pharmaceuticals, agrochemicals, and materials science. Moreover, 1,3,5-tri(4-methylphenyl)benzene (**6**) was tested under conditions for benzylic oxidation. To our delight, the expected product 1,3,5-Tris(4-formylphenyl)benzene (**7**), which is a versatile synthon for the preparation of COFs can be obtained in good yield (Figure 10 c).

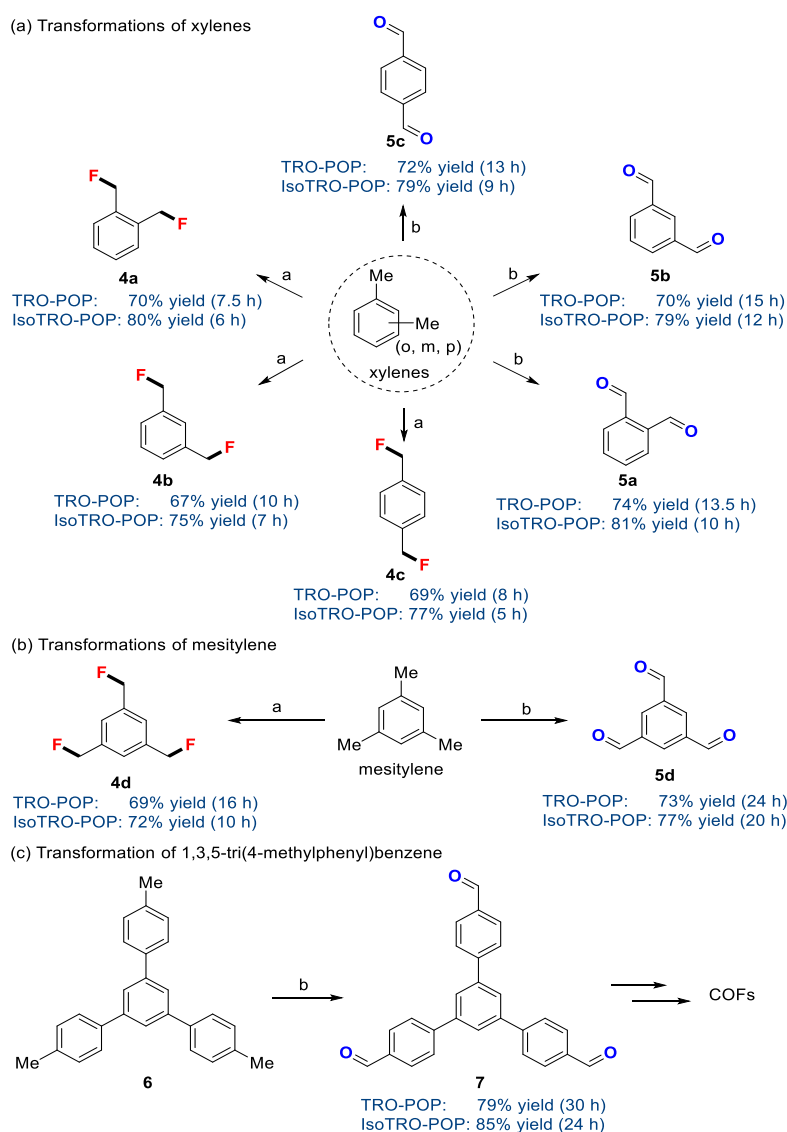


**Figure 10** Transformations. Condition a: **1** (0.2 mmol), Selectfluor (0.48 or 0.72 mmol) in CH<sub>3</sub>CN (0.1 M) were stirred at room temperature under the irradiation with a 12 W CFL. Condition b: **1** (0.2 mmol), Selectfluor (0.48 or 0.72 mmol) in CH<sub>3</sub>CN/H<sub>2</sub>O (1:1, 0.1 M) were stirred at room temperature under the irradiation with a 12 W CFL.

## 4 CONCLUSIONS

In conclusion, we have introduced a simple method for the synthesis of two new truxenone and isotruxenone-based POPs (TRO-POP and IsoTRO-POP) with truxene and isotruxene as the starting materials. These POPs are utilized as the first metal-free, heterogeneous photocatalysts for visible-light-induced tunable benzylic functionalization. By switching the solvents, either benzylic fluorination or benzylic oxidation is directed, resulting in the divergent synthesis of two types of products, namely fluorinated compounds and functionalized ketones or aldehydes in good to excellent yields from the same set of substrates. Decrease of the catalyst loading and recycling experiments reveal both POPs display excellent stability, high efficiency, and robust reusability. In addition, the optical and electronic characterizations suggest IsoTRO-POP is more in favor of charge transfer and separation, giving rise to superior photocatalytic activity compared to that of TRO-POP. Preliminary mechanistic studies account for the divergent reaction pathway. When water is used as the co-solvent, a sequence involving benzylic fluorination/nucleophilic substitution with water/oxidation occurs instead. Finally, the synthetic utility is illustrated in the elaborations of chemical feedstocks such as xylenes and mesitylene, and the product was used to reduce the reproduction of lung cancer A549 cells. A variety of important multi-fluorinated compounds as well as

polyaldehydes can be accessed in a precisely controlled fashion with a single operation. To the best of our knowledge, this is the first example that porous materials can catalyze tunable organic synthesis under visible-light irradiation. Our lab is focusing on reducing the incidence of respiratory disease with porous organic polymers.

## COMPETING INTERESTS

The authors have no relevant financial or non-financial interests to disclose.

## ACKNOWLEDGEMENT

Thank you for the laboratory provided by the Institute of Geriatrics, Hunan Provincial People's Hospital.

## REFERENCES

- [1] T.P. Yoon, M.A. Ischay, J. Du. Visible Light Photocatalysis as a Greener Approach to Photochemical Synthesis. *Nat. Chem.* 2010, 2(7): 527-532. DOI: <https://doi.org/10.1038/nchem.687>.
- [2] J. Xuan, W.J. Xiao. Visible-Light Photoredox Catalysis. *Angew. Chem. Int. Ed.* 2012, 51(28): 6828-6838. DOI: <https://doi.org/10.1002/anie.201200223>.
- [3] C.K. Prier, D.A. Rankic, D.W.C. MacMillan. Visible Light Photoredox Catalysis with Transition Metal Complexes: Applications in Organic Synthesis. *Chem. Rev.* 2013, 113(7): 5322-5363. DOI: <https://doi.org/10.1021/cr300503r>.
- [4] N.A. Romero, D.A. Nicewicz. Organic Photoredox Catalysis. *Chem Rev.* 2016, 116(17): 10075-10166. DOI: <https://doi.org/10.1021/acs.chemrev.6b00057>.
- [5] Z.-Y. Xu, Y. Luo, H. Wang, D.-W. Zhang, Z.-T. Li. Porous Organic Polymers as Heterogeneous Catalysts for Visible Light-Induced Organic Transformations. *Chin. J. Org. Chem.* 2020, 40(11): 3777-3793. DOI: <https://doi.org/10.6023/cjoc202003070>.
- [6] T.-X. Wang, H.-P. Liang, D.A. Anito, X. Ding, B.-H. Han. Emerging Applications of Porous Organic Polymers in Visible-Light Photocatalysis. *J. Mater. Chem. A.* 2020, 8(15): 7003-7034. DOI: <https://doi.org/10.1039/D0TA00364F>.
- [7] T. Zhang, G. Xing, W. Chen, L. Chen. Porous Organic Polymers: A Promising Platform for Efficient Photocatalysis. *Mater. Chem. Front.* 2020, 4(2): 332-353. DOI: <https://doi.org/10.1039/C9QM00633H>.
- [8] C.T.J. Ferguson, K.A.I. Zhang. Classical Polymers as Highly Tunable and Designable Heterogeneous Photocatalysts. *ACS Catal.* 2021, 11(15): 9547-9560. DOI: <https://doi.org/10.1021/acscatal.1c02056>.
- [9] H.-P. Liang, Q. Chen, B.-H. Han. Cationic Polycarbazole Networks as Visible-Light Heterogeneous Photocatalysts for Oxidative Organic Transformations. *ACS Catal.* 2018, 8(6): 5313-5322. DOI: <https://doi.org/10.1021/acscatal.7b04494>.
- [10] J. Luo, J. Lu, J. Zhang. Carbazole-Triazine Based Donor-Acceptor Porous Organic Frameworks for Efficient Visible-Light Photocatalytic Aerobic Oxidation Reactions. *J. Mater. Chem. A.* 2018, 6(31): 15154-15161. DOI: <https://doi.org/10.1039/c8ta05329d>.
- [11] X. Li, X. Ma, F. Zhang, X. Dong, X. Lang. Selective photocatalytic formation of sulfoxides by aerobic oxidation of sulfides over conjugated microporous polymers with thiazolo[5,4-d] thiazole linkage. *Appl. Catal. B: Environ.* 2021, 298: 120514-120623. DOI: <https://doi.org/10.1016/j.apcatb.2021.120514>.
- [12] H. Hao, F. Zhang, X. Dong, X. Lang. 2D sp<sup>2</sup> carbon-conjugated triazine covalent organic framework photocatalysis for blue light-induced selective oxidation of sulfides with O<sub>2</sub>. *Appl. Catal. B: Environ.* 2021, 299: 120691-120702. DOI: <https://doi.org/10.1016/j.apcatb.2021.120691>.
- [13] Z.J. Wang, S. Ghasimi, K. Landfester, K.A.I. Zhang. Molecular Structural Design of Conjugated Microporous Poly(Benzooxadiazole) Networks for Enhanced Photocatalytic Activity with Visible Light. *Adv. Mater.* 2015, 27(40): 6265-6270. DOI: <https://doi.org/10.1002/adma.201502735>.
- [14] V.R. Battula, H. Singh, S. Kumar, I. Bala, S.K. Pal, K. Kailasam, K. Natural Sunlight Driven Oxidative Homocoupling of Amines by a Truxene-Based Conjugated Microporous Polymer. *ACS Catal.* 2018, 8(8): 6751-6759. DOI: <https://doi.org/10.1021/acscatal.8b00623>.
- [15] H. Xu, X. Li, H. Hao, X. Dong, W. Sheng, X. Lang. Designing fluorene-based conjugated microporous polymers for blue light-driven photocatalytic selective oxidation of amines with oxygen. *Appl. Catal. B: Environ.* 2021, 285: 119796-119806. DOI: <https://doi.org/10.1016/j.apcatb.2020.119796>.
- [16] P. Wei, M. Qi, Z. Wang, S. Ding, W. Yu, Q. Liu, L. Wang, H. Wang, W. An, W. Wang. Benzoxazole-Linked Ultrastable Covalent Organic Frameworks for Photocatalysis. *J. Am. Chem. Soc.* 2018, 140(13): 4623-4631. DOI: <https://doi.org/10.1021/jacs.8b00571>.
- [17] Z.-Y. Xu, Y. Luo, D.-W. Zhang, H. Wang, X.-W. Sun, Z.-T. Li. Iridium complex-linked porous organic polymers for recyclable, broad-scope photocatalysis of organic transformations. *Green Chem.* 2020, 22(1): 136-143. DOI: <https://doi.org/10.1039/c9gc03688a>.

- [18] Y. Nailwal, A.D.D. Wonanke, M.A. Addicoat, S.K. Pal. A Dual-Function Highly Crystalline Covalent Organic Framework for HCl Sensing and Visible-Light Heterogeneous Photocatalysis. *Macromolecules*. 2021, 54(13): 6595-6604. DOI: <https://doi.org/10.1021/acs.macromol.1c00574>.
- [19] C. Song, J. Nie, C. Ma, C. Lu, F. Wang, G. Yang. 1,2,3-Triazole-based conjugated porous polymers for visible light induced oxidative organic transformations. *Appl. Catal. B: Environ.* 2021, 287: 119984-119996. DOI: <https://doi.org/10.1016/j.apcatb.2021.119984>.
- [20] Y. Zhi, S. Ma, H. Xia, Y. Zhang, Z. Shi, Y. Mu, X. Liu. Construction of donor-acceptor type conjugated microporous polymers: A fascinating strategy for the development of efficient heterogeneous photocatalysts in organic synthesis. *Appl. Catal. B: Environ.* 2019, 244: 36-44. DOI: <https://doi.org/10.1016/j.apcatb.2018.11.032>.
- [21] W. Zhang, S. Li, X. Tang, J. Tang, C. Pan, G. Yu. Phenothiazine core promoted charge transfer in conjugated microporous polymers for photocatalytic Ugi-type reaction and aerobic selenation of indoles. *Appl. Catal. B: Environ.* 2020, 272: 118982-118992. DOI: <https://doi.org/10.1016/j.apcatb.2020.118982>.
- [22] S. Purser, P.R. Moore, S. Swallow, V. Gouverneur. Fluorine in Medicinal Chemistry. *Chem. Soc. Rev.* 2008, 37(2): 320-330. DOI: <https://doi.org/10.1039/b610213c>.
- [23] R. Berger, G. Resnati, P. Metrangolo, E. Weber, J. Hulliger. Organic Fluorine Compounds: A Great Opportunity for Enhanced Materials Properties. *Chem. Soc. Rev.* 2011, 40(7): 3496-3508. DOI: <https://doi.org/10.1039/c0cs00221f>.
- [24] A.L. Ong, A.H. Kamaruddin, S. Bhatia. Current Technologies for the Production of (S)-Ketoprofen: Process Perspective, *Process Biochem.* 2005, 40(11): 3526-3535. DOI: <https://doi.org/10.1016/j.procbio.2005.03.054>.
- [25] J. Miao, H. Ge. Palladium-catalyzed chemoselective decarboxylative ortho acylation of benzoic acids with  $\alpha$ -oxocarboxylic acids, *Org. Lett.* 2013, 15(12): 2930-2933. DOI: <https://doi.org/10.1021/ol400919u>.
- [26] S.R. Khan, R.T. Berendt, C.D. Ellison, A.B. Ciavarella, E. Asafu-Adjaye, M.A. Khan, P.J. Faustino. Profiles of Drug Substances, Excipients and Related Methodology. 2016, 41: 79-438.
- [27] J.T. Brewster, S. Dell'Acqua, D.Q. Thach, J.L. Sessler. Classics in Chemical Neuroscience: Donepezil, *ACS Chem. Neurosci.* 2019, 10(1): 155-167. DOI: <https://doi.org/10.1021/acschemneuro.8b00517>.
- [28] A. Sagadevan, V.P. Charpe, A. Ragupathi, K.C. Hwang. Visible Light Copper Photoredox-Catalyzed Aerobic Oxidative Coupling of Phenols and Terminal Alkynes: Regioselective Synthesis of Functionalized Ketones via  $C\equiv C$  Triple Bond Cleavage. *J. Am. Chem. Soc.* 2017, 139(8): 2896-2899. DOI: <https://doi.org/10.1021/jacs.6b13113>.
- [29] S. Bloom, C.R. Pitts, D.C. Miller, N. Haselton, M.G. Holl, E. Urheim, T. Lectka. A Polycomponent Metal-Catalyzed Aliphatic, Allylic, and Benzylic Fluorination. *Angew. Chem. Int. Ed.* 2012, 51: 10580-10583. DOI: <https://doi.org/10.1002/ange.201203642>.
- [30] J.-B. Xia, C. Zhu, C. Chen. Visible Light-Promoted Metal-Free C-H Activation: Diarylketone-Catalyzed Selective Benzylic Mono- and Difluorination. *J. Am. Chem. Soc.* 2013, 135(46): 17494-17500. DOI: <https://doi.org/10.1021/ja410815u>.
- [31] B. Pieber, M. Shalom, M. Antonietti, P.H. Seeberger, K. Gilmore. Continuous Heterogeneous Photocatalysis in Serial Micro-Batch Reactors, *Angew. Chem. Int. Ed.* 2018, 57(31): 9976-9979. DOI: <https://doi.org/10.1002/ange.201712568>.
- [32] P. Mondal, M. Lovisari, B. Twamley, A.R. McDonald. Fast Hydrocarbon Oxidation by a High Valent Nickel-Fluoride Complex. *Angew. Chem. Int. Ed.* 2020, 59(31): 13044-13050. DOI: <https://doi.org/10.1002/anie.202004639>.
- [33] J.K. Bower, A.D. Cypcar, B. Henriquez, S.C.E. Stieber, S. Zhang.  $C(sp^3)$ -H Fluorination with a Copper(II)/(III) Redox Couple. *J. Am. Chem. Soc.* 2020, 142: 8514-8521. DOI: <https://doi.org/10.1021/jacs.0c02583>.
- [34] M.B. Andrus. Allylic and benzylic oxidation. In *Science of Synthesis, Stereoselective Synthesis*, 1st ed.; J.G.D. Vries, G.A. Molander, P.A. Evans, Eds.; Thieme Verlag: Stuttgart., 2011, 469-482.
- [35] F. Goubard, F. Dumur. Truxene: A Promising Scaffold for Future Materials. *RSC Adv.* 2015, 5: 3521-3551. DOI: <https://doi.org/10.1039/c4ra11559g>.
- [36] K. Shi, J.-Y. Wang, J. Pei.  $\pi$ -Conjugated Aromatics Based on Truxene: Synthesis, Self-Assembly, and Applications. *Chem. Rec.* 2015, 15(1): 52-72. DOI: <https://doi.org/10.1002/tcr.201402071>.
- [37] S. Das, H. Kim, K. Kim. Metathesis in Single Crystal: Complete and Reversible Exchange of Metal Ions Constituting the Frameworks of Metal-Organic Frameworks. *J. Am. Chem. Soc.* 2009, 131(11): 3814-3815. DOI: <https://doi.org/10.1021/ja808995d>.
- [38] L. Liu, S.G. Telfer. Systematic Ligand Modulation Enhances the Moisture Stability and Gas Sorption Characteristics of Quaternary Metal-Organic Frameworks. *J. Am. Chem. Soc.* 2015, 137(11): 3901-3909. DOI: <https://doi.org/10.1021/jacs.5b00365>.
- [39] Q. Zhang, C. Zhang, L. Cao, Z. Wang; B. An, Z. Lin, R. Huang; Z. Zhang, C. Wang, W. Lin., Förster Energy Transport in Metal-Organic Frameworks Is Beyond Step-by-Step Hopping. *J. Am. Chem. Soc.* 2016, 138(16): 5308-5315. DOI: <https://doi.org/10.1021/jacs.6b01345>.
- [40] X. Yang, Y. Hu, N. Dunlap, X. Wang, S. Huang, Z. Su, S. Sharma Y. Jin, F. Huang, X. Wang, S.-H. Lee, W. Zhang. A Truxenone-based Covalent Organic Framework as an All-Solid-State Lithium-Ion Battery Cathode with High Capacity. *Angew. Chem. Int. Ed.* 2020, 59: 20385-20389. DOI: <https://doi.org/10.1002/anie.202008619>.

- [41] K. Lin, Z. Wang, Z. Hu, P. Luo, X. Yang, X. Zhang, M. Rafiq, F. Huang, Y. Cao. Amino-Functionalised Conjugated Porous Polymers for Improved Photocatalytic Hydrogen Evolution. *J. Mater. Chem. A.* 2019, 7(32): 19087-19093. DOI: <https://doi.org/10.1039/c9ta06219j>.
- [42] H. Zhang, C. Zhou, Y. Zheng, X. Zhang. Isotruxene-Based Porous Polymers as Efficient and Recyclable Photocatalysts for Visible-Light-Induced Metal-Free Oxidative Organic Transformations. *Green Chem.* 2021, 23(22): 8878-8885. DOI: <https://doi.org/10.1039/D1GC03165A>.
- [43] E.V. Dehmlow, T. Kelle. Synthesis of New Truxene Derivatives: Possible Precursors of Fullerene Partial Structures? *Synth. Commun.* 1997, 27(11): 2021-2031. DOI: <https://doi.org/10.1080/00397919708006804>.
- [44] C. Zhou, W. Xuan, S.-P. Luo, Y.-H. Bao. One-step, Large-scale Synthesis of Isotruxene. *J. Chem. Res.* 2018, 42(11): 556-557. DOI: <https://doi.org/10.3184/174751918x15403823022089>.

# DEEP APPLICATION OF BIM + 3D SCANNING IN STEEL STRUCTURE AND CURTAIN WALL ENGINEERING

XueLiang Qiao<sup>1\*</sup>, XiYan Wang<sup>2</sup>, GuangYu Qiao<sup>3</sup>, SuYao Wei<sup>3</sup>, Hang Xing<sup>3</sup>, XingBin Tang<sup>3</sup>

<sup>1</sup>Beijing Shijingshan District Planning and Natural Resources Comprehensive Affairs Center, Beijing 100043, China.

<sup>2</sup>China National Botanical Garden, Beijing, 100093, China.

<sup>3</sup>The Third Construction Engineering Company Ltd. of China Construction Second Engineering Bureau, Beijing 100070, China.

Corresponding Author: XueLiang Qiao, Email: Qiaoxueliang1991@163.com

**Abstract:** There are many factors that affect the deformation and stress of steel structure in the construction process. Therefore, it is necessary to consider the deformation of steel structure affected by many factors before pre-assembly. How to control the machining and installation accuracy of these complex steel components is a difficult problem in the industry. BIM + 3D laser scanning technology is used to collect three-dimensional data of steel body construction, and accurate three-dimensional point cloud model is obtained. The deviation value of steel structure and design concept model can be easily judged by professional three-dimensional analysis software, which can not only effectively control the machining and installation accuracy of steel body structure, but also fully record the engineering site condition, and provide strong support for the reliability of data.

**Keywords:** Special-shaped steel structure; 3D laser scanning technology; BIM application; Point cloud data; Installation and measurement

## 1 INTRODUCTION

In recent years, China's steel structure industry has developed rapidly, especially in the civil high-rise, public buildings, industrial buildings and other fields are mostly steel structure design, high-rise buildings have been more than 500m, such as Shanghai center height of 632m, Dubai Khalifa height of 828m. The maximum span of public buildings has exceeded 100 m, such as the span of Beijing Wukesong Blue Ball Stadium is 120 m, the long axis span of the National Stadium is 332.3 m, and the short axis is 296.4 m. With the development of large-span and super high-rise buildings and the increasing improvement of people's aesthetic concepts, steel structure, as an advantageous structural system, is widely used. However, due to the large number of multi-directional and multi-angle complex steel members in its complex structural system, how to control their processing and installation accuracy is a big problem in the industry[1]. At present, a better way to solve this problem is to use a three-dimensional laser scanner to measure the three-dimensional steel components to obtain an accurate three-dimensional model. The deviation of the steel components is obtained through software analysis, which plays a more accurate role in the implementation of installation[2].

## 2 APPLICATION OF 3D SCANNING IN STEEL STRUCTURE ENGINEERING

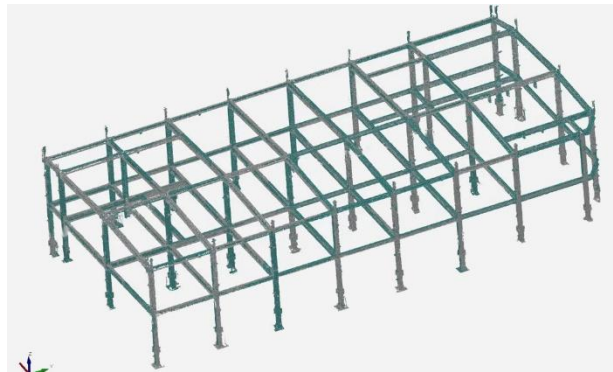
### 2.1 Three-dimensional Scanning of Steel Structure



Figure 1 On-site scanning

The large space 3D scanner is used to scan the overall architecture. The inclinometer function of the equipment is used to process the scanning data, which can effectively make the scanning data reach the horizontal state[3]. Through professional comparative analysis software, compared with the design model, the actual deviation is reflected in the form of chromatomap, and the specific deviation degree is determined by measuring the deviation size.

### 2.2 Steel Structure Model Analysis



**Figure 2** Three-dimensional scanning point cloud data

Due to the point cloud data acquisition process, redundant data and noise data will inevitably be generated. Manually delete the noise points that can be recognized by the naked eye, and delete the noise points that cannot be recognized by the naked eye with professional software. After denoising, the point cloud is merged.

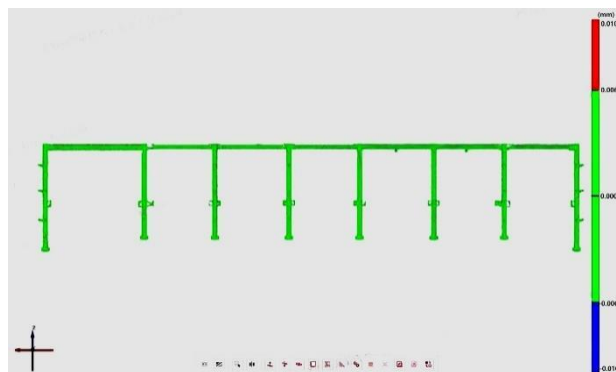


**Figure 3** Model analysis

Import the complete point cloud data into the modeling software to establish the overall three-dimensional model of the steel structure. The whole three-dimensional model is imported into the professional software to match the design model, and the deformation and displacement values of the solid model relative to the design model are compared and analyzed to detect the deformation of the steel structure.

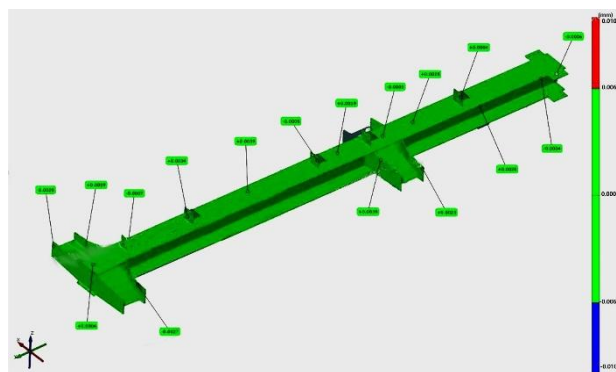


**Figure 4** Three-dimensional detection data of steel members

Through the chromatomap, the actual deviation of the steel structure can be intuitively analyzed, and the specific deviation degree can be determined by measuring the deviation size. After scanning all the constructions that need to be assembled, the real model obtained by scanning is assembled in real time in the software, and the conclusion that can be assembled is obtained intuitively.

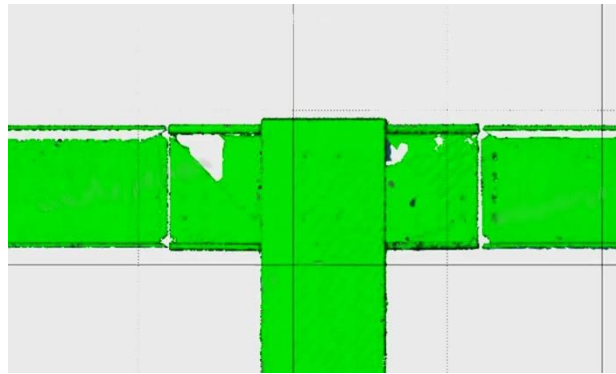


**Figure 5** Three-dimensional scanning point cloud data of some steel members

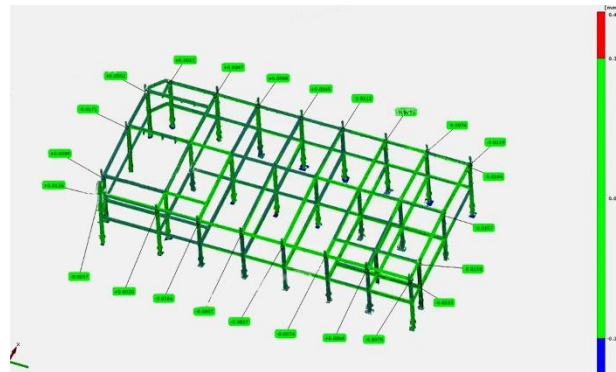


**Figure 6** Deviation Analysis of Bottom Pipe

Through the above model deviation analysis, the deviation parts can be clearly captured, and the accurate deviation data can be obtained, which plays a vital role in controlling the quality of the project. Compared with the traditional entity detection and pre-installation process, three-dimensional scanning technology has the advantages of saving construction investment, reducing a large number of construction sites, manpower and machinery investment, and can greatly improve construction efficiency and construction quality, and reduce construction costs. Truly achieve low cost, high efficiency, high efficiency standards[4].

### 3 APPLICATION OF 3D SCANNING IN CURTAIN WALL CONSTRUCTION

With the demand of large-scale urban construction, some unique 'landmark buildings' have emerged in various places. The special-shaped buildings with large space and large span are increasing, and the application of building curtain wall with special-shaped space modeling is becoming more and more extensive[5]. How to accurately detect the size of the special-shaped curtain wall is an important part to ensure the construction quality.

#### 3.1 Technical Difficulties of Steel Structure Curtain Wall Construction

- 1) Such buildings often use complex steel structures as the main base. Due to the large manufacturing and installation errors, large temperature deformation, and many changes in spatial angles of such steel structures.
- 2) The traditional wire measuring blanking and installation technology can not meet the needs of such projects in terms of operational safety, accuracy, schedule, cost and quality.

#### 3.2 Three-dimensional Scanning of Steel Curtain Wall



**Figure 7** Curtain wall three-dimensional scanning site

The engineering structure and architectural modeling of this project are complex. Due to the difficulty of detailing design, construction and installation of the curtain wall, the first step is to carry out on-site investigation in the scanning area, understand the on-site environment, analyze and deploy the whole scanning task, and use the total station and 3D laser scanner to carry out 3D scanning of the installed steel members.



**Figure 8** Curtain wall point cloud data

Preprocessing the collected point cloud data is generally to process the original data, check the consistency of the point cloud data and the integrity of the data, smooth the noise data in the point cloud data, fill the missing part of the point cloud, and remove the impurity point cloud data.

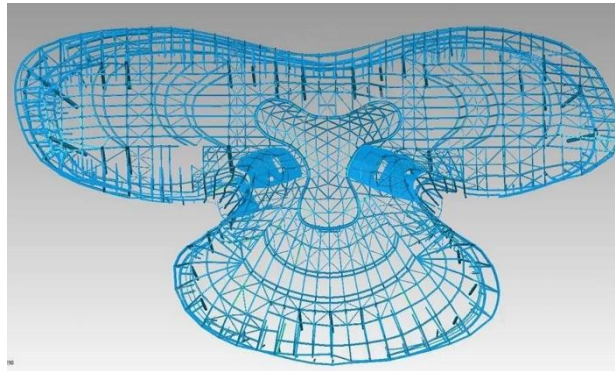


**Figure 9** Three-dimensional model of curtain wall

Noise point mainly refers to the external environment such as moving vehicles, pedestrians and trees on the road that mask or block the scanned target. In addition, the uneven reflection characteristics of the surface quality of the measured target itself lead to the situation that the scanned point cloud data we finally obtained contains unstable points or error points. For the more obvious noise points ( such as scattered points and outliers ) discrimination ,we generally used to determine through naked eye and then directly delete.

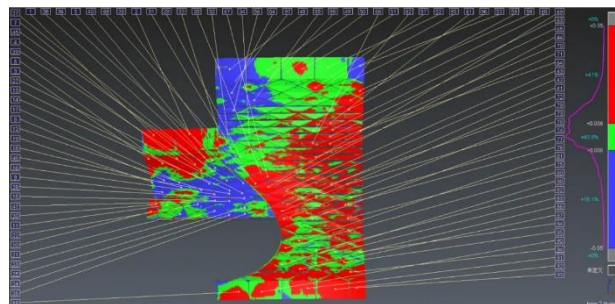


**Figure 10** Noise reduction

In order to ensure the quality of these point cloud data, it is necessary to simplify and smooth these point cloud data, so that the application of the whole data is more stable and fast.

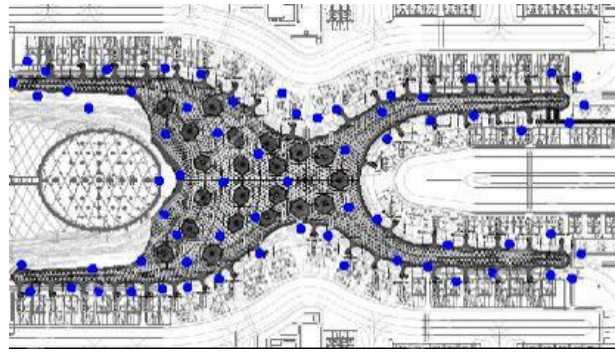


**Figure 11** Curtain wall point cloud data processing

The three-dimensional laser scanner is used to obtain the point cloud data of the object. After data preprocessing, the three-dimensional modeling of the building is carried out, so as to quickly determine the size of the building curtain wall and carry out batch cutting.

Thus, three-dimensional laser scanning high-density acquisition technology greatly shortens the data acquisition cycle, and the traditional single-point measurement efficiency of tens of thousands of times ; high-precision measurement greatly meet the high-precision installation requirements for the design of buildings is construction and technology provides a strong guarantee.

#### **4 APPLICATION OF 3D LASER SCANNING TECHNOLOGY IN STEEL STRUCTURE DEFORMATION DETECTION**

For large steel structure buildings, due to the good ductility of steel, the deformation is more complicated when it is stressed, and single point detection cannot reflect the deformation of the tower well.



**Figure 12** Three-dimensional scanning scene diagram of pressure equalization chamber

In order to obtain complete, comprehensive, continuous and related panoramic point cloud data. Technical team used FRAO three-dimensional scanner to measure the multi-angle and multi-directional structural deformation of the tower pressure cabin, and quickly obtained accurate data on the surface of the steel structure.



**Figure 13** Three-dimensional scanning station distribution map of ballast steel structure

Because of redundant data and noise data will inevitably be generated in the process of point cloud data acquisition. The noise points that can be identified by the naked eye are manually deleted, and the noise points that cannot be directly identified are automatically identified will be deleted by software. After denoising, point cloud splicing processing is performed. The complete point cloud data is imported into the modeling software to build a three-dimensional model of the whole steel structure.

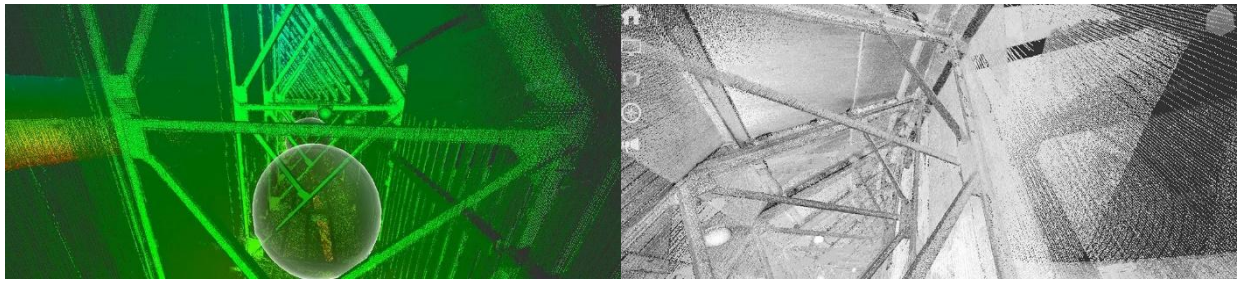


**Figure 14** Point cloud diagram of steel structure of pressure equalizing cabin

The overall three-dimensional model is imported into professional software to match the design model, and the deformation and displacement values of the solid model relative to the design model are compared and analyzed to detect the deformation of the steel structure.

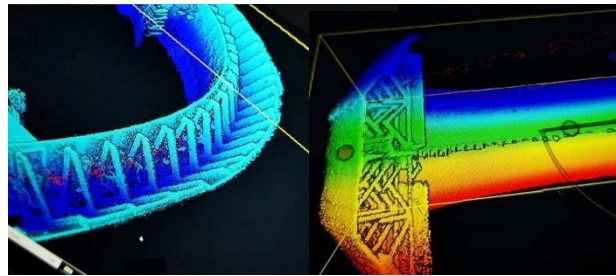


**Figure 15** Value brought in

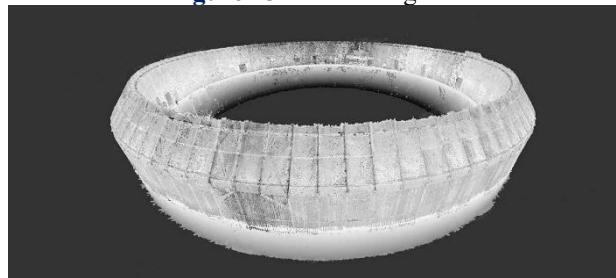


**Figure 16** Integral point cloud map of equalizing cabin steel structure

Therefore, it can be seen that the three-dimensional laser scanning technology has the advantages of fast, accurate and comprehensive acquisition, processing and analysis of data in the deformation detection technology of special-shaped steel structure, and can be fully applied to the deformation detection application requirements of special-shaped steel structure[6]. At the same time, three-dimensional scanning technology is also gradually changing the traditional measurement methods. More and more fields that cannot be completed or difficult to complete by conventional measurement are being overcome by three-dimensional laser scanning technology.

## 5 GENERALIZE

Modern public building design should not only meet the functional requirements, but also pursue the beauty of the building, the suitability of the function, and the comfort of the environment. It is necessary to conduct in-depth research on various decorative elements to meet the requirements of modeling, function, use, and perception. Therefore, the combination of super-large steel structure framework and decorative curtain wall structure has become the main method to realize complex modeling. Among them, in the processing, hoisting and installation process of the steel structure framework will produce large deviation that caused great difficulty to decorative shaped curtain wall installation. The rapid and comprehensive characteristics of BIM + 3D laser scanning technology can quickly obtain the three-dimensional data of each stage of construction, which not only avoids the limitations of manual measurement, but also accelerates the production and installation of subsequent components, and provides a new measurement method for the detection of special-shaped steel structures.

## COMPETING INTERESTS

The authors have no relevant financial or non-financial interests to disclose.

## REFERENCES

- [1] HAN Lei, YU Cun-hai, LIU Xiao-hui, et al. Study on Manufacturing Process of Multidirectional Complex Steel Structure/ / Proceedings of the 4th National Steel Structure Engineering Technology Exchange Conference. Tsinghua University ; construction Technology Editorial Department, 2012.
- [2] Application of 3D laser scanning technology in deformation measurement of steel structure plant. Journal of Heilongjiang Institute of Engineering, 2016, 30(5): 5.
- [3] Tian Liqun.Faru introduced the large space three-dimensional space scanner Photon 120. Ship Engineering, 2009, 31(4): 1.
- [4] Gong, Dong, Li, et al. Comprehensive application of BIM technology in Shenye Shangcheng Super Tall Tower 1 Project. Chinese Science and Technology Journal Database ( Citation Edition ) Engineering Technology, 2017(2): 00023-00023.
- [5] Zhu Hongwei.Conceptual design of curtain wall structure and calculation of glass deflection. Shanghai Construction Technology, 2009(4): 3.
- [6] Application of 3D laser scanning technology in deformation measurement of steel structure plant. Journal of Heilongjiang Institute of Engineering, 2016, 30(5): 5.



